論文 / 著書情報
Article / Book Information

題目(和文)	電子吸収分光法を用いたイオン液体を構成するカチオン-アニオン間電荷移動相互作用に関する研究
Title(English)	Charge transfer interactions of cation and anion components in ionic liquids studied by electronic absorption spectroscopy
著者(和文)	小倉隆宏
Author(English)	Takahiro Ogura
出典(和文)	学位:博士(理学), 学位授与機関:東京工業大学, 報告番号:甲第9011号, 授与年月日:2013年3月26日, 学位の種別:課程博士, 審査員:河合 明雄
Citation(English)	Degree:Doctor (Science), Conferring organization: Tokyo Institute of Technology, Report number:甲第9011号, Conferred date:2013/3/26, Degree Type:Course doctor, Examiner:
学位種別(和文)	博士論文
Type(English)	Doctoral Thesis

Charge Transfer Interactions of Cation and Anion Components in Ionic Liquids Studied by Electronic Absorption Spectroscopy

Takahiro Ogura

Department of Chemistry

Graduate School of Science and Engineering

Tokyo Institute of Technology

2013

Contents

Contents 1

List of Tables 5

List of Figures 6

List of Charts 9

Chapter 1. General introduction

1-1 Room Temperature Ionic Liquids (RTILs) 11

1-2 Unique structure of RTILs 12

1-3 Charge transfer interaction in RTILs 14

1-4 Goal and outline of the present thesis 15

References of Chapter 1 18

Chapter 2. Experimental

2-1 Room Temperature Ionic Liquids (RTILs) 24

2-2 Unique structure of RTILs 24

Chapter 3. Solvent effect for RTILs in the gas and liquid phases studied by electronic absorption spectroscopy

3-1 Introduction

-1. *Solvation in RTILs* 26

-2. *Gaseous RTILs* 27

-3. *Purpose of the present study* 28

3-2 Experimental

-1. *Samples* 29

-2. *Single path absorption spectroscopy* 29

-3. *Cavity ring-down laser absorption spectroscopy (CRDS)* 29

-4. *Quantum chemical calculation* 32

3-3 Results and discussion

-1. *Gas phase absorption spectra of EmpyTf$_2$N and BmimTf$_2$N* 32

-2. *Spectral features of RTILs in the gas and liquid phases* 35

-3. *Solvation in neat RTILs* 37

3-4 Conclusion 38

References of Chapter 3 39

Chapter 4. Transition energies of imidazolium-based cations affected by charge transfer interaction between cation and various counter anions

4-1 Introduction 50

4-2 Experimental 51

4-3 Results and discussion

-1. *Spectral shifts of $S_1(\pi\pi^*)\leftarrow S_0$ absorption bands due to counter anions* 51

-2. *Relationship between spectral shifts and solvatochromic shifts* 52

-3. *Transition energy difference determined by CT interaction* 53

4-4 Conclusion 54

References of Chapter 4 55

Chapter 5. Charge transfer interaction between pyridinium-based cation and anion in diluted solution

5-1 Introduction 59

5-2 Experimental

-1. *Samples* 60

-2. *Steady state absorption spectroscopy* 61

-3. *Conductivity measurement* 61

-4. *Nuclear magnetic resonance (NMR) spectroscopy* 61

-5. *Quantum chemical calculation* 62

5-3 Results and discussion

-1. *Absorption spectra of 1-ethylpyridinium-based ILs dissolved in solvents* 62

-2. *Assignment of CT bands for EpyX in solutions* 63

-3. *Oscillator strength for CT transitions of EpyX in dichloromethane* 65

-4. *Nature of the CT complex of EpyX ILs in dichloromethane* 68

-5. *Determination of ion pair conformation* 69

5-4 Conclusion 71

References of Chapter 5 72

Appendix 73

Chapter 6. Charge transfer interaction within ion pairs formed in RTILs

6-1 Introduction 87

6-2 Experimental 88

6-3 Results and discussion

-1. *Absorption spectra for neat imidazolium- and pyridinium-based ILs in neat liquid* 88

-2. *Analysis of absorption spectra in neat liquid* 91

-3. *Estimation of charge transfer interaction in neat liquid phase* 94

6-4 Conclusion 97

References of Chapter 6 98

Chapter 7. Charge transfer interaction near ionic liquid-solid interface studied by evanescent wave absorption spectroscopy

7-1 Introduction

-1. *Structure of RTILs near solid-liquid interface* 107

-2. *Experimental results indicating interface's specialty* 108

-3. *Purpose of the present study* 109

7-2 Experimental

-1. *Samples* 110

-2. *Attenuated total reflection (ATR) –UV/visible (ATR-UV/Vis) spectroscopy* 110

7-3 Results and discussion

-1. *Principle of evanescent wave absorption spectroscopy* 111

-2. *ATR-UV/Vis absorption spectra of toluene and RTILs as neat liquids* 114

-3. *Simulation of ATR-UV/Vis absorption spectra* 115

-4. *ATR-UV/Vis absorption spectra of RTILs depending on chromophore concentration* 121

-5. *ATR-UV/Vis absorption spectra of dyes diluted in RTILs* 122

-6. *Charge transfer interaction near solid-liquid interface* 123

7-4 Conclusion 124

References of Chapter 7 124

Chapter 8. Summary and concluding remarks 141

Acknowledgements 145

List of Tables

1-1. Snapshots of simulation boxes containing 700 ions of $C_n$mimPF_6. The application of a coloring code enables clear identification of the (red) and nonpolar (green) domains that form in ionic liquids. The lengths of the box sides are given: (a) n=2, CPK coloring; (b) n=2, same configuration as in a with red/green (charged/nonpolar) coloring; (c) n=4, *l* = 49.8 Å; (d) n=6, *l* = 52.8 Å; (e) n=8, *l* = 54.8 Å; (f) n=12, *l* = 59.1 Å. Graph from Lopes *et al*., *J. Phys. Chem. B*, **110**, 3330 (2006) (ref.[9]).

1-2. Sketch for the 1,1-butylmethylpyrrolidinium tris(pentafluoroethyl)trifluoro-phosphate-Al_2O_3 interface. (D and E) Different possible layering arrangements of correlated ions at a hard wall with checkerboard-type stacking (D) and double-layer stacking (E). Graph from Mezger *et al*., *J. Chem. Phys.*, 131, 094701 (2009). (ref.[18]).

3-1. The list of parameters used in theoretical calculation of spectral shifts.

3-2. Observed and calculated spectral shifts.

4-1. Observed values of $S_1(\pi\pi^*) \leftarrow S_0$ transition energy of $Bmim^+$-based RTILs, literature values of dielectric constant, E_N^T, donor number (DN) of RTILs, and DN of anions .

5-1. Molar absorption coefficients of $S_1(\pi\pi^*) \leftarrow S_0$ electronic transition of 1-ethylpyridinium-based RTILs in typical solvent. λ_{max} is 258.2 nm in water and acetonitrile solution, and 258.9 nm for $EpyTf_2N$ and 258.7 nm for $EpyPF_6$ in dichloromethane solution.

5-2. Electron affinity(E_A), solvation energy(E_S), ionic radius(r),and spin-orbit coupling(ΔE_{SO}) of halogen atom, X.

5-3. Ion association constant (K_A) of Epy^+ and various anions in solutions.

5-4. Molar absorption coefficients and oscillator strengths of CT transition of EpyBr and EpyI in dichloromethane solution.

5-5. Chemical shifts of EpyCl and $EpyTf_2N$ in deuterated water, acetonitrile, and dichloromethane. Δ indicates difference in chemical shifts of the two ILs.

6-1. The parameters of CT ($^2P_{3/2}$) transition bands.

7-1. Estimated reflection angle of incident light depending on light wavelengths and refractive indices of sapphire prism depicted in Figure 6-3 (b).

List of Figures

3-1. Temperature-dependent single-path absorption spectra of vaporized (a) $EmpyTf_2N$ and (b) $BmimTf_2N$.

3-2. Clausius-Clapeyron plots and their fitting lines [$\ln (p/p^*)=-(\Delta_{vap}H(T_{ave})/R)(1/T-1/T^*)$] of vaporized $EmpyTf_2N$ (open circle, gray line) and $BmimTf_2N$ (closed circle, black line). T^* and p^* are standard temperature and pressure for each ionic liquid, respectively.

3-3. Absorption spectra (closed circles) of vaporized (a) $EmpyTf_2N$ at 453 K and (b) $BmimTf_2N$ in red edge of the band at 443 K measured by CRDS. The solid lines are single-path absorption spectra (in arbitrary units) of neat liquids at almost the same temperature as in the gas phase.

3-4. Normalized single path absorption spectra of (a) $EmpyTf_2N$ and (b) $BmimTf_2N$ in gas phase and in neat liquid condition.

3-5. Normalized single path absorption spectra of pyridine in neat liquid condition (green) and in the gas phase (red). Arrows indicate 0-0 band of $\pi-\pi^*$ transition.

3-6. Transition energy shifts ΔE of chromophore compounds from vapor to neat liquid condition. Both observed (ΔE_{obs}) and calculated (ΔE_{ORF}) values were plotted for each compound. For pyrimidine and pyridine, the chromophores correspond to molecular pyrimidine and pyridine, respectively, while they are pyridinium and imidazolium cations in the ion pairs of each RTIL.

4-1. Normalized absorption spectra of $Bmim^+$ in two polar solvents and four neat RTILs. Inset is a structure of $Bmim^+$ caluculated by DFT method: blue atom is for nitrogen, dark grey for carbon and light grey for hydrogen.

4-2. The $\pi\pi^*$ transition energy of $Bmim^+$ in various ionic liquids and in molecular solvents. The black bar is for observed transition energy, red bar for predicted transition energy of ion pair in vacuum, and orange bar for estimated transition

energy from Onsager Reaction Field Theory and dielectric constant.
Transition energy in gas phase is assumed to be above 47640 cm^{-1}.
Solvation energies in molecular solvents for isolated $Bmim^+$ ion and those in RTILs for ion pair are not quantitative values because of unknown gas phase $Bmim^+$ u_{max} value. Transition energy for RTILs were also reduced by CT interaction between anion and cation of ion pairs. These estimated values were displayed by colored bars.

5-1. Absorption spectra of N-ethylpyridinium-based ILs in (left) water and (right) acetonitrile. Asterisks in EpyBr and EpyI spectra indicate CTTS band from halide ions.

5-2. Absorption spectra of N-ethylpyridinium-based ILs in dichloromethane.
An asterisk in EpyI spectrum indicates CTTS band from iodide ion.

5-3. Absorption spectra of (a) EpyCl, (b) EpyBr, and (c) EpyI at various concentrations in dichloromethane.

5-4. Experimental plots and their fitting lines calculated by Shedlovsky method.

5-5. IL concentration vs. dissociation degree curves of some solutions. Arrows indicate concentration region in the present absorption experiments.

5-6. ^{1}H-NMR spectra of EpyCl and EpyTf_2N in three deuterated solvents. S and * indicate peaks of solvent and impurity, respectively. The concentrations were about constant around 100 mM.

5-7. The most stable (a) and the second-most stable (+9.88 kJ mol^{-1}) (b) structures of Epy^+Cl^- ion pair in dichloromethane optimized by DFT calculations at the RB3LYP/6-311++G(3df,3pd) level of theory. Dotted lines indicate the nearest and the second nearest bonds distance between cation and anion.

6-1. Normalized absorption spectra of BmimTf_2N, BmimI and their mixture at 363 K. Molar ratios of the mixture are given.

6-2. Normalized absorption spectra of (a) neat PmmimI and neat PmmimTf_2N liquids at 363 K and (b) neat EpyI and neat EpyTf_2N liquids at 373 K.

6-3. Normalized absorption spectra of neat I^- salt (orange line), Tf_2N^- salt (green dotted line), their mixture (blue line), and simulated spectra (red dotted lines) with molar

fraction of X_I- as (a) 0.40, (b) 0.50, and (c) 0.75 for $Pmmim^+$-based ILs at 363 K and (d) 0.23, (e) 0.48, and (f) 0.79 for Epy^+-based ILs at 373 K.

6-4. Plots of absorbance ratio vs. molar fraction of X_I- in (a) EpyI / $EpyTf_2N$ mixture, (b) PmmimI / $PmmimTf_2N$ mixture and their fitting curves.

6-5. Absorption spectrum of neat PmmimI (grey) and its deconvoluted spectra with 4 bands.

6-6. Normalized absorption spectrum of neat EpyI (grey) and its deconvoluted spectra with 5 bands.

6-7. Schematic picture of CT transitions with spin-orbit splitting due to iodine atom. Weak CT complex gives large splitting in absorption bands, while strong CT complex gives small one.

7-1. (a) Absorption spectra of neat [2PA-Hmim]Tf_2N during thermal isomerization after UV irradiation stopped. (b) The measured change in absorbance during thermal isomerization, and their fitting curves by single exponential and biexponential decay functions.

7-2. Normalized absorption spectra of (a) toluene, (b) pyridine, and (c) $EmpyTf_2N$ as neat liquids and acetonitrile solutions.

7-3. (a) Experimental apparatus for ATR-UV/Vis absorption spectroscopy, and (b) a view of incident light and sapphire prism.

7-4. (a) Principle of evanescent wave generation, (b) estimated wavelength dispersion of refractive indices, and (c) estimated depth of penetration (d_p) depending on light wavelength in the case of toluene on sapphire.

7-5. Absorption spectra of neat liquids by using reflection method (red), transmission method (blue), and that of toluene solution by using transmission method (black) as (a) toluene, (b) $EmpyTf_2N$, and (c) [2PA-MOEmim]Tf_2N

7-6. Plots of calculated values for refractive index (n) and extinction coefficient (κ) vs. excitation light wavenumber of (a) toluene, (b) $EmpyTf_2N$, and (c) [2PA-MOEmim]Tf_2N..

7-7. Theoretically estimated depth of penetration (d_p) depending on reflection angle comparing with band shape of κ for (a) toluene, (b) $EmpyTf_2N$, and (c)

[2PA-MOEmim]Tf_2N.

7-8. Calculated absorption band for various reflection angle and observed one by transmission method. (a) toluene (z=4), (b) EmpyTf_2N (z=2), and (c) [2PA-MOEmim]Tf_2N (z=1).transmission method.

7-9. Observed ATR and simulated absorption spectra of (a) toluene, (b) EmpyTf_2N, and (c) [2PA-MOEmim]Tf_2N. The numbers in parenthesis mean the reflection angle.

7-10. Absorption spectra by ATR method for various concentration of (a) EmpyTf_2N in EmpyTf_2N/TMPATf_2N mixture, and (b) [2PA-MOEmim]Tf_2N in [2PA-MOEmim]Tf_2N/BmimTf_2N mixture . The numbers in vertical axis of (b) are arbitrary units due to various number of reflections for each samples.

7-11. (a) Calculated depth of penetration (d_p) against light wavelength for BpyTf_2N which is the representative of RTILs on sapphire. Absorption spectra of neat liquids by using transmission method (blue), reflection method (red), and that after calibration of dp (green) for (b) rhodamine 6G/TMPATf_2N and (c) coumarin 153/TMPATf_2N.

7-12. Absorption spectra of neat liquid by using reflection method (red), and transmission method (blue) at about 473 K. Arrows indicate absorption peaks of CT bands.

List of Charts

1-1. Common cations and anions in typical RTILs : I : 1-alkyl-3-methyl-imidazolium ($Rmim^+$) ; II : 1-alkylpyridinium (Rpy^+) ; III : tetraalkylammonium (N_{ijkl}^+) ; IV : tetra-alkylphosphonium (P_{ijkl}^+) ; V : 1,1-alkylmethylpyrrolidinium ($Rmpyrr^+$) ; VI : bis(trifluoromethanesulfonyl)amide (Tf_2N^-) ; VII : trifluoromethanesulfonate (TfO^-) ; VIII : hexafluorophosphate (PF_6^-) ; IX : tetrafluoroborate (BF_4^-) ; X : iodide (I^-)

5-1. Structure formula of EpyTf_2N [N-ethylpyridinium bis(trifluoromethanesulfonyl)amide].

6-1. Chemical structures and abbreviations of cations (left) and anions (right)

composing RTILs in the present experiment.

7-1. Photochemical and thermal E–Z isomerization reaction of $[2PA\text{-}Rmim]^+$ cation.

[2PA-MOEmim] Tf_2N : 2-phenylazo-1-metoxyethyl-3-methylimidazolium bis(trifluoromethanesulfonyl)amide.

Chapter 1. General introduction

1-1 Room Temperature Ionic Liquids (RTILs)

In 1914, a room temperature molten salt, ethylammonium nitrate was firstly discovered [1]. However in those days, researchers were not much interested in this salt. After about 40 years, in 1951, organic chloroaluminates were mentioned for the first time [2] and studied in details [3]. This is considered as the first generation of ionic liquids. However, these salts hydrolyze easily and needed to be handled in inert gas atmosphere. 40 years later, various air and water stable ionic liquids were discovered in early 1990s [4,5]. Since then, ionic liquids have attracted much interest in academia and industry.

Room temperature ionic liquids (RTILs) are organic salts consisting solely of cations and anions. Chart 1-1 shows some important typical ions and introduces their abbreviations. They normally have melting points near room temperature, and this character is very important. Sodium chloride, simple inorganic salts, melts at about 800 ^{o}C, and conventional inorganic salts have much higher melting points than room temperature. It is thus impossible to use these inorganic salts at room temperature as solvent. RTILs have other very unique physicochemical properties such as non-volatility, non-flammability, high viscosity, and high ionic conductivity. Considerable number of cation and anion families and their many substitution patterns allow the desired properties for specific applications to be selected, therefore RTILs are denoted as

"designer solvents" [6].

1-2 Unique structure of RTILs

As described above, RTILs have many unique physicochemical properties. Understanding of liquid structure formed in RTILs is much important to elucidate the reason why their properties depart from conventional solvents. Coulombic nature imposes a degree of order on the short range scale, and combination of polar and nonpolar components leads to correlations on long range scale. It is well known that high-temperature molten salts display charge ordering. Specifically, the structure of cation-cation and anion-anion peaks and valleys in the pair distribution are diametrically out of phase with the cation-anion pair distribution [7]. MD simulations of RTILs also display similar charge-ordering, though the anticoincidence between the cation-anion and self-ion peaks in the pair distribution function are usually not as clearly defined in systems of larger, flexible cations and anions compared with alkali halides [8]. One of the most striking findings about RTILs has been that they can display remarkable structural heterogeneity. Self-aggregation effects between alkyl chains of imidazolium based RTILs can lead to strongly ordered local environments depending on the alkyl chain length of R substituents (Chart 1-1). MD simulations by Canongia Lopes and Pádua [9,10] presented convincing evidence of this nanostructural organization, which was corroborated by X-ray experiments from Triolo and coworkers [11,12]. Lopes *et al.* also presented famous snapshot of simulation boxes by MD simulation as shown in

Figure 1-1 [9]. This figure is a powerful visual insight into the nature and evolution of the observed structures as the length of the nonpolar chain is increased. It is thought that this domain formation may be the cause of many of the anomalous properties of RTILs. There are also many spectroscopic studies focusing on RTIL structure utilizing various techniques such as Raman scattering [13], IR absorption [14], Kerr effect [15], dielectric absorption [16], NMR [17], and fluorescence anisotropy measurement [18].

More recently, the interfaces of RTILs with their environment, such as liquid-liquid, liquid-gas, and solid-liquid interfaces, have attracted considerable attention because they play a decisive role in multiphasic reactions [19,20]. For all processes near solid-liquid interfaces, a detailed understanding of the chemical structure, coordination behavior, reactivity, stability, and phase transitions of RTILs at the solid surfaces is important relevance. There are many usage of solid-RTIL interface, for examples, catalytic processes, lubricants, nanocomposites, and solar cells [20-22]. Various different methods such as atomic force microscopy (AFM) [23], X-ray reflectivity studies [24], and sum-frequency generation (SFG) measurement [20,25,26] have been applied for the investigation of solid-RTIL interfaces. Mezger *et al.* presented the unique structure sketch derived from X-ray reflectivity experimental results as shown in Figure 1-2 [24]. They suggested that the ordering structure of RTILs is formed by influence from solid-liquid interaction. This structure is composed up to about 1 nm from solid surface. However, much more recently, there was a report that there are longer unique structure with about 100 nm thickness that have an influence on

translational diffusion of solutes [27]. As described above, there are many outstanding and interesting problems near solid-RTIL interface.

1-3 Charge transfer interaction in RTILs

It is important to understand microscopic interactions in neat RTILs because unique structures in RTILs introduced in previous sections would be due to the balance of these interactions. RTILs are composed of cations and anions therefore major and important interactions are Coulomb interaction and charge transfer (CT) interaction. This study focuses on CT interaction in RTILs as the most important interaction, and tried to understand the interaction by spectroscopic measurements on electronic transition energy and oscillator strength of CT and other related absorption bands in RTILs.

Electronic state is a quantum state of a system of electrons. Electronic ground and excited states in condensed media are much influenced by surroundings like solvent-solute interaction, therefore absorption spectroscopy is great useful tool to study electronic states of object substance, solvation for them, and microscopic interactions of them. Absorption spectra are related to fundamental properties of liquids and have characteristic features that allow the determination of the type of electronic interactions that occur among molecules in the liquid. In neat RTILs, there are many cations and anions, which is a different character from other conventional liquids with neutral molecules. This is the most interesting point in a study of CT interactions in RTILs.

In general**,** the electronic absorption spectra of molecular liquids are understood on

the basis of the electronic structure of corresponding solvent molecule itself. However, RTILs may show additional CT bands of ion pairs, ion pair clusters, and ions to surroundings known as CTTS (Charge Transfer To Solvent) band [28,29], which are not expected in conventional neat molecular liquids. Because of this complicated nature of RTILs, there remain debates about their electronic absorption. As for their electronic structure in the condensed phase, there are several spectroscopic studies measuring photoelectron [30], UV/VIS absorption [31-33], and fluorescence [32,33]. Paul *et al.* measured absorption and fluorescence spectra of imidazolium-based RTILs, and found the broad and weak absorption bands in the neat liquid phase. They suggested these bands might relate to association of the cationic species [32,33]. Meanwhile, Katoh also measured absorption spectra of neat imidazolium-based RTILs which are 1-butyl-3-methylimidazolium bis(trifluoromethanesulfonyl)amide ($BmimTf_2N$) and $BmimPF_6$, and concluded that electronic structure of the liquid is interpreted by a simple sum of those of isolated cation and anion [31]. The electronic structure would be complicated due to coexistence of ions, ion pairs, and ion clusters. Moreover, dynamic heterogeneous structure of ion clusters as shown in Figure 1-1 suggested by MD simulation [9] gives additional complicated nature of RTILs.

1-4 Goal and outline of the present thesis

The goal of the present thesis is to understand CT interactions of RTILs by using electronic absorption spectroscopic method. The outlines of the subsequent chapters in

the present thesis are described below.

In Chapter 3, solvent effect for electronic states of RTILs was examined by using Cavity Ring-Down Spectroscopy for gas and liquid phases. Liquid phase of neat RTILs is much complicated due to interaction between cation and anion, domain structure of ions, and so on. Meanwhile, their gas phase is very simple system as details described in Chapter 3. Therefore, comparison with measured electronic transition energies of gas and liquid phases are important to evaluate solvent effect for RTILs in neat liquid. The measured spectral shifts were examined by Onsager Reaction Field theory for solvation energy, and solvent effect for RTILs is discussed.

In Chapter 4, electronic state of cations affected by CT interaction from nearby anion was examined. In this study, ion pair is considered as a basic unit of RTILs, which is an important result of chapter 3. CT interaction between cation and anion within the ion pair was elucidated from analysis of cation electronic state. There are many kinds of anions as given in Chart 1-1 composing RTILs, and these anions are characterized by various molecular properties such as donor number, molecular size, and mass. These properties result in variety of CT interactions with cation. Absorption spectroscopy of imidazolium provides red-shifted electronic transition energies which is a key measure for discussion of CT interactions.

In Chapter 5, CT complex between pyridinium-based cation and halide anion in diluted solution was studied. Study on electronic states of the CT complex of cation and anion in diluted solution gives important and fundamental information to understand

those of neat RTILs which would have CT interaction among ions. Molar absorption coefficients of CT transitions were determined by absorption spectroscopy combined with electric conductivity measurements, and relative conformation of the CT complex was determined by Nuclear Magnetic Resonance (NMR) spectroscopy. According to Mulliken theory for CT transition, nature of the isolated CT complex in diluted solution was discussed.

In Chapter 6, CT complexes of cation and anion pair in RTILs of EpyI, PmmimI and BmimI were studied by absorption spectroscopy for the neat RTILs. In these samples, there found many kinds of transitions such as those of cations, CT transition of ion pairs, and CTTS transition from ions to surroundings. These complicated absorption spectra measured for the RTILs were carefully analyzed to elucidate CT interaction of ion pairs in RTILs.

In Chapter 7, CT interaction of ion pair in RTILs near solid-liquid interface was examined. There are many reports that unique structure of RTILs evolves near solid-liquid interface. These structures of surroundings may lead to different solvation characters for RTILs, and electronic states of RTILs would be different from bulk liquid phase. However, there is no information of CT interaction of RTILs near solid-liquid interface. The present study introduces evanescent wave absorption spectroscopy to measure absorption spectra. Electronic states of RTILs near solid-liquid interface were discussed by comparing experimental results and theoretical analysis.

References of Chapter 1

[1] P. Walden, *Bull. Acad. Imp. Sci. St-Petersbourg* **8**, 405 (1914).

[2] F.H. Hurley, T.P. Wier, Jr., *J. Electrochem. Soc.* **98**, 207 (1951).

[3] T. Welton, *Chem. Rev.* **99**, 2071 (1999).

[4] J.S. Wilkes, M.J. Zaworotko, *J. Chem. Soc. Chem. Commun.* **965**, (1992).

[5] P. Bonhôte, A.P. Dias, N. Papageorgiou, K. Kalyanasundaram, M. Grätzel, *Angew. Inorg. Chem.* **35**, 1168 (1996).

[6] H. Weingärtner, *Angew. Chem. Int. Ed.* **47**, 654 (2007).

[7] K.S. Pitzer, *J. Phys. Chem.* **88**, 2689 (1984).

[8] C. Schröder, T. Rudas, G. Neumayr, W. Gansterer, and O. Steinhauser, *J. Chem. Phys.* **127**, 044505 (2007).

[9] J.N.A. Canongia Lopes and A.A.H. Pádua, *J. Phys. Chem. B* **110**, 3330 (2006).

[10] A.A.H. Pádua, M.F. Costa Gomes, and J.N.A. Canongia Lopes, *Acc. Chem. Res.* **40**, 1087 (2007).

[11] A. Triolo, O. Russina, H.J. Bleif, and E. Di Cola, *J. Phys. Chem. B* **111**, 4641 (2007).

[12] O. Russina, A. Triolo, L. Gontrani, R. Caminiti, D. Xiao, L.G. Hines, Jr., R.A. Bartsch, E.L. Quitevis, N. Pleckhova, and K.R. Seddon, *J. Phys.: Condens. atter.* **21**, 424121 (2009).

[13] H. Hamaguchi, S. Saha, R. Ozawa, S. Hayashi, ACS. Symp. Ser. **901**, 68 (2005).

[14] N. Akai, A. Kawai, K. Shibuya, *Chem. Lett.* **37**, 256 (2008).

[15] H. Shirota, J.F. Wishart, E.W. Castner Jr., *J. Phys. Chem. B* **111**, 4819 (2007).

[16] M.-M. Huang, Y. Jiang, P. Sasisanker, G.W. Driver, H. Weingärtner, *J. Chem. Eng. Data* **56**, 1494 (2011).

[17] H. Tokuda, K. Hayamizu, K. Ishii, Md.A.B.H. Susan, M. Watanabe, *J. Phys. Chem. B* **108**, 16593 (2004).

[18] D.C. Khara, A. Samanta, *Phys. Chem. Chem. Phys.* **12**, 7671 (2010).

[19] V.I. Parvulescu, C. Hardacre, *Chem. Rev.* **107**, 2615 (2007).

[20] S. Baldelli, *Acc. Chem. Res.* **41**, 421 (2008).

[21] T. Fukushima, A. Kosaka, Y. Ishimura, T. Yamamoto, T. Takigawa, N. Ishii, T. Aida, *Science* **300**, 2072 (2003).

[22] W. Xu, C. A. Angell, *Science* **302**, 422 (2003).

[23] R. Hayes, G.G. Warr, R. Atkin, *Phys. Chem. Chem. Phys.* **12**, 1709 (2010).

[24] M. Mezger, S. Schramm, H. Schroder, H. Reichert, M. Deutsch, E.J. De Souza, J.S. Okasinski, B.M. Ocko, V. Honkimaki, H. Dosch, *J. Chem. Phys.* **131**, 094701 (2009).

[25] B.D. Fitchett, J.C. Conboy, *J. Phys. Chem. B* **108**, 20255 (2004).

[26] T. Iimori, T. Iwahashi, H. Ishii, K. Seki, Y. Ouchi, R. Ozawa, H. Hamaguchi, D. Kim, *Chem. Phys. Lett.* **389**, 321 (2004).

[27] Kimura *et al.*, Annual Meeting of Japan Society for Molecular Science (2011).

[28] R. Katoh, Y. Yoshida, Y. Katsumura, K. Takahashi, *J. Phys. Chem. B* **111,** 4770 (2007).

[29] R. Katoh, M. Hara, S. Tsuzuki, *J. Phys. Chem. B* **112**, 15426 (2008).

[30] D. Yoshimura, T. Yokoyama, T. Nishi, H. Ishii, R. Ozawa, H. Hamaguchi, K. Seki, *J. Electron. Spectrosc. Relat. Phenom.* **319,** 144 (2005).

[31] R. Katoh, *Chem.Lett.* **36**, 1256 (2007).

[32] A. Paul, P. K. Mandal, A. Samanta, *Chem.Phys.Lett.* **402**, 375 (2005).

[33] A. Paul, A. Samanta, *J.Chem.Sci.* **118**, 335 (2006).

Cations

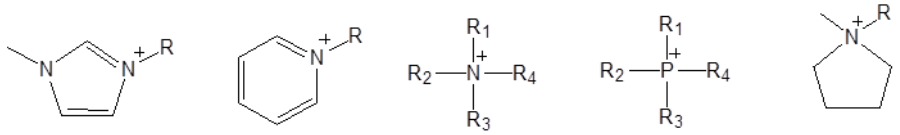

I II III IV V

Anions

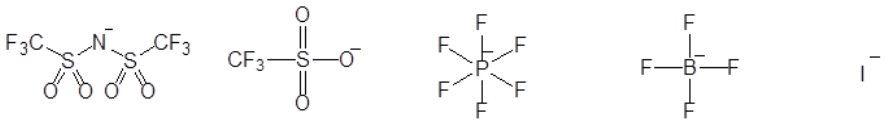

VI VII VIII IX X

Chart 1-1. Common cations and anions in typical RTILs : I : 1-alkyl-3-methyl-imidazolium ($Rmim^+$) ; II : 1-alkylpyridinium (Rpy^+) ; III : tetraalkylammonium (N_{ijkl}^+) ; IV : tetra-alkylphosphonium (P_{ijkl}^+) ; V : 1,1-alkylmethylpyrrolidinium ($Rmpyrr^+$) ; VI : bis(trifluoromethanesulfonyl)amide (Tf_2N^-) ; VII : trifluoromethanesulfonate (TfO^-) ; VIII : hexafluorophosphate (PF_6^-) ; IX : tetrafluoroborate (BF_4^-) ; X : iodide (I^-)

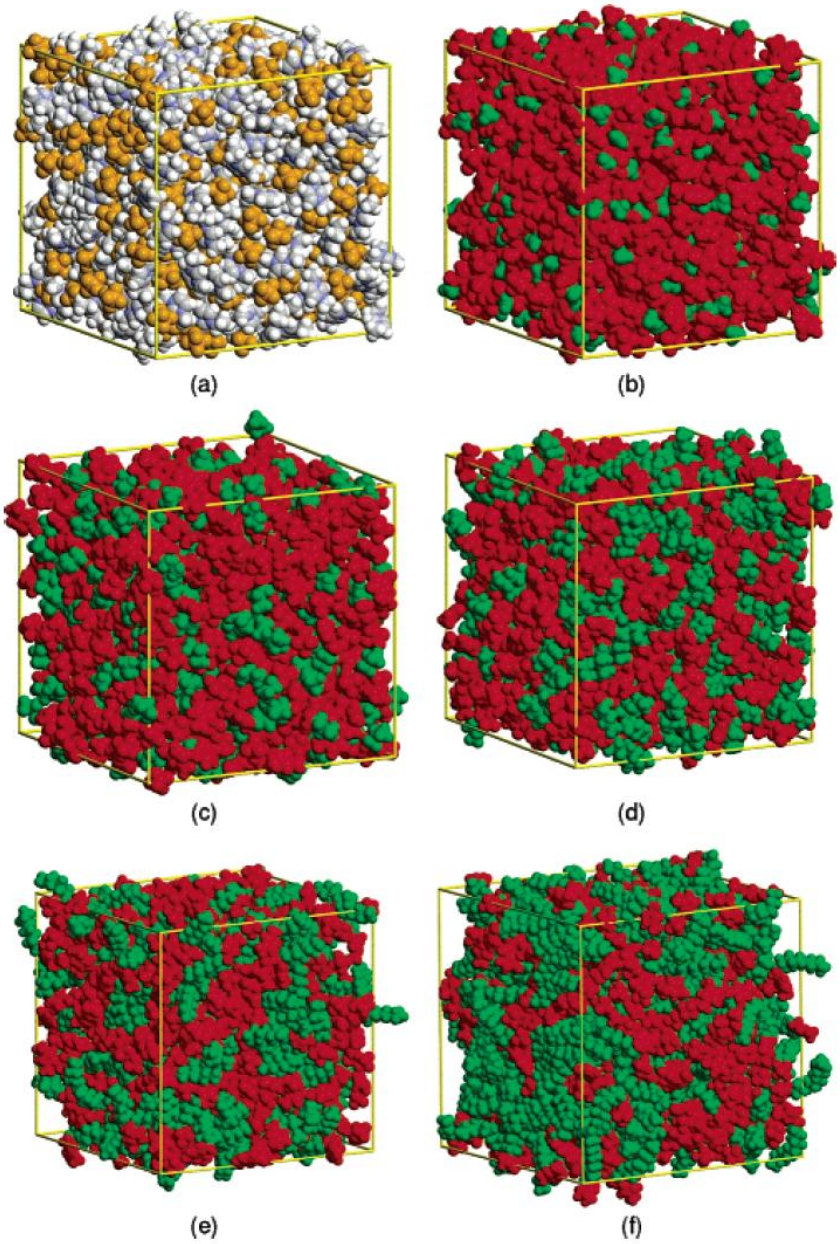

Figure 1-1. Snapshots of simulation boxes containing 700 ions of $C_n$mimPF_6. The application of a coloring code enables clear identification of the charged (red) and nonpolar (green) domains that form in ionic liquids. The lengths of the box sides are given: (a) n=2, CPK coloring; (b) n=2, same configuration as in a with red/green (charged/nonpolar) coloring; (c) n=4, *l* = 49.8 Å; (d) n=6, *l* = 52.8 Å; (e) n=8, *l* = 54.8 Å; (f) n=12, *l* = 59.1 Å. Graph from Lopes *et al., J. Phys. Chem. B*, **110**, 3330 (2006) (ref.[9]).

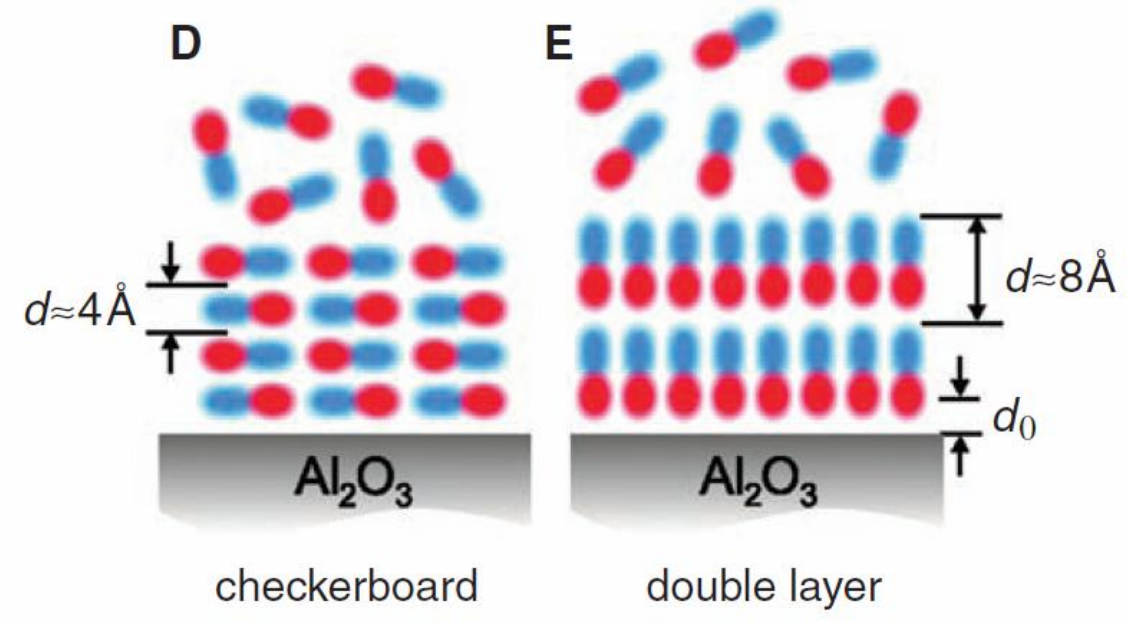

Figure 1-2. Sketch for the 1,1-butylmethylpyrrolidinium tris(pentafluoroethyl)trifluorophosphate-Al_2O_3 interface.

(D and E) Different possible layering arrangements of correlated ions at a hard wall with checkerboard-type stacking (D) and double-layer stacking (E). Graph from Mezger *et al.*, *J. Chem. Phys.*, **131**, 094701 (2009). (ref.[18]).

Chapter 2. Experimental

2-1. *Samples*

BmimTf$_2$N (Kanto Chemical, >97%), BmimPF$_6$ (Kanto Chemical, >99%), BmimBF$_4$ (Kanto Chemical, >99%), BmimTfO (Iolitec, >99%), BmimI (Kanto Chemical, >99%), EpyTf$_2$N (Tokyo Chemical Industry, >98%), and EmpyTf$_2$N (Tokyo Chemical Industry, >98%) were optically transparent and colorless. 1,2-dimethyl-3-propylimidazolium Tf$_2$N (PmmimTf$_2$N) (Kanto Chemical, >99%) and EpyI (Iolitec, >98%) were colorless solid at room temperature. They were used after purification by freeze-pump-thaw cycles in vacuum to remove volatile impurities such as oxygen, water and residual synthetic materials such as *n*-alkanes, imidazole and pyridine. Non-volatile alkali halide impurities have negligibly low vapor pressures as compared with BmimTf$_2$N and EmpyTf$_2$N, making no contribution to absorption spectroscopy in the gas phase. EpyPF$_6$ (Iolitec, >99%), EpyBr (Tokyo Chemical Industry, >98%), EpyCl (Tokyo Chemical Industry, >98%) were used as received. Other molecular solvents (Kanto Chemical) were used as received.

2-2. *Steady state absorption spectroscopy*

Absorption spectra were measured by using a UV/VIS spectrophotometer (Shimadzu, UV-2450). For solution samples, a fused-silica cubic cell with 1 cm optical path length was used. For neat liquids, thin layer samples between two fused-silica

plates were utilized. Thickness of thin liquids is on the order of μm. Wavelength resolution was 0.1 nm.

Chapter 3. Solvent effect for RTILs in the gas and liquid phases studied by electronic absorption spectroscopy

3-1. Introduction

3-1-1. *Solvation in RTILs*

Electronic states of molecules are very important in molecular photochemistry as details described in Chapter 1-3. Physical and chemical processes occur after absorbing photons, therefore electronically excited states of molecules are at the most important part of photoprocesses. There are many studies about the electronic states of molecules, and it is well known that the electronic states of molecules are affected by surroundings. Transition energy between electronic excited and ground states is observed by absorption spectroscopy, and the absorption band position depends on the solvation conditions. Thus, the experimental study of solvent effects and solvatochromic shift on UV/Vis absorption spectra provides an important insight on the electronic properties of molecules. Though there are many studies for solvatochromism of organic compounds up to current times, studies for that of RTILs are scarce.

As described in Chapter 1-1, RTILs are organic salts consisting solely of cations and anions. Their unique physicochemical properties are characterized by a balance among the Coulomb force, van der Waals interaction, and hydrogen bonds. Many spectroscopic studies have been reported to understand these intermolecular interactions,

For example, C. Reichardt studied solvatochromism of betaine dye in RTILs focusing on the polarity of RTILs, and found that solvatochromism occur in RTILs [1]. There are other studies for solvatochromism in RTILs [2,3].

In general**,** the electronic absorption spectra of molecular liquids are understood on the basis of the electronic structure of corresponding solvent molecule itself. However, RTILs may show additional electronic transition bands which are not expected in conventional neat molecular liquids as details described in Chapter 1-3. Because of this complicated nature of RTILs, there remain debates about the electronic absorption of RTILs. Therefore, the present study is focused on the electronic absorption spectra of RTILs, in particular in the gas phase, to understand the intermolecular interaction in RTILs.

3-1-2. *Gaseous RTILs*

To understand the solvent effect for RTILs, it is very important to obtain the electronic states of vaporized RTILs which have no surroundings. However, the studies of the vaporized RTILs are rather less common. One of the reasons is widely accepted view that RTILs have no vapor pressure. However in 2005, Rebero *et al*. measured vapor pressures of RTILs [4], and they exploded the established common view as RTILs have no vapor pressure. In 2006, Earle *et al*. demonstrated that Tf_2N salts based on imidazolium cations are vaporized in vacuum and also are separated by distillation [5]. After that, researches of vaporized RTILs have been done actively. In 2007, Leal *et al.*

studied the RTIL conformations in the gas phase by using Fourier transform ion cyclotron resonance mass spectrometry experiments, and they concluded that the gas phase of RTILs were consisting of discrete 1:1 anion-cation pairs [6], and gas phase spectroscopy is expected to be helpful for discussion about their electronic structure in the liquid phase. Actually, gas-phase spectroscopy is available because of the recent discovery of slightly volatile RTILs by Rebero *et al.* [4] and some related gas phase studies [5-15].

3-1-3. *Purpose of the present study*

In the present study, measurements of the gas-phase UV/Vis absorption spectra of isolated ion pairs of $EmpyTf_2N$ and $BmimTf_2N$ were carried out. These RTILs are advantageous for gas-phase spectroscopy because (1) RTILs involving Tf_2N anion have relatively high vapor pressure, and (2) Tf_2N anion is thermally-stable, which enables us to heat their samples. Absorption spectra of simple ion pairs in the gas phase were discussed by comparing those of liquid phase RTILs which include both ion pair character and complicated solvation networks.

3-2. Experimental

3-2-1. *Samples*

Used samples were as details described in Chapter 2.

3-2-2. *Single path absorption spectroscopy*

Absorption spectra of solution samples and neat liquids were measured by the method as described in Chapter 2. For gas phase spectroscopy of RTIL vapors, a fused-silica cell with 8 cm optical path was used. Temperatures of the sample and the cell were controlled by a home-made cell holder. RTIL samples were encapsulated into the cell under vacuum (< 10 mPa) after purification. Wavelength resolution was 0.1 nm.

3-2-3. *Cavity ring-down laser absorption spectroscopy (CRDS)*

Cavity ring-down spectroscopy (CRDS) is the relatively-new technique of the spectroscopy field developed by O'Keefe and Deacon, in 1988 [16]. Laser light beam was trapped in two high reflectivity concave mirrors, and the light absorption of the sample in the cavity was determined to measure the laser light beam intensity. When the laser light beam introduced in the mirror cavity reflects on the mirror, the laser light beam leaks from the mirror and the laser light beam reciprocates between two mirrors. The leaked laser light beam intensity is expressed by eq. (1),

$$I(t) = I(0)\exp\left(\left(-\frac{1}{\tau_0}\right)t\right) \qquad (1)$$

where $I(t)$ and I_0 stand for the leaked laser light beam intensity on the time of t and $t = 0$, respectively. τ_0 for the lifetime of the laser light beam. It is called “ring-down time”. The τ_0 for expressed eq. (2) for the empty cavity.

$$\tau_0 = \frac{L}{c}(1-R) \qquad (2)$$

Where L stands for distance between two mirrors, c for velocity of light, and R for reflectance of the mirrors. Number of reflection times N for τ_0 is expressed by eq. (3)

$$R^{2N} = \frac{1}{\mathrm{e}} \qquad (3)$$

For example, using the mirror of R = 99.99%, N = 5000 and the effective optical path length corresponds to 10 km with 100 cm of the length cavity. Therefore, CRDS is high sensitive absorption spectroscopy to use the long path length.

When the sample which absorbs light exists in the cavity, the decay of the light intensity is faster. The laser light beam intensity is expressed eq. (4) and (5).

$$I(t) = I(0)\exp\left(\left(-\frac{1}{\tau}\right)t\right) = I(0)\exp\left(\left(-\frac{1}{\tau_0} - \sigma nc\right)t\right) \qquad (4)$$

$$\Delta\frac{1}{\tau} = \frac{1}{\tau} - \frac{1}{\tau_0} = \sigma nc \qquad (5)$$

where σ stands for the light absorption cross-section of the sample in the cavity, n for number density of the sample and τ for ring-down time in the presence of sample. The deference between inverse of τ and inverse of τ_0 is proportional to the number density of

the sample in the cavity. Therefore, Lambert-Beer's law is valid.

The requirement to construct cavity is given by eq. (6),

$$L < 2r \quad (L \neq r) \tag{6}$$

where r stands for the curvature radius. In addition, ring-down signal cannot be measured to occur the interference of light in the case of the laser light beam pulse duration is longer than the cavity length. The requirement is expressed as eq. (7),

$$L < c\Delta t \tag{7}$$

where Δt is the laser light beam pulse duration.

A tunable dye laser (Lambda Physik, SCANMate) pumped by a third harmonics (355 nm) of a pulsed Nd:YAG laser (Continuum, Surelite I) was employed as the light source. Visible light outputs of the dye laser were frequency-doubled by automatic angle tuning of BBO-B crystal (Indeco, Autotracker II). The UV beam was injected into an optical cavity which consists of a stainless steel vacuum chamber and a pair of high reflective concave mirrors attached on the chamber. The reflectance of the mirrors used were 99.95 % at 235 nm (Japan Aviation Electronics) and 99.6 % at 270 nm (Optical Coatings Japan). Both mirrors have a radius of curvature of 6 m. The back pressure in the chamber was ~ 60 mPa. In this chamber, a 30 cm stainless steel tube without optical windows at both ends was set on the laser path. RTIL samples were accommodated in the tube and were vaporized by heating. As there was no optics along the laser path inside the vacuum chamber, vaporized sample was the only carrier of measured absorbance. The tube was movable in the chamber, which enabled

measurements of ring-down times with and without the sample tube. The ring-down decay signal was monitored by a photomultiplier tube (Hamamatsu photonics, R3896) and was averaged 1500 times at each laser wavelength.

3-2-4. *Quantum chemical calculation*

Density functional theoretical (DFT) calculations were performed using Gaussian09 Program [17]. The single-point energies, Onsager radii, dipole moments, and optimized structures were calculated at RB3LYP/6-311++G(3df,3pd) level of theory.

3-3. Results and discussion

3-3-1. *Gas phase absorption spectra of EmpyTf$_2$N and BmimTf$_2$N*

Figure 3-1 shows single pass spectra of vaporized (a) EmpyTf$_2$N and (b) BmimTf$_2$N measured under various temperatures in the closed gas cell. During the heating process to raise temperature, it was found that RTIL vapor formed thin liquid layer on the cell window surface. This adsorbed sample gave background absorbance. Hence, the temperature was first raised to 430 K to make RTIL adequately adsorbed on the surface and then reduced the temperature to decrease RTIL concentration in gas phase. Adsorbed RTIL quantity did not change drastically during this cooling process as compared to the change in gas phase concentration; this enables us to obtain the temperature dependence of gas phase absorbance.

This tentative conclusion was confirmed by the vapor pressure estimation (see below). The spectra measured under 410 K were mostly from the background absorbance of adsorbed RTILs on the window; thus the background spectrum at 410 K was subtracted from the measured spectra at various temperatures. The resultant absorption spectra are shown in Figure 3-1. The spectral shape is almost identical at any temperature. The peak wavelengths of $EmpyTf_2N$ and $BmimTf_2N$ are around 265.5 and 212 nm, respectively, which show slight red-shift at higher temperatures. The absorbance increased as the temperature was raised, which reflects an increase in the gas-phase concentration at high temperature. Based on these liquid-phase studies, these bands are attributed to $\pi\pi^*$ transitions of pyridinium and imidazolium rings [18].

To confirm the assignment of the spectral carrier to gas phase RTILs, vaporization enthalpy [$\Delta_{vap}H(T_{ave})$] was determined by analyzing the absorbance at various temperatures with the Clausius-Clapeyron equation. The T_{ave} stands for the mean value of temperature for measurements. Vapor pressure ratio was estimated from Lambert-Beer's law ($A=\varepsilon cl$) and gas equation of state ($p=cRT$) described as

$$\frac{p}{p^*} = \frac{cRT}{c^* RT^*} = \frac{(A/\varepsilon l)T}{(A^*/\varepsilon l)T^*} = \frac{AT}{A^* T^*} \qquad (8)$$

where p stands for pressure, c for molar concentration, R for gas constant, T for temperature, A for absorbance, ε for molar absorption coefficient, and l for light path length. The standard temperature, T^* is 432 K. Figure 3-2 shows plots of the vapor pressure ratio of $EmpyTf_2N$ and $BmimTf_2N$ with the best fitting lines. The $\Delta_{vap}H$ (T_{ave})

values of 162 ± 35 and 137 ± 11 kJ mol^{-1} were determined for $EmpyTf_2N$ at T_{ave} =419 K and for $BmimTf_2N$ at T_{ave} =418 K respectively. The value of $BmimTf_2N$ agrees well with literature values of ~ 130 kJ mol^{-1} [14,15,19-21]. These $\Delta_{vap}H$ (T_{ave}) values are reasonably higher than those of conventional molecular solvents, which supports our assignment of the measured absorbance to the vaporized RTILs.

Wang *et al.* reported the absorption spectrum of vaporized $BmimTf_2N$ at 550 K, which had an additional absorption band in the region shorter than the 211 nm ππ* band [22]. This additional band did not appear in our spectrum. Earle *et al.* reported that 2 % of $BmimTf_2N$ thermally decomposed after heating for 8 h at 573 K under vacuum [5]. To the contrary, the present study investigated thermal decomposition at 473 K for 2 h in vacuum but no decomposition was recognized by NMR, FT-IR, and Raman spectroscopic measurements. These examinations on thermal stability suggest that the reported heat decomposition that occurred at 550 K was related to the additional absorption peak mentioned above.

To confirm that measured absorption spectra were due to vaporized RTIL, CRDS experiments were carried out for RTIL vapor. Figure 3-3(a) shows the absorption spectra of vaporized $EmpyTf_2N$ observed by CRDS in the stainless steel tube at 443 K equipped in a vacuum chamber. The α mark in the vertical axis means the absorbance per 1cm optical length. This cell had no optical window at both ends. As a reference, a single-path absorption spectrum of thin layer neat liquid is also shown. The spectra clearly show that the absorption band shape of $EmpyTf_2N$ measured by CRDS is

identical to that of neat liquids. Because the stainless steel tube in the vacuum chamber has no optical windows on the laser path, the observed absorption can certainly be assigned to gas-phase EmpyTf$_2$N.

Figure 3-3(b) shows that the absorption spectra of vaporized BmimTf$_2$N measured by CRDS and single pass method using thin layer neat liquid. Although the spectral range of CRDS is limited to the region of 230 ~ 240 nm, the spectral feature in this red-edge region is analogous to each other. The extinction coefficient of RTIL vapors were not determined by the present CRDS, because the cell is opened to vacuum and the molecular density inside the cell cannot be estimated. It is noteworthy that the absorption spectra of vaporized RTILs were solely observed by CRDS without any trapped liquids on the light path, although the entire band shapes and the extinction coefficients of RTILs could not be observed.

3-3-2. *Spectral features of RTILs in the gas and liquid phases*

Figure 3-4 shows normalized absorption spectra of (a) EmpyTf$_2$N and (b) BmimTf$_2$N in neat liquid and under vaporized conditions. The $S_1 \leftarrow S_0$ absorption peak wavelength of neat EmpyTf$_2$N is red-shifted from 264.9 nm at 308 K to 265.2 nm at 423 K. The latter spectrum resembles that measured in the gas phase at 427 K with a peak at 265.4 nm. Similarly, $S_2 \leftarrow S_0$ absorption peak in neat liquid at 423 K is similar to that of vapor at 427 K; the peak shift is only 0.4 nm. These spectral features were also observed for BmimTf$_2$N. The peak of neat liquid at 428 K is close to that of vaporized

BmimTf$_2$N at 429 K. Note that the shapes and peaks of the absorption band of vaporized RTILs are close to those of neat ones, whereas their intermolecular interactions may be different; Coulomb interaction among cations and anions are important in the neat liquid, while single cation-anion interaction in the pair works in gas phase. Slightly larger absorbance was observed in the S_2 band of EmpyTf$_2$N gas, which may be caused by the spectral shift of allowed transition band in the vacuum-UV region overlapping the S_2 band.

To understand intermolecular interaction on the electronic transition energy of RTILs, spectral shift between the gas and neat liquid phases were examined for conventional organic compounds such as pyrimidine and pyridine, which have similar size heteroaromatic ring as compared to imidazolium and pyridinium cations. In the normalized absorption spectra of pyridine, shown in Figure 3-5, the 0-0 band of S_2 ($\pi\pi^*$) $\leftarrow S_0$ transition indicated by arrows is red-shifted on going from vapor (260.0 nm) to neat liquid (264.0 nm). This red-shift of 4.0 nm is much more eminent than those of RTILs. As summarized in Figure 6, the spectral shifts in molecular liquids, ~ 500 cm^{-1}, significantly exceed those in RTILs, ~ 100 cm^{-1}. As $S_1 \leftarrow S_0$ transition of pyridine and pyrimidine are $\pi\pi^*$ type, the solvation through reaction field and/or local interactions such as hydrogen bonding give rise to evident red-shift in transition energy. Meanwhile, relatively small spectral shift was observed for RTILs even though $S_1 \leftarrow S_0$ transition is $\pi\pi^*$ type. This characteristic feature is discussed in the following subsection.

3-3-3. *Solvation in neat RTILs*

The spectral shift of transition energy is explained by the Onsager reaction field theory, where electric dipole moments interact with dielectric solvents. According to this model [23], spectral shift, ΔE_{ORF} is expressed by

$$\Delta E_{\mathrm{ORF}} = \frac{1}{4\pi\varepsilon_0}\left\{\frac{\left(\mu_{\mathrm{g}}{}^2 - \mu_{\mathrm{e}}{}^2\right)}{a^3}\frac{n^2-1}{2n^2+1} + \frac{2\mu_{\mathrm{g}}\left(\mu_{\mathrm{g}}-\mu_{\mathrm{e}}\right)}{a^3}\left(\frac{\varepsilon-1}{\varepsilon+2} - \frac{n^2-1}{n^2+2}\right)\right\} \qquad (9)$$

where a stands for the cavity radius, μ_{g} and μ_{e} for the dipole moments of electronic ground and excited states, respectively, ε for the dielectric constant, and n for the refractive index of the solvent. Parameter a was estimated by quantum chemical calculation at the RB3LYP/6-311++G(3df, 3pd) level. The a value of the ion pair for RTILs was calculated, because we expected that the dominant species in liquid phase RTIL were ion pairs or cluster of ion pairs. For the vapor phase, we also considered ion pairs according to previous mass spectroscopic studies about gas phase RTILs [21]. For discussion of ion pairs of RTILs, abbreviation for ion pairs as $Empy^+Tf_2N^-$ and $Bmim^+Tf_2N^-$ were used. The values of μ_{g} and μ_{e} for the cations were obtained by the DFT calculation using the parameters summarized in Table 1. The calculated spectral shifts for pyrimidine, pyridine, and ion pairs of $Empy^+Tf_2N^-$ and $Bmim^+Tf_2N^-$ are shown in Figure 3-6 and Table 3-2.

The calculated spectral shifts of $Bmim^+$ and $Empy^+$ chromophores are much smaller than those of molecular pyrimidine and pyridine, which agrees well with the present

observations. Therefore, it is concluded that the present model for spectral shift is reasonable. In general the ππ* absorption bands of RTILs show no remarkable spectral shift from gas phase to neat liquid. This is because ion pairs are dominant in the gas phase and solution of ion pairs due to the reaction field of such a large volume becomes negligible in comparison with organic molecules with conventional sizes such as pyridine, and thus results in smaller solvation effects.

3-4. Conclusion

Electronic absorption spectra were measured for ionic liquids, $EmpyTf_2N$ and $BmimTf_2N$ in the gas phase and neat liquid. Absorption spectra of ionic liquids in the gas phase were obtained using a closed cell for a conventional single-path absorption spectrometer and a cell equipped in a vacuum chamber for cavity ring down laser spectroscopy.

Contrary to conventional molecular liquids, no remarkable differences were observed between the absorption spectra of ionic liquids in the gas and neat liquid phases. The absorption spectra of ionic liquid samples show clear bands of $S_1(\pi\pi^*)\leftarrow S_0$ and $S_2(\pi\pi^*)\leftarrow S_0$ transitions for $EmpyTf_2N$ and a band of $S_1(\pi\pi^*)\leftarrow S_0$ transition for $BmimTf_2N$. Vaporization enthalpies are determined by measuring the temperature-dependent absorbance of gas phase spectra, and the value for $BmimTf_2N$ agrees well with literature values. Small spectral shifts of the absorption bands of these ionic liquids from gas to neat liquid phases are discussed on the basis of ion pair

absorption both for gas phase and for neat liquid. A large volume of ion pair reduces the spectral shifts due to the reaction field of liquids, which can account for the reason why gas-phase spectra is similar to that of neat liquid. We expect that a relatively small spectral shift in electronic absorption spectra between the gas and neat liquid phases is common for RTILs.

References of Chapter 3

[1] C. Reichardt, *Green Chemistry* **7**, 339 (2005).

[2] R. Byrne, Kevin J. Fraser, E. Izgorodina, D.R. MacFarlane, M. Forsyth, D. Diamond, *Phys.Chem.Chem.Phys.* **10**, 5919 (2008).

[3] Kristin A. Fretcher and Siddharth Pandey, *Applied Spectroscopy* **56**, 266 (2002).

[4] L.P.N. Rebelo, J.N.C. Lopes, J.M.S.S. Esperança, E. Filipe, *J. Phys. Chem. B* **109**, 6040 (2005).

[5] M.J. Earle, J.M.S.S. Esperança, M.A. Gilea, J.N.C. Lopes, L.P.N. Rebelo, J.W. Magee, K.R. Seddon, J.A. Widegren, *Nature* **439**, 831 (2006).

[6] J.P. Leal, J.M.S.S. Esperança, M.E.M. da Piedade, J.N.C. Lopes, L.P. N. Rebelo, K.R. Seddon, *J. Phys. Chem. A* **111**, 6176 (2007).

[7] D. Strasser, F. Goulay, M. S. Kelkar, E. J. Maginn, S. R. Leone, *J. Phys. Chem. A* **111**, 3191 (2007).

[8] D. Strasser, F. Goulay, L. Belau, O. Kostko, C. Koh, S. D. Chambreau, G. L.Vaghjiani, M. Ahmed, S. R. Leone, *J. Phys. Chem. A* **114**, 879 (2010).

[9] N. Akai, A. Kawai, K. Shibuya, *J. Phys. Chem. A* **114**, 12662 (2010).

[10] N. Akai, D. Parazs, A. Kawai, K. Shibuya, *J. Phys. Chem. B* **113**, 4756 (2009).

[11] J. H. Gross, *J. Am. Soc. Mass Spectrom.* **19**, 1347 (2008).

[12] K. R. J. Lovelock, A. Deyko, Jo-Anne Corfield, P. N. Gooden, P. Licence, R. G. Jones, *Chem. Phys. Chem.* **10**, 337 (2009).

[13] R. W. Berg, A. Riisager, R. Fehrmann, *J. Phys. Chem. A* **112**, 8585 (2008).

[14] Y. U. Paulechka, Dz. H. Zaitsau, G. J. Kabo, A. A. Strechan, *Thermochimica Acta* **439**, 158 (2005).

[15] D. H. Zaitsau, G. J. Kabo, A. A. Strechan, Y. U. Paulechka, *J. Phys. Chem. A* **110**, 7303 (2006).

[16] A. O'Keefe, D.A.G. Deacon, *Rev. Sci. Instrum.* **59**, 2554 (1998).

[17] M.J. Frisch et al., Gaussian 09, Revision **A.1**, Gaussian, Inc., Wallingford CT, 2009.

[18] A. Bolovinos, P. Tsekeris, J. Philis, E. Pantos, G. Andritsopoulos, *J. Mol. Spectrosc.* **103**, 240 (1984).

[19] J. P. Armstrong, C. Hurst, R. G. Jones, P. Licence, K. R. J. Lovelock, C. J. Satterley, I. J. Villar-Garcia, *Phys. Chem. Chem. Phys.* **9**, 982 (2007).

[20] L.M.N.B.F. Santos, J.N.C. Lopes, J.A.P. Coutinho, J.M.S.S. Esperança, L.R. Gomes, I.M. Marrucho, L.P.N. Rebelo, *J. Am. Chem. Soc.* **129**, 284 (2007).

[21] H. Luo, G. A. Baker, S. Dai, *J. Phys. Chem. B* **112**, 10077 (2008).

[22] C. Wang, H. Luo, H. Li, S. Dai, *Phys. Chem. Chem. Phys.* **12**, 7246 (2010).

[23] O. Kajimoto, M. Futakami, T. Kobayashi, K. Yamasaki, *J. Phys. Chem.* **92**, 1347 (1988), and references therein.

[24] K. B. Wilberg, Laboratory Technique in Organic Chemistry, McGraw-Hill, New York, 1970.

[25] H. Bredereck, *Chem. Ber.* **93**, 1402 (1960).

[26] B. A. Middleton, *Nature* **141**, 516 (1938).

[27] N. M. Yunus, M. I. A. Mutalib, Z. Man, M. A. Bustam, T. Murugesan, *J. Chem. Thermodyn.* **42**, 491 (2010).

[28] M. Tariq, P.A.S. Forte, M.F.C. Gomes, J.N.C. Lopes, L.P.N. Rebelo, *J. Chem. Thermodyn.* **41**, 790 (2009).

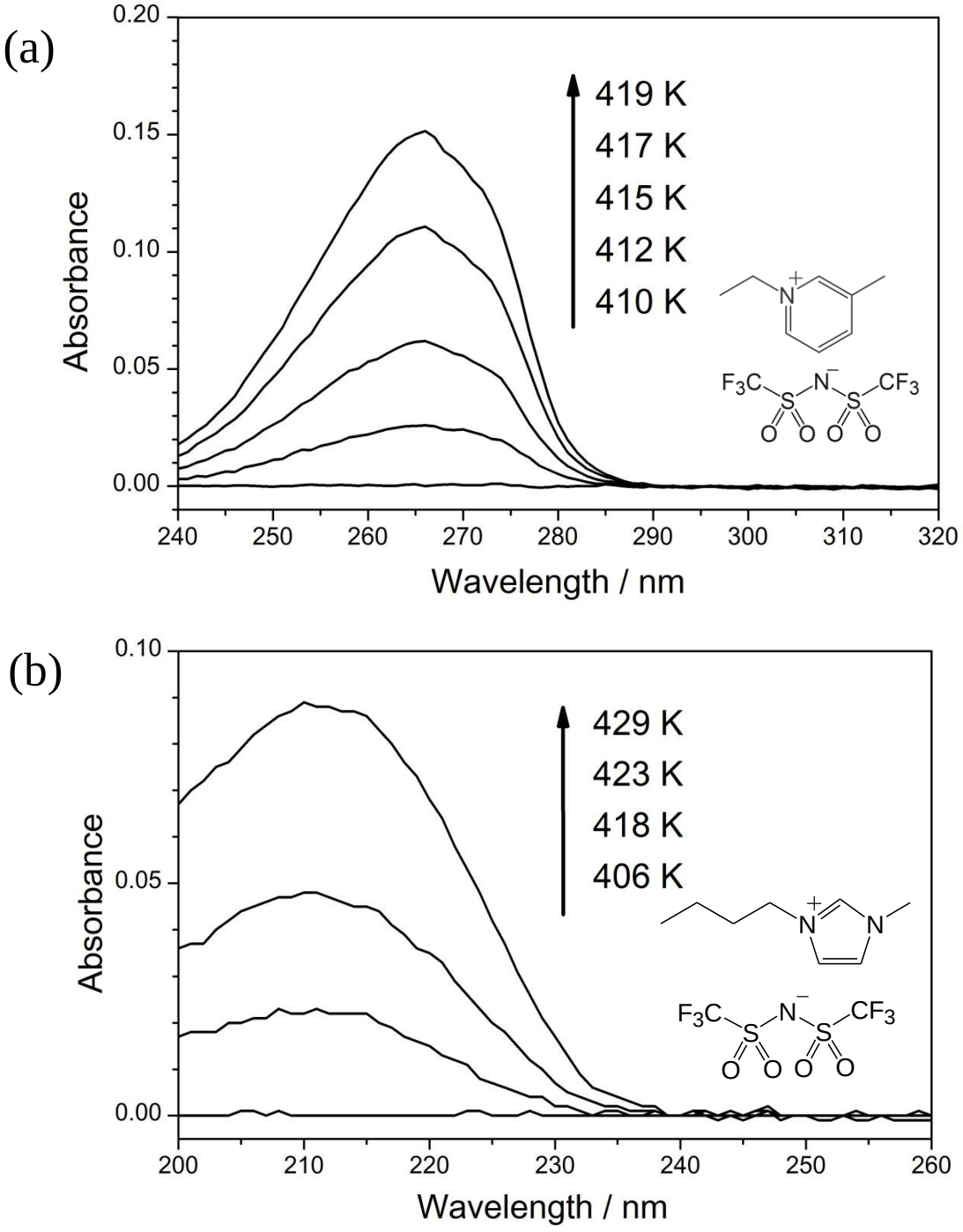

Figure 3-1. Temperature-dependent single-path absorption spectra of vaporized (a) EmpyTf2N and (b) BmimTf2N.

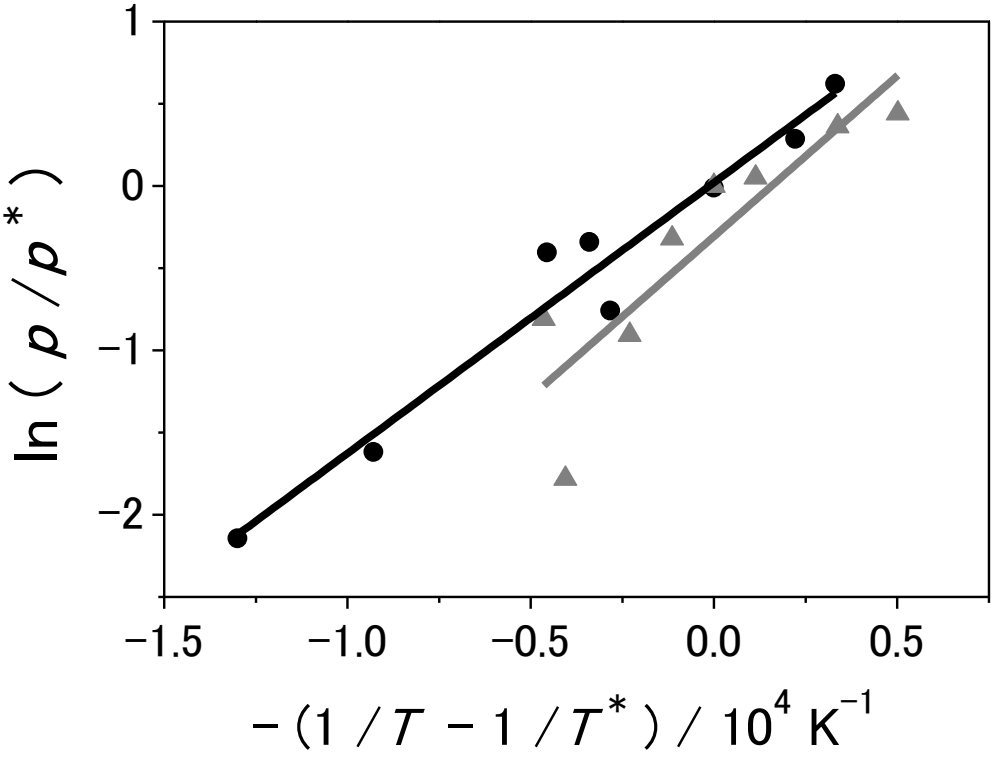

Figure 3-2. Clausius-Clapeyron plots and their fitting lines [ln (p/p^*)=--($\Delta_{vap}H(T_{ave})/R$) (1/T-1/T^*)] of vaporized EmpyTf$_2$N (open circle, gray line) and BmimTf$_2$N (closed circle, black line). T^* and p^* are standard temperature and pressure for each ionic liquid, respectively.

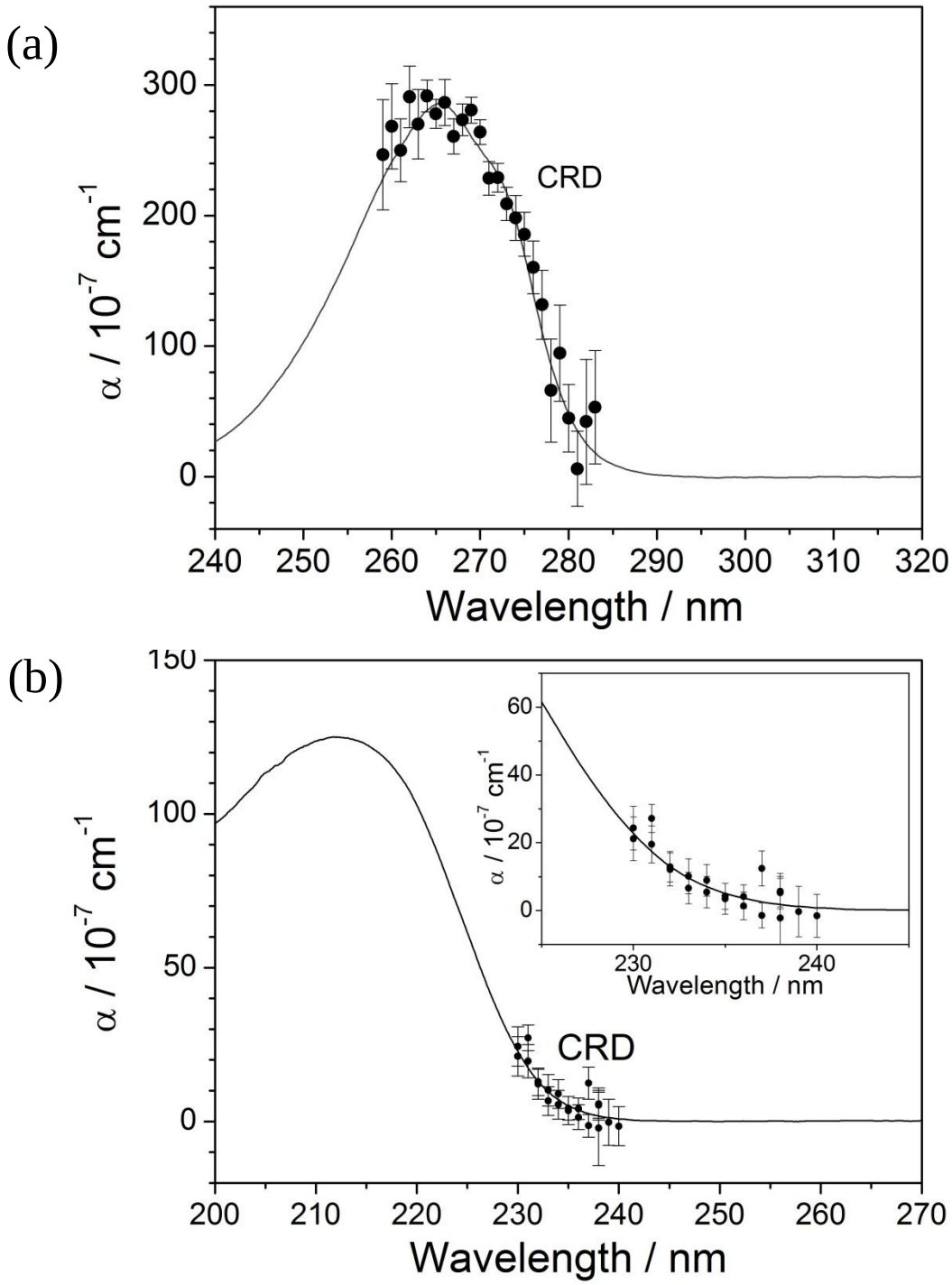

Figure 3-3. Absorption spectra (closed circles) of vaporized (a) $EmpyTf_2N$ at 453 K and (b) $BmimTf_2N$ in red edge of the band at 443 K measured by CRDS. The solid lines are single-path absorption spectra (in arbitrary units) of neat liquids at almost the same temperature as in the gas phase.

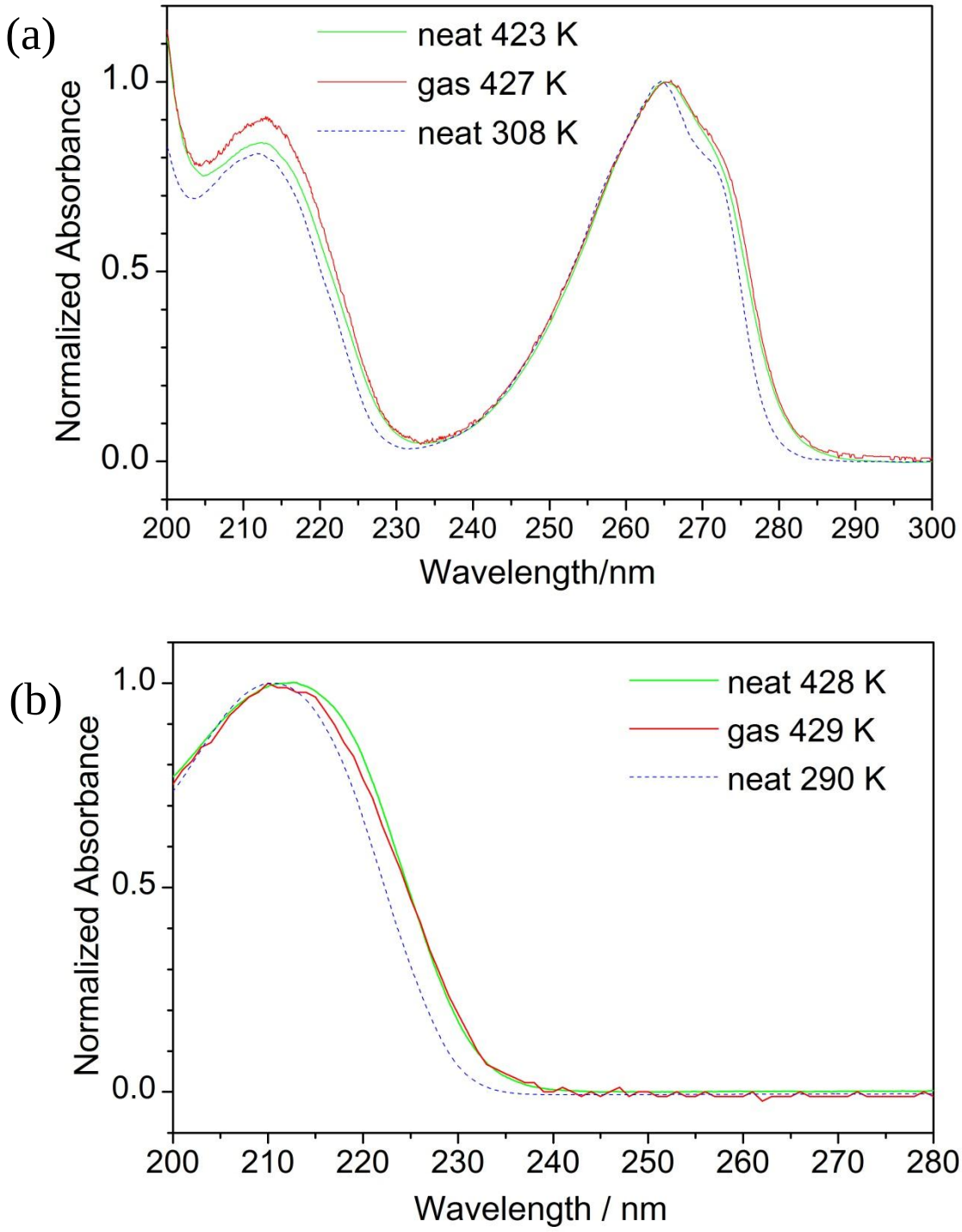

Figure 3-4. Normalized single path absorption spectra of (a) $EmpyTf_2N$ and (b) $BmimTf_2N$ in gas phase and in neat liquid condition.

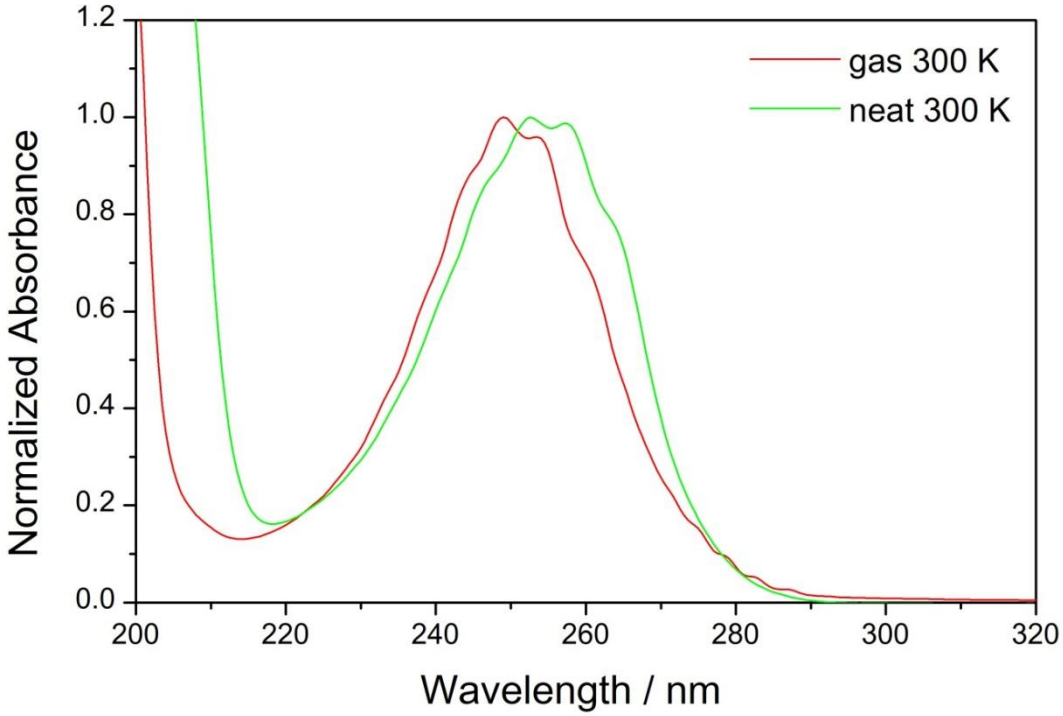

Figure 3-5. Normalized single path absorption spectra of pyridine in neat liquid condition (green) and in the gas phase (red). Arrows indicate 0-0 band of ππ* transition.

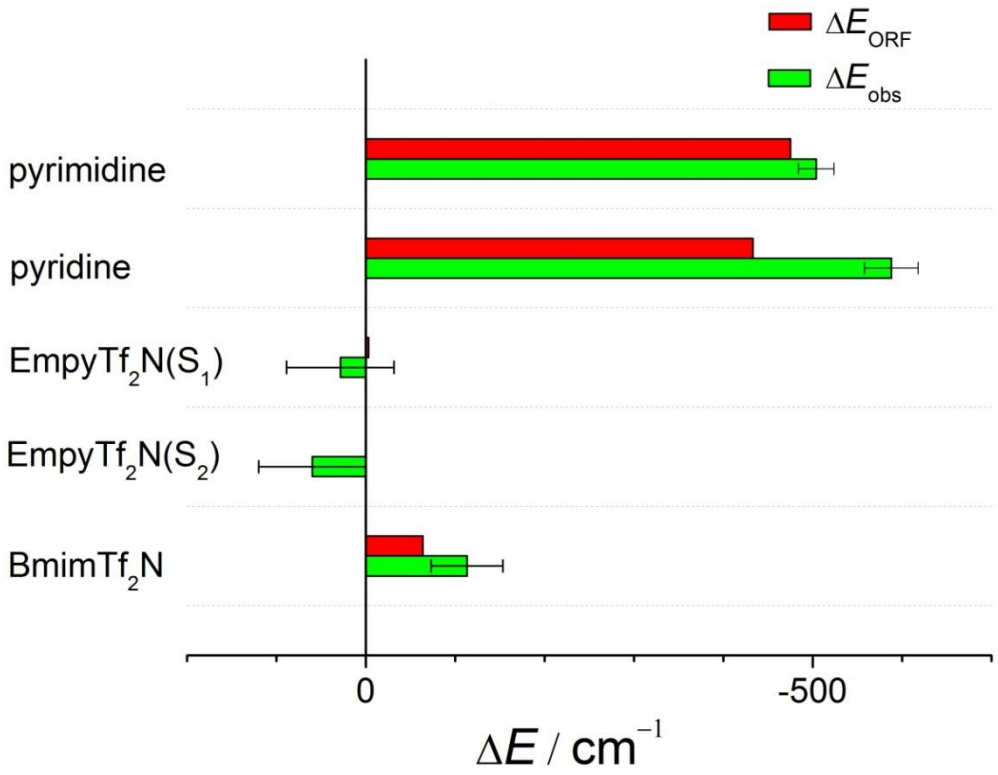

Figure 3-6. Transition energy shifts Δ*E* of chromophore compounds from vapor to neat liquid condition. Both observed (Δ E_{obs}) and calculated (Δ E_{ORF}) values were plotted for each compound. For pyrimidine and pyridine, the chromophores correspond to molecular pyrimidine and pyridine, respectively, while they are pyridinium and imidazolium cations in the ion pairs of each RTIL.

Table 3-1. The list of parameters used in theoretical calculation of spectral shifts.

material	molecular volume	electric dipole [a] / D		optical properties	
	a^3 / 10^{-23} cm^3	μ_g	μ_e	ε	n_D
pyrimidine	9.3	2.36	4.57	13 [b]	1.4951 [f]
pyridine	8.7	2.27	4.26	12.4 [c]	1.5092 [g]
$Empy^+Tf_2N^-$	34.4	0.79	0.97(S_1) 0.82(S_2)	15.3 [d]	1.44537 [h]
$Bmim^+Tf_2N^-$	32.4	1.62	3.11	14 [e]	1.4408 [i]

[a] For ionic liquids, electric dipole of cation is calculated.

[b] Estimated value from Onsager equation for dielectric constant using n_D and μ_g of pyrimidine.

[c] Ref .[39].

[d] Ref .[4]. Value of N-butylpyridinium bistrifluoromethylsulfonylamide is cited.

[e] Ref .[4].

[f] Ref .[40].

[g] Ref .[41].

[h] Ref .[42]. Value of N-butylpyridinium bistrifluoromethylsulfonylamide is cited.

[i] Ref .[43].

Table 3-2. Observed and calculated spectral shifts.

Electronic transition	energy shift / cm^{-1}	
	ΔE_{ORF}	ΔE_{obs}
Molecular liquid		
$S_2 \leftarrow S_0$ pyrimidine	-475	-501 ±20
$S_2 \leftarrow S_0$ pyridine	-433	-583 ±30
Ion pairs		
$S_1 \leftarrow S_0$ $Empy^+Tf_2N^-$	-3	28 ±60
$S_2 \leftarrow S_0$ $Empy^+Tf_2N^-$	-1	60 ±60
$S_1 \leftarrow S_0$ $Bmim^+Tf_2N^-$	-64	-110 ±40

Chapter 4. Transition energies of imidazolium-based cations affected by charge transfer interaction between cation and various counter anions

4-1. Introduction

According to absorption spectroscopy of liquid and gas phases of ionic liquids in Chapter 3, ion pairs were found to be major components in neat RTILs [1]. The observed spectral shifts for ion pairs were very small as described in Chapter 3, which reflects solvation for ion pairs by surroundings is nearly negligible. Therefore it is possible that charge transfer (CT) interaction between nearest anion and cation determine the electronic states of cation. There are various anions which are components of RTILs, for example, Tf_2N^-, PF_6^-, BF_4^-, TfO^-, and halide anions. These anions have various sizes with different electronic structure but the same negative charge, therefore the mean density of the excess electron within one anion is different. Because of this feature, CT interaction against other ions significantly depends on anion. Since ion pair is major spectral carrier in RTILs, CT interaction between cation and anion would change the electronic transition energies of cations.

Gas phase spectroscopy has been providing better understanding of these features of molecular interactions. However, it is difficult to apply this technique for study of RTILs because no sufficient vapor pressure for gas phase measurements can be obtained,

except small numbers of RTILs with Tf_2N^-. Therefore, in the present study, anion dependence of CT interaction was evaluated by comparing UV absorption spectra of cations in ion pairs which is isolated in molecular solvents and in neat liquids. For this purpose, $Bmim^+$-based RTILs having various anion components were used, because (1) $Bmim^+$ has strong absorption in UV wavelength region, which is appropriate for spectroscopy, and (2) these RTILs are well known typical RTILs which are commercially available with good quality. According to spectroscopic results for electronic transition energies of cations, intermolecular Coulomb interaction was discussed on the basis of both macroscopic and microscopic solvent properties such as anions' donor number (DN), dielectric constant, and empirical parameter (E_N^T) in neat liquid phase.

4-2. Experimental

Used samples and purification method were as details described in Chapter 2. Absorption spectra of solution samples and neat liquids were measured as details described in Chapter 2.

4-3. Results and discussion

4-3-1. *Spectral shifts of $S_1(\pi\pi^*)\leftarrow S_0$ absorption bands due to counter anions*

Figure 4-1 shows the normalized absorption spectra of $BmimTf_2N$ diluted in water and acetonitrile, and for neat liquids of $BmimTf_2N$, $BmimPF_6$, $BmimBF_4$, and

BmimTfO. In water and acetonitrile solution, some $Bmim^+$-based ILs are almost completely dissociated to cation and anion [2], which indicates that spectral carrier is $Bmim^+$ in these measurements. It is clear that the absorption peak wavelength of $S_1(\pi\pi^*)\leftarrow S_0$ absorption band depends significantly on the solution and liquids, and their absorption band shapes are very similar. This result suggests that the S_0 and S_1 electronic states of the cation do not change in these solvents and neat liquids. There are small spectral shifts of peak wavelength; the electronic transition energy was the highest in neat $BmimPF_6$, and decreases in the order of $BmimBF_4$, $BmimTf_2N$, BmimTfO, acetonitrile solution, and water solution. Spectral shifts are normally derived from solvation by surroundings, which is explained by Onsager reaction field theory [3]. According to Onsager reaction field theory, spectral shift are determined by dielectric constant, refractive index of solvent, electric dipole moments of the ground and excited states, and Onsager volume of solutes. These values are the same in all the samples examined here. However in the present case, spectral shifts are not explained by this theory as details described below.

4-3-2. *Relationship between spectral shifts and solvatochromic shifts*

$S_1(\pi\pi^*)\leftarrow S_0$ transition energy of $Bmim^+$-based RTILs, dielectric constant [4], E_N^T [5] as macro polarity parameter, donor number (DN) of RTILs [6] are listed in Table 4-1. It is noteworthy that DN increases in the order of PF_6^- (6.2), BF_4^- (7.3), Tf_2N^- (11.2) and TfO^- (20.4) in $Emim^+$ based RTILs. This order is in good correlation with the order

of decrease in the transition energy of $Bmim^+$ measured in the present study. No other macro polarity parameters show any correlation with the transition energy, which indicates that spectral shifts cannot be explained by Onsager reaction field theory as described above.

Tokuda *et al*. reported clear correlation between the molar conductivity ratio ($\Lambda_{imp}/\Lambda_{NMR}$) and λ_{Cu} for $[Cu(acac)(tmen)]^+$ (acac = acetylacetone, tmen = *N*,*N*,*N'*,*N*'-tetramethylethylenediamine). Since λ_{Cu} is a good measure of DN for anions, their results indicates that $\Lambda_{imp}/\Lambda_{NMR}$ is clearly correlated with anions' DN [7-10]. In RTILs with large anions' DN such as $CF_3CO_2^-$, about 50% of ions are composing ion pairs. This result is inconsistent with the present result in chap. 2 which indicates that whole ions in neat liquid phase are composing ion pairs [1]. This inconsistence might be explained as follows. In ion conductivity measurement, dissociated ions diffuse freely in slower time region. Actual amount of dissociated ions should be negligibly small according to absorption spectroscopy. They diffuse through interspace among ion clusters; one ion diffuses from one cluster to another then the latter cluster pushes one ion to another ion cluster and the similar process continues to show ion conductivity. This process may be similar to the proton diffusion in water with Grotthuss mechanism.

4-3-3. *Transition energy difference determined by CT interaction*

Figure 3-5 shows the transition energies of $Bmim^+$ measured by absorption spectroscopy and theoretically estimated from solvent polarity. The dotted line is

estimated transition energy of $Bmim^+$ in the gas phase, and this value which is above 47650 cm^{-1} is larger than that of $BmimPF_6$ in neat liquid phase. In water and acetonitrile solutions, decrease of transition energy is simply due to solvation by surroundings. Meanwhile, in neat RTILs, there is another effect due to CT interaction with counter anion to reduce transition energy. After that, solvation for ion pair occurs and reduces transition energy. However, ion pair has large Onsager volume and are not affected largely by surroundings, therefore stabilization by solvation for ion pairs is small. It is concluded that transition energies in neat RTILs are larger than those estimated from solvent polarity and Onsager reaction field theory.

4-4. Conclusion

The electronic absorption spectra of RTILs were measured for RTILs such as $BmimTf_2N$, $BmimPF_6$, $BmimBF_4$, and BmimTfO as neat liquid phases. $S_1(\pi\pi^*)\leftarrow S_0$ transition energies of $Bmim^+$ are large in the order of $TfO^- < Tf_2N^- < BF_4^- < PF_6^-$ as corresponding to the inversed order of RTILs' DN. Meanwhile, there is no correlation between transition energies and solvent polarities such as dielectric constant and empirical parameter (E_N^T), and this result also suggests that transition energy changes due to CT interaction between cation and counter anion.

References of Chapter 4

[1] T. Ogura, N. Akai, A. Kawai, K. Shibuya, *Chem. Phys. Lett.* **535**, 110 (2013).

[2] H. Shekaari, S.S. Mousavi, *Fluid Phase Equilibria* **286**, 120 (2009).

[3] O. Kajimoto, M. Futakami, T. Kobayashi, K. Yamasaki, *J. Phys. Chem.* **92**, 1347 (1988), and references therein.

[4] M.-M. Huang, Y. Jiang, P. Sasisanker, G.W. Driver, H. Weingärtner, *J. Chem. Eng. Data* **56**, 1494 (2011).

[5] C. Reichardt, *Green Chemistry* **7**, 339 (2005).

[6] M. Schmeisser, P. Illner, R. Puchta, A. Zahl, R. van Eldik, *Chem. Eur. J.* **18**, 10969 (2012).

[7] H. Tokuda, K. Hayamizu, K. Ishii, M.A.B.H. Susan, M. Watanabe, *J. Phys. Chem. B* **108**, 16593 (2004).

[8] H. Tokuda, K. Hayamizu, K. Ishii, M.A.B.H. Susan, M. Watanabe, *J. Phys. Chem. B* **109**, 6103 (2005).

[9] H. Tokuda, K. Ishii, M.A.B.H. Susan, S. Tsuzuki, K. Hayamizu, M. Watanabe, *J. Phys. Chem. B* **110**, 2833 (2006).

[10] H. Tokuda, S. Tsuzuki, M.A.B.H. Susan, K. Hayamizu, M. Watanabe, *J. Phys. Chem. B* **110**, 19593 (2006).

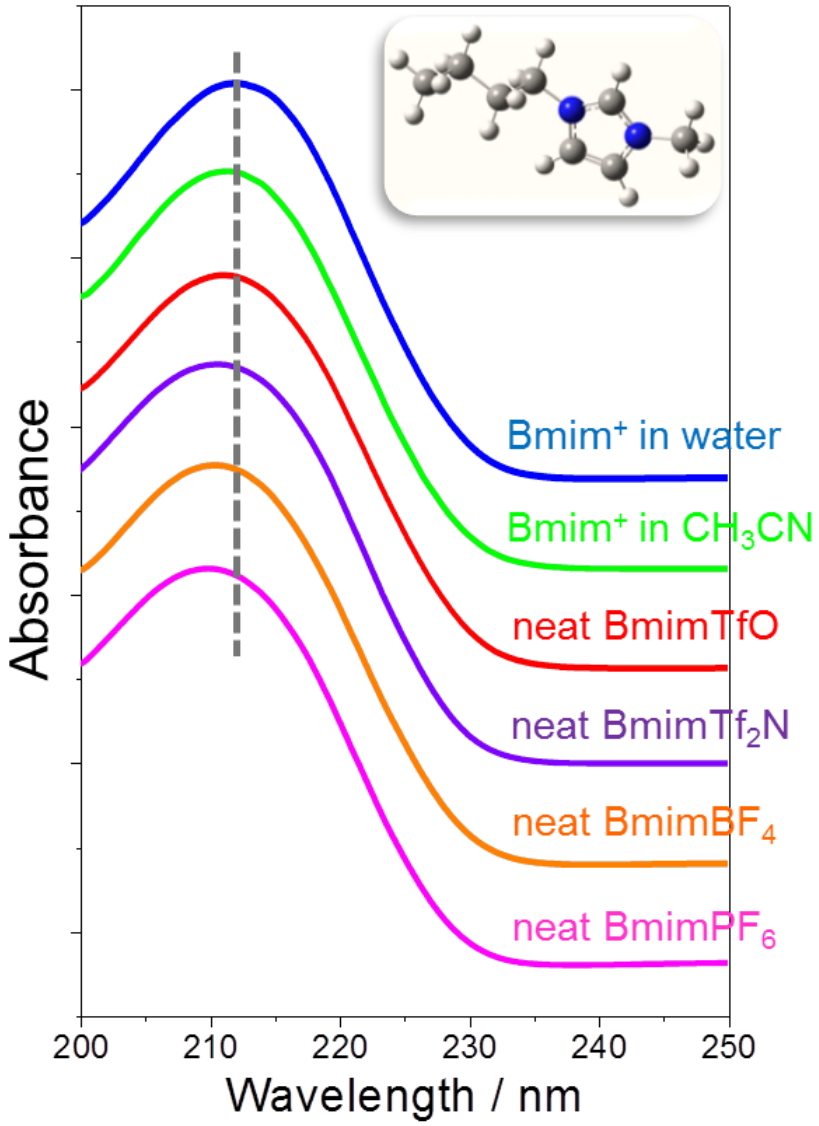

Figure 4-1. Normalized absorption spectra of $Bmim^+$ in two polar solvents and four neat RTILs. Inset is a structure of $Bmim^+$ caluculated by DFT method: blue atom is for nitrogen, dark grey for carbon and light grey for hydrogen.

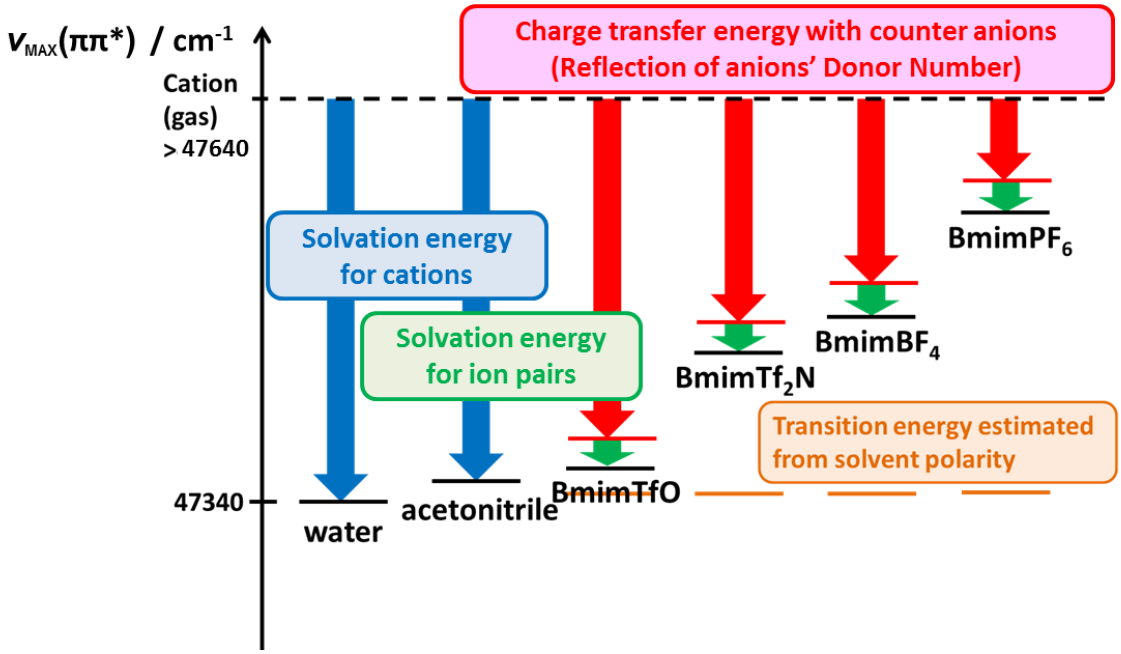

Figure 4-2. The ππ* transition energy of $Bmim^+$ in various ionic liquids and in molecular solvents. The black bar is for observed transition energy, red bar for predicted transition energy of ion pair in vacuum, and orange bar for estimated transition energy from Onsager Reaction Field Theory and dielectric constant. Transition energy in gas phase is assumed to be above 47640 cm^{-1}. Solvation energies in molecular solvents for isolated $Bmim^+$ ion and those in RTILs for ion pair are not quantitative values because of unknown gas phase $Bmim^+$ υ_{max} value. Transition energy for RTILs were also reduced by CT interaction between anion and cation of ion pairs. These estimated values were displayed by colored bars.

Table 4-1. Observed values of $S_1(\pi\pi^*) \leftarrow S_0$ transition energy of $Bmim^+$-based RTILs, literature values of dielectric constant, E_N^T, donor number (DN) of RTILs, and DN of anions .

	Bmim$^+$-based				Emim$^+$-based
	Transition energy / cm^{-1}	dielectric constant [a]	E_N^T [b]	DN [c]	DN [c]
PF_6^-	47640	14.0±0.7	0.676	-	6.2
BF_4^-	47530	13.9±0.4	0.673	-	7.3
Tf_2N^-	47490	14.0±0.5	0.642	10.2	11.2
TfO^-	47370	12.9±0.5	0.667	20.5	20.4

a) Ref. [4].

b) Ref. [5].

c) Ref. [6].

Chapter 5. Charge transfer interaction between pyridinium-based cation and anion in diluted solution

5-1. Introduction

In this chapter, charge transfer (CT) absorption of RTILs is focused to understand the electronic states constructed in RTILs. In general**,** the electronic absorption spectra of molecular liquids are understood on the basis of the electronic structure of corresponding solvent molecule itself. However, RTILs may show additional CT bands of ion pairs, ion pair clusters, and ions to surroundings known as the CTTS (charge transfer to solvent) band [1,2]; these bands are not expected in conventional neat molecular liquids. Because of this complicated nature of RTILs, there remain debates about the electronic absorption of RTILs [3-6]. Moreover, dynamic heterogeneous structure of ion clusters suggested by MD simulation [7] gives additional complicated nature of RTILs.

In chapter 3, solvation effect for N-ethyl-3-methylpyridinium Tf_2N ($EmpyTf_2N$) and $BmimTf_2N$ was found to be almost negligible by comparing absorption spectra of the gas and neat liquid phases [8]. This experimental results show that a counter anion play dominant role for electronic states of a cation within an ion pair. Moreover, no additional absorption such as CT and CTTS absorption of ions have been found in these neat liquid. This might be due to large anion size of Tf_2N^-, because large anion size

makes Coulomb force between ions small. It was a contrast to study by Katoh *et al*. who successfully measured CT absorption bands in neat BmimI [1]. However, their results were simple broad spectrum and no detailed information has not been extracted yet.

In the present study, the absorption spectra were measured for isolated ions and ion pairs of halide anions by using UV/Vis spectroscopic method. Since RTILs having halide ions are not able to be vaporized, RTILs diluted in solution was examined here. Pyridinium-based RTILs which have halide ion are advantageous for measuring CT transition between cation and anion because CT band appears lower energy region as compared to imidazolium-based or other RTILs. Absorption spectra of ion pairs were analyzed based on Mulliken theory for CT complex and oscillator strengths of CT absorption bands were obtained by using absorption spectroscopic method and electric conductivity measurement. Relative configurations of ion pair were determined from NMR spectroscopy.

5-2. Experimental

5-2-1. *Samples*

Chart 5-1 shows structure of $EpyTf_2N$ (1-ethylpyridinium Bis(trifluoromethylsulfonyl)amide). Used samples were as details described in Chapter 2. Deuterated water, acetonitrile, and dichloromethane (Acros Organics) were used as solvent for NMR spectroscopy.

5-2-2. *Steady state absorption spectroscopy*

Steady state absorption spectra of solution samples and neat liquids were measured as details described in Chapter 2.

5-2-3. *Conductivity Measurement*

Conductivities were measured by using a conductivity meter (TOA, CM-20S) with a custom made cell whose inner volume was 50 cm^3 . The cell was placed in a water bath and the temperature was adjusted at 25.0 ± 0.2 ^oC. The cell constant was determined as 0.976 cm^{-1} at 25.0 ^oC. In the series of conductivity measurements for various ion concentrations, a sample of the highest concentration with 20 cm^3 volume was first examined and then, the solution was diluted in the cell by stepwise addition of a certain amount of solvent for next step. Conductivity for ion concentration range from 10^{-1} to 10^{-5} M was determined for each pyridinium salt.

5-2-4. *Nuclear magnetic resonance (NMR) spectroscopy*

400-MHz NMR spectrometer (JEOL, JMTC-400) was used to obtain ^{1}H-NMR spectra. Chemical shifts (ppm) were measured with reference to solvent peak. Solutions were prepared at the concentration of ca. 10^{-1} mol dm^{-3}.

5-2-5. *Quantum chemical calculation*

Density functional theoretical calculations were performed using Gaussian09 program [9]. The geometry of EpyCl were optimized with RB3LYP/6-311++G(3df,3pd) level of theory. The effect of dichloromethane polarity was simulated within the framework of a polarized continuum model calculation using the integral equation formalism model (IEFPCM).

5-3. Results and discussion

5-3-1. *Absorption spectra of 1-ethylpyridinium-based ILs dissolved in solvents*

Figure 5-1 shows absorption spectra of pyridinium-based ILs dissolved in water and in acetonitrile (dielectric constant, D=78.4 and 37.5, respectively) measured for 220 ~ 360 nm wavelength region. The spectra are dominated by the $S_1(\pi\pi^*)\leftarrow S_0$ electronic transition of the pyridinium cation with a peak wavelength, λ_{max}, of 258.2 nm. The molar absorption coefficient of the $S_1(\pi\pi^*)$ band is around 4000 $M^{-1}cm^{-1}$ as listed in Table 1. In the solutions of EpyI / water, EpyBr / acetonitrile and EpyI / acetonitrile, an additional band appears in higher energy region. These bands are attributed to an electronic transition due to a charge transfer to solvent (CTTS) from the halide anion [10]. A peak wavelength of the CTTS band of the iodide anion shows spectral red-shift as solvent polarity decreases from water to acetonitrile, which agrees well with the previous report [10].

Figure 5-2 shows absorption spectra of pyridinium-based ILs dissolved in dichloromethane (D=9.1). Absorption bands of $EpyTf_2N$ and $EpyPF_6$ are well characterized by the $S_1(\pi\pi^*)\leftarrow S_0$ electronic transition and spectral parameters are summarized in Table 1. λ_{max} and $\varepsilon(\lambda_{max})$ of $EpyTf_2N$ and $EpyPF_6$ in dichloromethane are almost the same with those in water and acetonitrile. Contrary to $EpyTf_2N$ and $EpyPF_6$, absorption spectra for EpyX (X=Cl, Br, I) are quite different from those for $EpyTf_2N$ and $EpyPF_6$: broad absorption bands appear in lower energy region of the $S_1(\pi\pi^*)$ and the CTTS bands. Since halide anions are strong electron donor, these bands are temporary assigned to a charge transfer (CT) electronic transition within Epy^+ and X^- ion pairs formed in the solutions. In the following section, solvent polarity and anion dependence of the CT band spectra were discussed to confirm the band assignment.

5-3-2. *Assignment of CT bands for EpyX in solutions*

As shown in Figure 5-2, there are two additional bands below $\pi\pi^*$ transition band of EpyI in dichloromethane solution. As for the two bands at 4.30 and 3.35 eV of EpyI, it is noteworthy the energy difference of the bands, 0.95 eV, equals to the literature value of iodine spin-orbit coupling (ΔE_{SO} = 0.942 eV) between $^2P_{1/2}$ and $^2P_{3/2}$ states in the gas phase. This means that a spectral career of these bands includes iodine atom in the excited states. Since CT transition of Epy^+ and I^- ion pair accompanies electron transfer from I^- to Epy^+ giving Epy and I radical pair complex, the two bands of EpyI are reasonably assigned to CT transition bands with different spin-orbit state of iodine.

Another evidence for assignment of CT transition may be found by considering the energy difference of the bands between EpyI and EpyBr complexes, $\Delta h\nu_{CT}^{obs}$. For this discussion, Mulliken theory [11] is introduced for CT transition energy ($h\nu_{CT}$) of ion pairs, $Epy^{+\cdots}X^{-}$ (X=Cl, Br, I), which is approximately given by the equation,

$$h\nu_{CT} = I(X^-) - E_A(Epy^+) + (G_G - G_E) + (X_G + X_E) + \{E_S(Epy^+ \cdots X^-) - E_S(Epy \cdots X)\} \quad (1)$$

where $I(X^-)$ stands for ionization potentials of halide anions, $E_A(Epy^+)$ for electron affinity of Epy^+, G_G and G_E for stabilization energies of the ground and the excited states by intermolecular Coulomb interaction, X_G and X_E for resonant energies of the ground and the excited zero-order states by CT interaction, and E_S for solvation energies of the ion pair in the ground state ($Epy^+ \cdots X^-$) and of the neutral complex in the excited state ($Epy \cdots X$).

Then, energy difference of the bands, $\Delta h\nu_{CT}$, was estimated by the theory. In the calculation, CT interaction is assumed to be weak and that Coulomb interaction is almost same between the EpyI and EpyBr complexes. Under this approximation, eq. (1) is dominated by $I(X^-) - E_A(Epy^+)$ term. Since $I(X^-)$ is essentially equivalent to $E_A(X)$, $\Delta h\nu_{CT}$ is expressed by,

$$\Delta h\nu_{CT} = h\nu_{CT}(Br) - h\nu_{CT}(I) = E_A(Br) + E_S(Br^-) - \{E_A(I) + E_S(I^-)\}. \quad (2)$$

As for solvation energies, Born equation is introduced as follows,

$$E_S(X^-) = \frac{e^2}{2r}\left(1 - \frac{1}{D}\right) \quad (3)$$

where e stands for elementary electric charge, and r for ionic radius. According to eq.2

and 3, $\Delta h\nu_{CT}$ value of 0.78 eV was calculated. In the calculation, the values listed in Table 5-2 for each molecule was used.

The absorption maximum wavelengths of CT bands for EpyBr and EpyI were obtained from Figure 5-2; 369.6 nm (3.55 eV) and 288.0 nm (4.30 eV) for EpyI and 304.0 nm (4.08 eV) for EpyBr. For EpyI, the value, 3.35 eV of the lower energy band was adopted. Then $\Delta h\nu_{CT}{}^{obs}$ was calculated by the following equation,

$$\Delta h\nu_{CT}{}^{obs} = h\nu_{CT}{}^{obs}(\mathrm{Br}) - h\nu_{CT}{}^{obs}(\mathrm{I}) \sim 0.73 \text{ eV}. \qquad (4)$$

This experimental value is good consistent with the theoretically calculated value of 0.78 eV, which supports our assignment of the CT transitions in ion pair of EpyX. As for EpyCl complex, its CT transition energy was estimated as 4.70 eV (λ=264 nm) by a similar analogy mentioned above. Actually, this predicted CT band overlaps with $S_1(\pi\pi^*)$ band as seen in Figure 5-2.

5-3-3. *Oscillator strength for CT transitions of EpyX in dichloromethane*

Since it was found that the CT transitions occur in EpyX complexes, we determined their oscillator strength was determined to obtain important knowledge about the complexes. First, concentration of ion pairs in dichloromethane solutions was measured by electric conductivity measurements and then determined absorption coefficients of the CT transitions. By considering spectral band shape of the CT transitions, oscillator strength values were obtained. This procedure is given in the following.

Figure 5-3 shows absorption spectra of (a) EpyCl, (b) EpyBr, and (c) EpyI at various

concentrations in dichloromethane. As molar concentration increases absorbance of CT band and ππ* transition becomes larger and smaller, respectively. There are isosbestic points at 269.5 nm for EpyCl and at 271.0 nm for EpyBr. These results suggest that there is equilibrium between the ion pair and isolated ions. Unfortunately, no isosbestic point in EpyI absorption spectrum is recognized due to overlap of the CT, the CTTS, and the ππ* absorption bands.

Next, concentration of ion pairs and isolated ions were measured in these solutions with various EpyX concentrations. For this purpose, molar conductivity measurements was carried out and determine the ion association constant, K_A. For this measurement, Shedlovsky method for 1:1 electrolytes was refer [12] to determine K_A. The equations used were expressed by,

$$\frac{1}{\Lambda\, S(z)} = \frac{1}{\Lambda_0} + \frac{K_A}{{\Lambda_0}^2}\, c\, \Lambda\, S(z)\, {f_\pm}^2 \qquad (5)$$

$$S(z) = \left\{\frac{z}{2} + \sqrt{1 + \frac{z^2}{4}}\right\}^2 \qquad (6)$$

$$z = \frac{(\alpha\, \Lambda_0 + \beta)\sqrt{c\, \Lambda}}{{\Lambda_0}^{3/2}}. \qquad (7)$$

where Λ_0 stands for limiting molar conductivity, Λ for molar conductivities, and c for molar concentration of separated salt. ${f_\pm}^2$, α and β values were calculated from the experimental condition as explained in supporting information.

The experiment provides sets of Λ and c values. In the beginning of the analysis, Λ_0 value was estimated by the theoretical formula so-called limiting Onsager equation [12].

With this roughly estimated Λ_0 value, K_A and Λ_0 values were determined by an analysis of experimental values of Λ and c using eq. (5) combined with eqs.(6) and (7). Then, iterative analysis using the last Λ_0 value of each step was carried out until a unique set of K_A and Λ_0 values was obtained. Figure 5-4 shows examples of the fitting lines with experimental plots. Form this analysis, K_A values were determined as listed in Table 5-3.

For determination of molar absorption coefficients, it is necessary to know concentration of ion pairs which can be calculated from K_A. For this calculation, following equation [12],

$$K_A = \frac{1-\gamma}{c\gamma^2 f_{\pm}^{\ 2}}. \qquad (8)$$

was introduced. In this equation, γ stands for dissociation degree of ions. By using this relation, γ values for wide range of IL concentration were estimated and the results are plotted as shown in Figure 5-5.

Eventually, molar absorption coefficients of CT transition bands of EpyBr / CH_2Cl_2 and EpyI / CH_2Cl_2 were determined from absorption spectra in Figure 5-3 and dissociation degree shown in Figure 5-5. Ranges of IL concentration for spectral measurements were indicated by arrows in Figure 5-5, and mean values of molar absorption coefficients for the present data set are listed in Table 5-4.

According to these experimentally determined molar absorption coefficients, oscillator strength were calculated for CT transitions of EpyI and EpyBr complexes. For

the calculation, Gaussian line shapes was adopted for each CT transition. The full-width of half maximum of CT bands of EpyBr, EpyI($^2P_{3/2}$), and EpyI($^2P_{1/2}$) are 5760, 4680, and 4740 cm^{-1}, respectively. The calculated results are also listed in Table 4.

5-3-4. ***Nature of the CT complex of EpyX ILs in dichloromethane***

Nevertheless the observed absorption bands are assigned to intermolecular CT transitions of EpyX ion pairs, oscillator strengths of about 0.02 is quite small as compared to other CT complexes of organic molecules [13]. This experimental finding is argued based on CT transition theory by Mulliken as follows. Wave functions of electronic states for a complex at intermolecular distance *R* are simply expressed as,

$$\Psi_G = a\Psi_I + b\Psi_N \qquad (9)$$

$$\Psi_E = -b\Psi_I + a\Psi_N \qquad (10)$$

where Ψ_G and Ψ_E stand for electronic states of the ground and excited states. Ψ_I and Ψ_N are zero-order states of ion complex in the ground state and neutral complex in the excited state under assumption that CT interaction is dominant for cross terms of matrix elements for Hamiltonian. The values of a and b are coefficients of wave functions. A transition dipole moment, $\boldsymbol{\mu}_{CT}$, for CT band is expressed as follows,

$$\boldsymbol{\mu}_{CT} = ab(\boldsymbol{\mu}_N - \boldsymbol{\mu}_I) \sim eRb \qquad (11)$$

where *e* stands for elementary charge, $\boldsymbol{\mu}_I$ and $\boldsymbol{\mu}_N$ for permanent electric dipole of the ground and excited states, and *R* for the distance between cation and anion as an ion pair in the ground state.

According to eq.11, coefficient, b of eqs. 9 and 10 for the complex was roughly calculated with μ_{CT} of 1.28 and typical intermolecular distance of 0.3nm. This calculation gives b value of 0.1, which is nearly the smallest among a large number of CT complexes previously studied [13]. This small value of b suggests that the ion pair is categorized to the weakly interacting CT complex.

Since the complex in the ground state is ion pair, (Epy^+ X^-), charge is almost completely separated. As for the excited state, it is concluded from the spin orbit splitting value that the complex consists of electrically neutral molecules, which gives the picture of ($Epy^{\cdot}$ $X^{\cdot}$) complex. This feature suggests that the ground and the excited states are well represented by the zero-order wavefunctions, which leads to quite small value of coefficient, b. This conclusion agrees well with a small value of oscillator strength, namely, small transition dipole moment, μ_{CT}, for EpyX complexes.

5-3-5. *Determination of ion pair conformation*

Absorption spectroscopy reveals that there exits weakly coupled CT complexes of EpyX in dichloromethane. In this section, the ion pair conformation was mentioned based on NMR spectroscopic measurements and quantum chemical calculations. Figure 5-6 and Table 5-5 show ^{1}H-NMR experimental results for EpyCl which is a representative of ion pair complex spectra for EpyX series of complexes. $EpyTf_2N$ whose CT interaction is negligibly weak was also measured and the spectrum is used as a representative of isolated Epy^+ spectra. In d_2-water solution, chemical shifts of these

two ILs are almost the same values. This result means that there is no influence of anion for protons of counter cation. This is good consistent with molar conductivity experimental results that salts are completely separated in d_2-water solution. In d_3-acetonitrile solution, position (2) and (1') chemical shifts of EpyCl are larger than those of EpyTf$_2$N. There are small amount of ion pairs in solution and slight influence of halide ion for counter cation is seen for those ion pairs. In d_2-dichloromethane solution, position (2) and (1') chemical shifts of EpyCl are much larger values than EpyTf$_2$N. This clearly means that electron screening effects of (2) and (1') protons become smaller due to counter halide ion which has large electronegativity. Halide ions are implied to exist near position (2) and (1') in solution.

Besides NMR spectroscopy, optimized structure of EpyCl in dichloromethane was calculated to find the conformation of ion pair. Our RB3LYP/6-311++G(3df,3pd)-level calculations on EpyCl led to at least two possible structures. Figure 5-7 shows (a) the minimum energy structure (structure (a)), and (b) the second minimum structure (structure (b)). These structures show relative energy difference of 9.88 kJ mol^{-1}. The thermal distribution at 300K gives a population ratio of structure (a) to structure (b) as 98 : 2. Therefore, spectral carrier of the CT bands should have the structure (a). One remarkable feature of structure (a) is that chlorine ion is attached to hydrogen atoms at carbon atoms of 1' and 2 positions. This result agrees well with NMR observation. Because of the cost of DFT calculations, only EpyCl complex was examined in the present study, but the similar feature is well expected for other complexes, EpyBr and

EpyI.

Our conclusion for conformation of EpyX complexes is good consistent with the previous report by Lee *et al*. [14]. They measured Kamlet-Taft parameters of some pyridinium-based RTILs with Tf_2N, changing the position of side chain at pyridinium ring such as 1-octylpyridinium (Opy^+), 1-octyl-2-methylpyridinium ($2MOpy^+$), 1-octyl-3-methylpyridinium ($3MOpy^+$), and 1-octyl-4-methylpyridinium ($4MOpy^+$). One of the Kamlet-Taft parameters, α provides a measure of a solvent's hydrogen bond donating acidity. They showed that α of $OpyTf_2N$, $2MOpyTf_2N$, $3MOpyTf_2N$, and $4MOpyTf_2N$ as 0.51, 0.48, 0.50, and 0.50, respectively. It is obvious that the value of $2MOpyTf_2N$ is smaller than others, which may be due to lack of H atom at C2 position by masking of methyl group. Therefore, it is reasonable that anion attached to the H atom at C2 position in dichloromethane solution.

5-4. Conclusion

CT absorption bands of ion pairs composed of pyiridinium-based cation and halide anion were observed by using UV/Vis absorption spectroscopy. Oscillator strength of CT bands of ILs in dichloromethane solution were estimated to be 0.02 by absorbance of the spectra and by measured concentration of ion pairs derived from electric conductivity measurements. Remarkable experimental finding is that CT interaction between the cation, Epy^+ and halide anions is very small as compared to usual CT complexes studied previously. From NMR spectroscopy and DFT calculation on EpyCl

and $EpyTf_2N$ ion pairs, configuration was determined for EpyCl ion pair which is isolated in dichloromethane solution. The complex is well characterized by the weak bonding of Cl^- anion attached to the hydrogen atoms at carbon atoms of 1' and 2 positions of Epy^+ cation.

References of Chapter 5

[1] R. Katoh, Y. Yoshida, Y. Katsumura, K. Takahashi, *J. Phys. Chem. B* **111**, 4770 (2007).

[2] R. Katoh, M. Hara, S. Tsuzuki, *J. Phys. Chem. B* **112**, 15426 (2008).

[3] D. Yoshimura, T. Yokoyama, T. Nishi, H. Ishii, R. Ozawa, H. Hamaguchi, K. Seki, *J. Electron. Spectrosc. Relat. Phenom*, **319**, 144 (2005).

[4] R. Katoh, *Chem. Lett.* **36**, 1256 (2007).

[5] A.Paul, P. K. Mandal, A. Samanta, *Chem. Phys. Lett.* **402**, 375 (2005).

[6] A. Paul, A. Samanta, *J. Chem. Sci.* **118**, 335 (2006).

[7] J.N.A. Canongia Lopes and A.A.H. Pádua, *J. Phys. Chem. B* **110**, 3330 (2006).

[8] T. Ogura, N. Akai, A. Kawai, K. Shibuya, *Chem. Phys. Lett.* **535**, 110 (2013).

[9] M.J. Frisch et al., Gaussian 09, Revision **A.1**, Gaussian, Inc., Wallingford CT, 2009.

[10] M.J. Blandamer, M.F. Fox, *Chem.Rev.* **70**, 59 (1970).

[11] R.S. Mulliken, W.B. Person, *Ann. Rev. Phys. Chem.* **13**, 107 (1962).

[12] S. Okazaki, I. Sakamoto, *"Solvents and Ions - Chemistry of Non-aqueous Electrolyte Solutions, in Japanese"*, Sanei, Kyoto (1990).

[13] N. Mataga, *"Molecular Interactions and Electronic Spectra"*, M. Dekker, New York (1970).

[14] J.M. Lee, S. Ruckes, J.M. Prausnitz, *J.Phys.Chem.B* **112**, 1473 (2008).

Appendix

As for calculation of ${f_{\pm}}^2$, α and β values, the following equations,

$$\alpha = \frac{2.801 \times 10^6 |z_+ z_-| \times 0.5}{(DT)^{3/2}(1 + 0.5^{1/2})} \quad \text{(S1)}$$

$$\beta = \frac{41.25(|z_+| + |z_-|)}{\eta (DT)^{1/2}} \quad \text{(S2)}$$

$$\log f_{\pm} = \frac{-1.8246 \times 10^6 |z_+ z_-| c}{(DT)^{3/2}} \quad \text{(S3)}$$

were used. In these equations, $|z_+|$ and $|z_-|$ stand for magnitude of ionic valency as unity, *D* for dielectric constant, *T* for temperature, and η for viscosity of solvent. The values of these parameters are T=25.0 ^{o}C for all measurement, η=0.890, 0.35, 0.43 mPa s for water, acetonitrile, dichloromethane solvent, respectively.

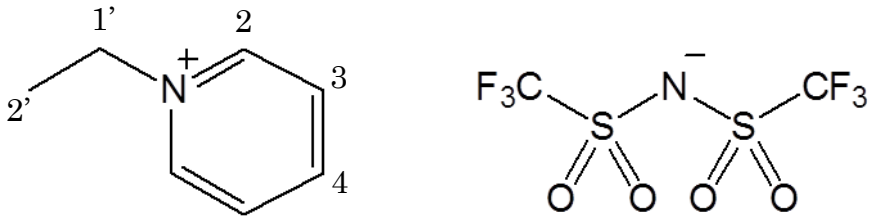

Chart 5-1.

Structure formula of $EpyTf_2N$ [N-ethylpyridinium bis(trifluoromethanesulfonyl)amide].

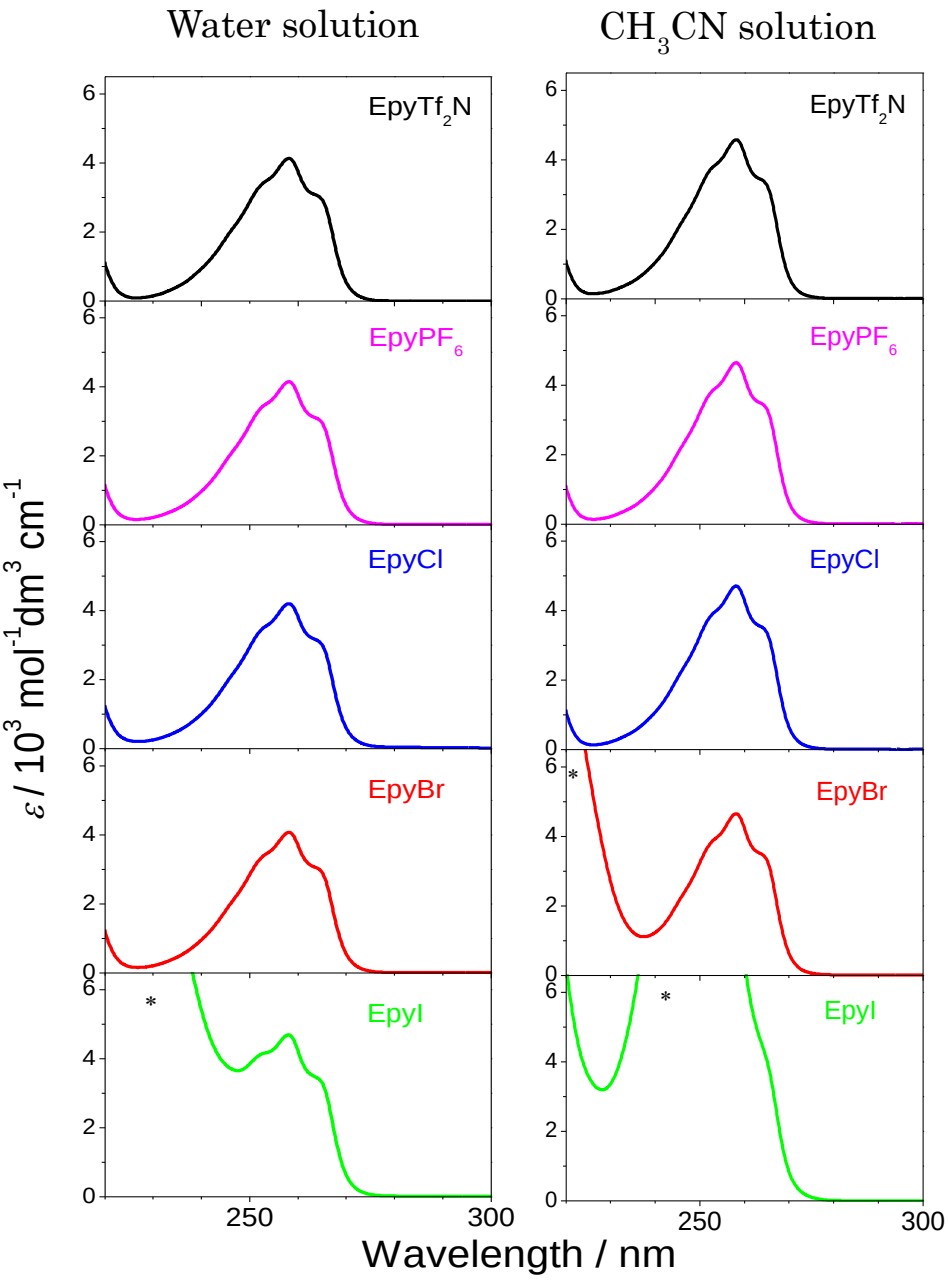

Figure 5-1.

Absorption spectra of N-ethylpyridinium-based ILs in (left) water and (right) acetonitrile. Asterisks in EpyBr and EpyI spectra indicate CTTS band from halide ions.

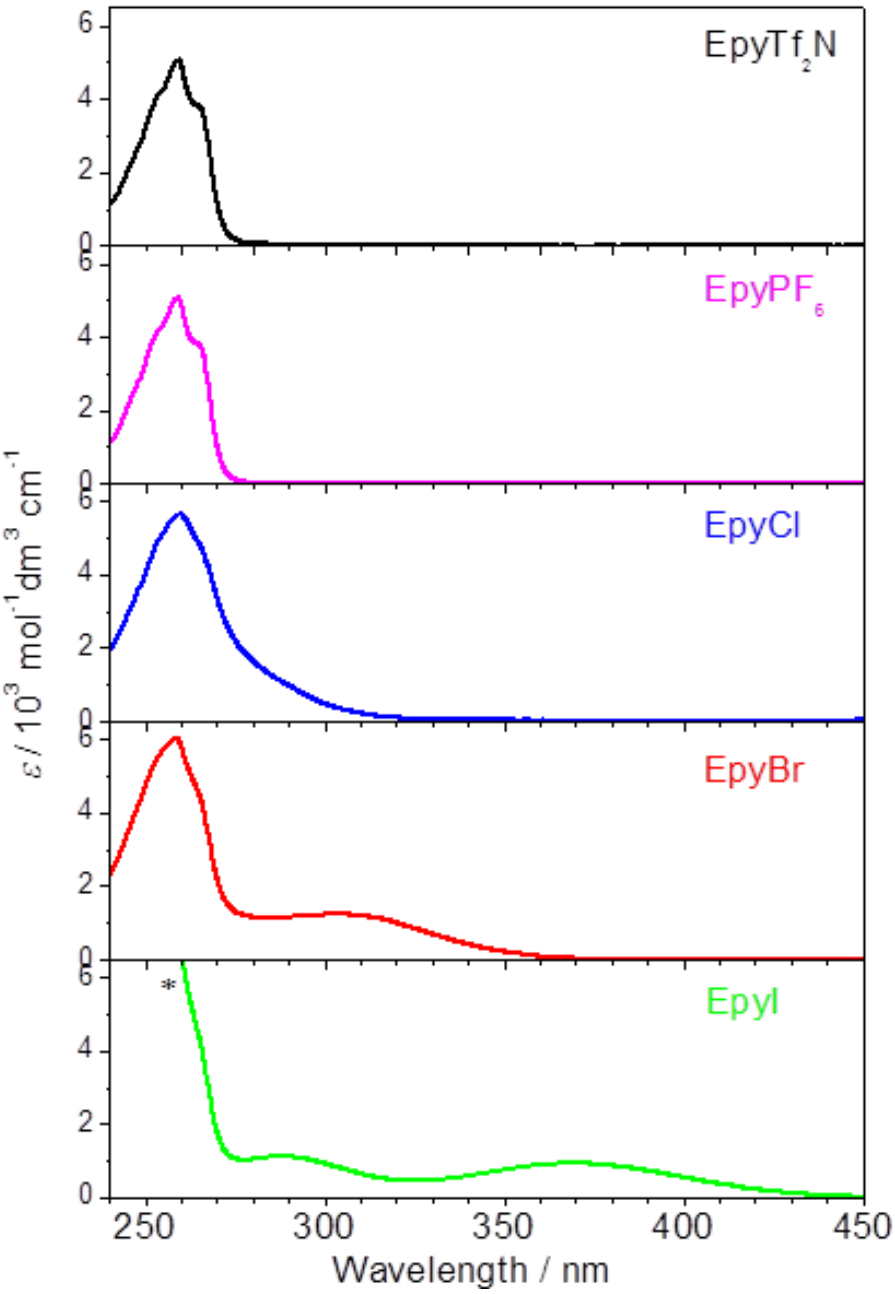

Figure 5-2.

Absorption spectra of N-ethylpyridinium-based ILs in dichloromethane. An asterisk in EpyI spectrum indicates CTTS band from iodide ion.

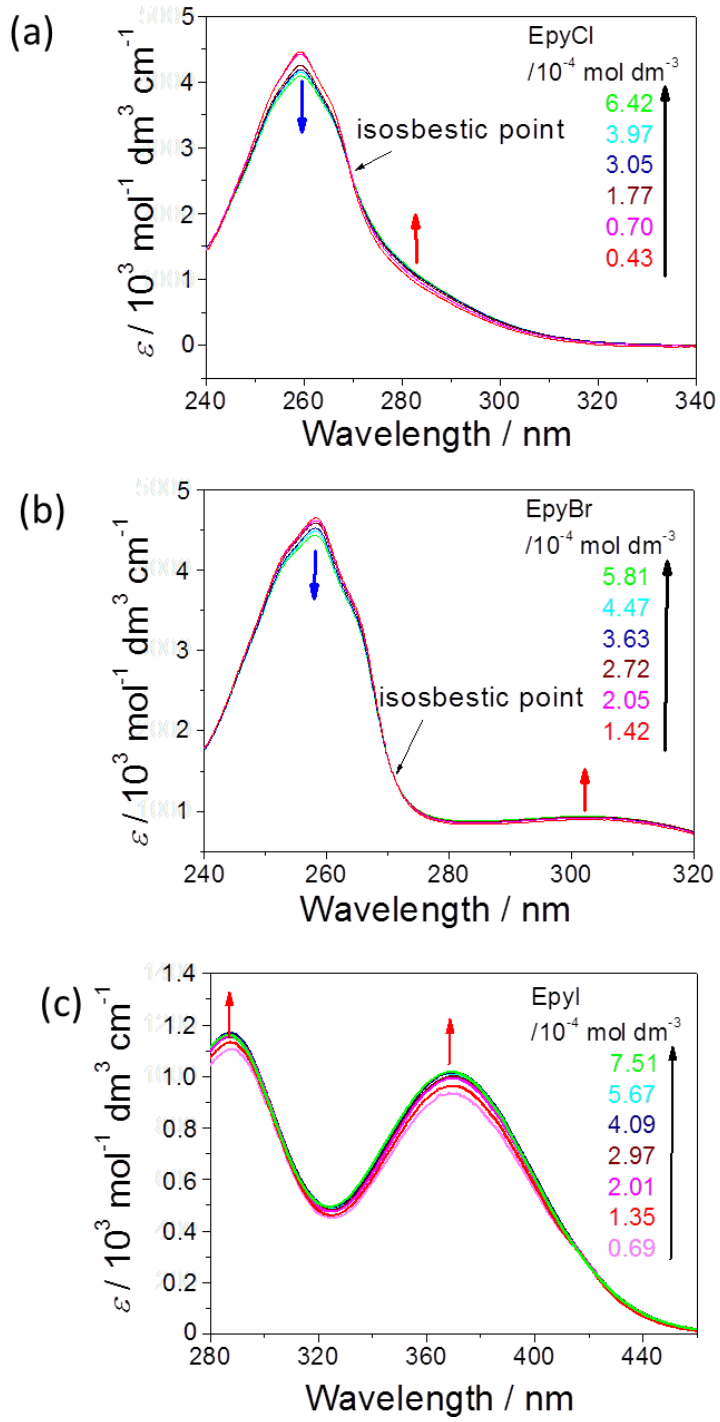

Figure 5-3.

Absorption spectra of (a) EpyCl, (b) EpyBr, and (c) EpyI at various concentrations in dichloromethane.

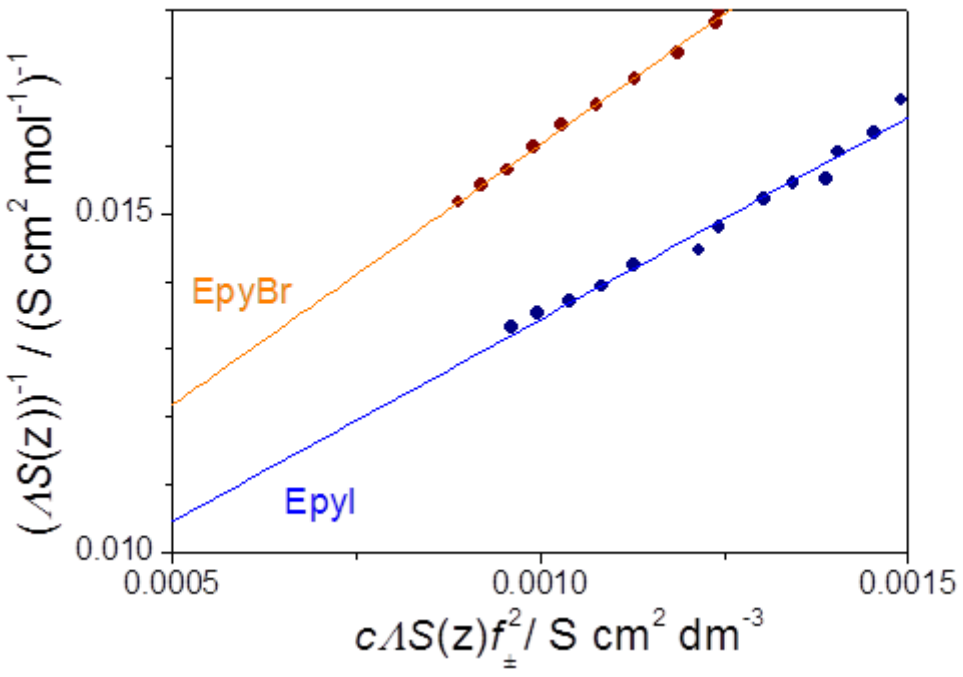

Figure 5-4.

Experimental plots and their fitting lines calculated by Shedlovsky method.

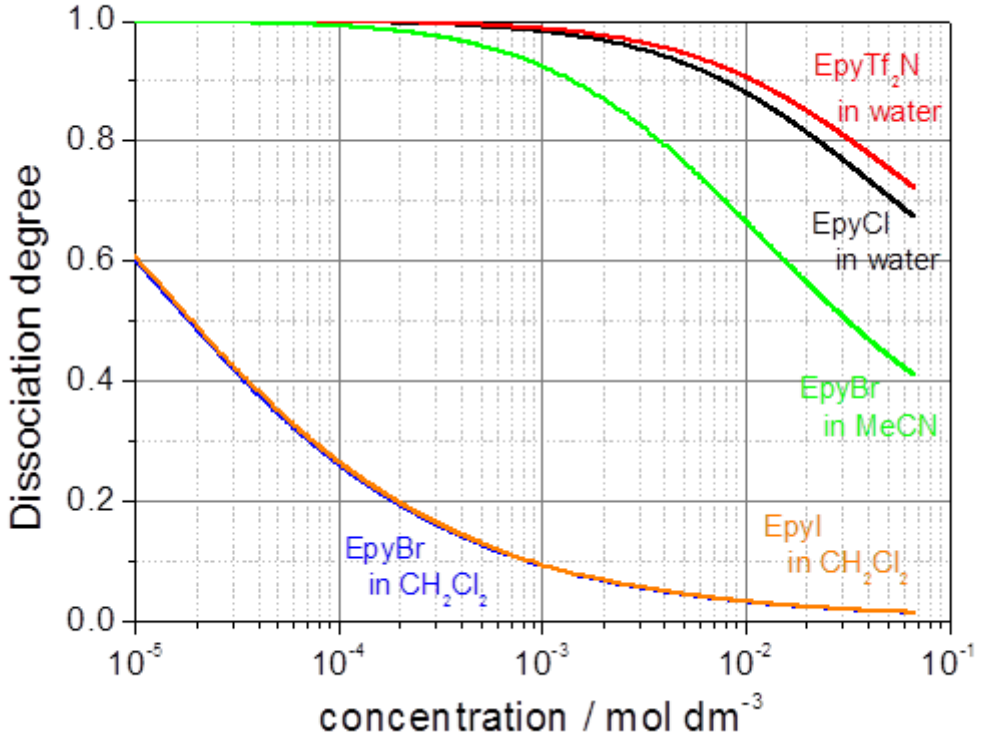

Figure 5-5.

IL concentration vs. dissociation degree curves of some solutions. Arrows indicate concentration region in the present absorption experiments.

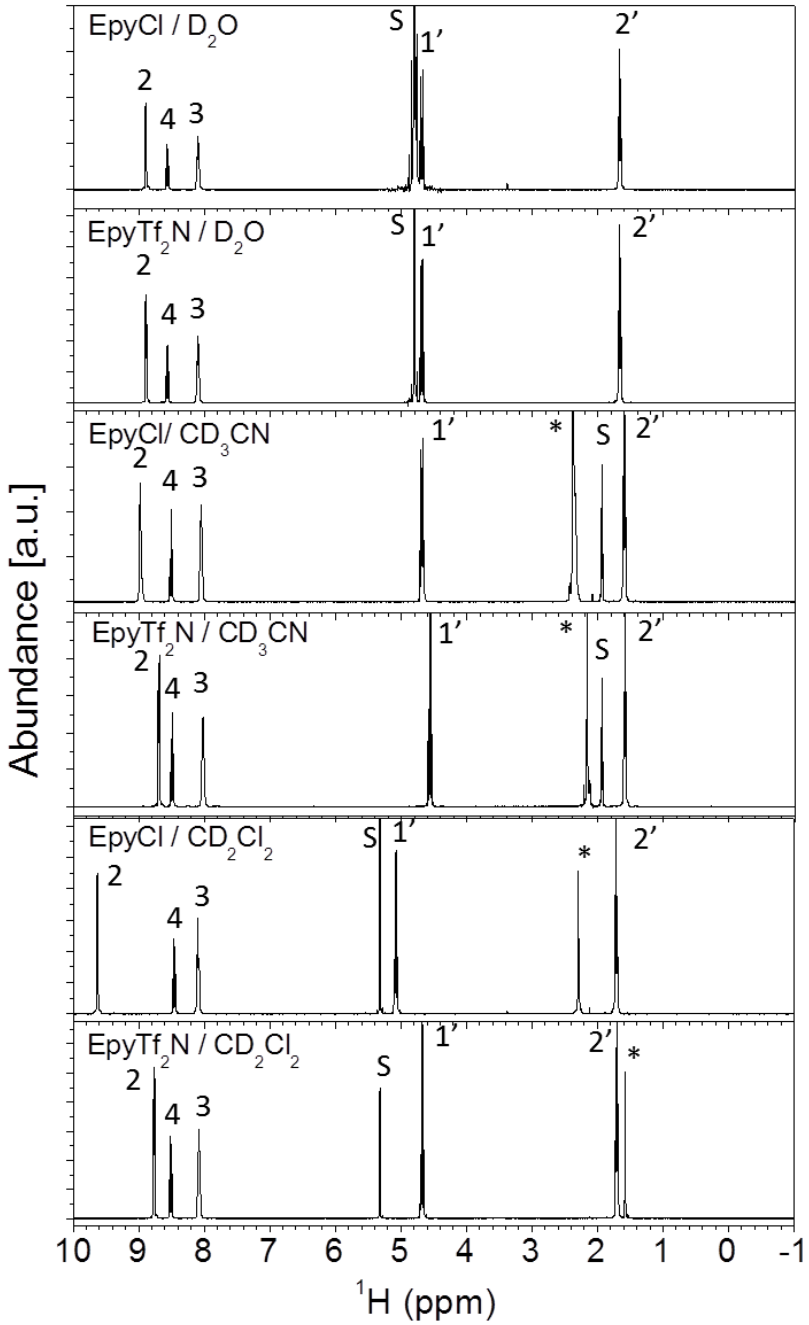

Figure 5-6.

^{1}H-NMR spectra of EpyCl and EpyTf$_2$N in three deuterated solvents.

S and * indicate peaks of solvent and impurity, respectively. The concentrations were about constant around 100 mM.

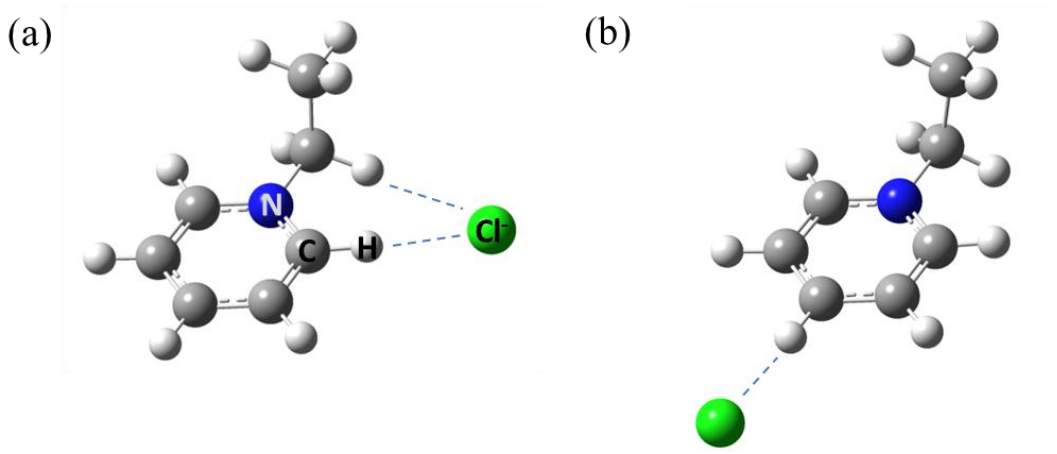

Figure 5-7.

The most stable (a) and the second-most stable (+9.88 kJ mol^{-1}) (b) structures of Epy^{+} Cl^{-} ion pair in dichloromethane optimized by DFT calculations

at the RB3LYP/6-311++G(3df,3pd) level of theory. Dotted lines indicate the nearest and the second nearest bonds distance between cation and anion.

Table 5-1.

Molar absorption coefficients of $S_1(\pi\pi^*)\leftarrow S_0$ electronic transition of 1-ethylpyridinium-based RTILs in typical solvent. λ_{max} is 258.2 nm in water and acetonitrile solution, and 258.9 nm for $EpyTf_2N$ and 258.7 nm for $EpyPF_6$ in dichloromethane solution.

X^- of Epy^+X^-	$\varepsilon(\lambda_{max})$ / 10^3 dm^3 mol^{-1} cm^{-1}		
	Water (D=78.4)	Acetonitrile (D=37.5)	Dichloromethane (D=9.1)
Tf_2N^-	4.1±0.1	4.6±0.2	5.0±0.3
PF_6^-	4.1±0.1	4.5±0.2	4.9±0.3
Br^-	4.1±0.1	4.3±0.2	-
Cl^-	4.2±0.1	4.5±0.2	-

Table 5-2.

Electron affinity(E_A), solvation energy(E_S), ionic radius(r),and spin-orbit coupling(ΔE_{SO}) of halogen atom, X.

X	E_A(X) / eV	E_S(X^-) / eV	r / Å	ΔE_{SO} / eV
Cl	3.61	4.35	1.64	0.109
Br	3.36	3.96	1.80	0.459
I	3.06	3.48	2.05	0.942

Table 5-3.

Ion association constant (K_A) of Epy^+ and various anions in solutions.

Solute	Solvent	K_A / dm^3 mol^{-1}
$EpyTf_2N$	H_2O	$(1.5 \pm 0.2) \times 10^1$
EpyCl	H_2O	$(1.9 \pm 0.2) \times 10^1$
EpyBr	CH_3CN	$(1.0 \pm 0.1) \times 10^2$
EpyBr	CH_2Cl_2	$(11.0 \pm 0.8) \times 10^4$
EpyI	CH_2Cl_2	$(10.6 \pm 1.3) \times 10^4$

Table 5-4.

Molar absorption coefficients and oscillator strengths of CT transition of EpyBr and EpyI in dichloromethane solution.

X of Epy^+X^-	λ_{max}	$\varepsilon(\lambda_{max})$	f
	nm	10^3 mol dm^{-3} cm^{-1}	
I ($^2P_{3/2}$)	369.6	1.2±0.1	0.021±0.002
I ($^2P_{1/2}$)	288.0	1.3±0.1	0.024±0.002
Br ($^2P_{3/2}$)	304.0	1.2±0.1	0.022±0.002

Table 5-5.

Chemical shifts of EpyCl and $EpyTf_2N$ in deuterated water, acetonitrile, and dichloromethane. Δ indicates difference in chemical shifts of the two ILs.

	Chemical shifts / ppm								
	Water			Acetonitrile			Dichloromethane		
C atom	EpyCl	$EpyTf_2N$	Δ	EpyCl	$EpyTf_2N$	Δ	EpyCl	$EpyTf_2N$	Δ
2	8.893	8.889	0.004	8.982	8.692	0.290	9.628	8.764	0.864
3	8.096	8.096	0.000	8.048	8.021	0.024	8.093	8.077	0.016
4	8.568	8.564	0.004	8.505	8.492	0.013	8.457	8.509	-0.052
1’	4.684	4.681	0.003	4.683	4.564	0.119	5.073	4.671	0.402
2’	1.571	1.670	-0.099	1.599	1.589	0.010	1.716	1.704	0.012

Chapter 6. Charge transfer interaction within ion pairs formed in RTILs

6-1. Introduction

In this thesis, CT absorption of RTILs is focused to understand CT interaction between cation and anion in neat liquid. In chap 5, estimation of CT interaction between isolated pyridinium-based cation and halide anion dissolved in non-polar solvent was mentioned by using electronic absorption spectroscopy [1]. It was concluded that CT interaction between cation and anion within an ion pair in non-polar solution is weak. Next step is to understand electronic states of RTILs that have CT transition in neat liquid phases. Katoh *et al*. studied electronic absorption of neat BmimI, and they suggested that there are only ion pairs in the neat liquid phase due to stabilization induced by the Madelung energy of RTILs [2].

In the present study, electronic absorption spectra were measured for RTILs that have halide anion in neat liquid phase by using UV/Vis spectroscopic method to understand CT interaction. Difference of CT interaction strength was evaluated for isolated ion pairs [1] and neat liquids by comparing these absorption band shapes, transition energies, and oscillator strength.

6-2. Experimental

Details of samples and purification method were described in Chapter 2. Chart 6-1 shows structures of these samples. The temperature of the sample cell is controlled by a flow of temperature adjusted water in a cell-holder.

Absorption spectra of solution samples and neat liquids were measured as details described in Chapter 2.

6-3. Results and discussion

6-3-1. *Absorption spectra for neat imidazolium- and pyridinium-based ILs*

Figure 6-1 shows the normalized absorption spectra of neat $BmimTf_2N$, neat BmimI and their mixture at 363 K. In neat $BmimTf_2N$, simple $\pi\pi^*$ transition absorption band was observed. This observation is quite similar to that of $BmimTf_2N$ in diluted solution [3]. This result clearly shows that there are no other electronic absorption in this wavelength region such as CT, CTTS, and those of cluster in neat liquid phase. Meanwhile, a broad and non-structural absorption band was observed in neat BmimI, which is the same result with the study of Katoh *et al*. measured at room temperature [2]. They concluded that this absorption band was assigned to CT transition within $Bmim^+$ and I^- ion pair, and band shapes of BmimI and $BmimTf_2N$ mixture was explained by simple sum of absorption bands of isolated $Bmim^+$ and ion pair of $Bmim^+I^-$. Then, they suggested that there exits only ion pair in the neat liquid phase, which is reasonably explained by stabilization due to the Madelung energy of RTILs [2].

$Bmim^+$ has strong hydrogen bond donating ability at hydrogen atom attached to C(2) carbon of imidazolium ring. This ability may assist cation in forming contact ion pair and makes the analysis of CT interaction difficult. Thus, low hydrogen donor cations were examined. The cations used were $Pmmim^+$ and Epy^+ whose hydrogen in C(2) is replaced by methyl group. Figure 6-2 (a) shows normalized absorption spectra of neat $PmmimTf_2N$ and neat PmmimI at 363 K. In neat $PmmimTf_2N$, there appears only the $\pi\pi^*$ absorption band, which is same observation as that in neat $BmimTf_2N$. As compared to neat $PmmimTf_2N$, absorption spectrum of neat PmmimI is characterized by two prominent bands. These bands in neat PmmimI might be assigned to CT transitions between cation and anion as seen in neat BmimI. Figure 6-2 (b) shows normalized absorption spectra of neat $EpyTf_2N$ and neat EpyI at 373 K. Those two spectra are obviously different : Neat $EpyTf_2N$ spectrum is dominated by dual absorption bands of S_1 ($\pi\pi^*$) $\leftarrow S_0$ and S_2 ($\pi\pi^*$) $\leftarrow S_0$ transitions, while neat EpyI has multiple bands. The absorption bands around 330 nm of neat EpyI may be attributed to CT transitions from iodide ions to Epy^+ cation. Meanwhile, band at 225nm cannot be the second CT band with different spin-orbit state, because energy separation between the 225 nm band and CT band at 330 nm is 14100 cm^{-1} which is much larger than splitting energy due to spin-orbit coupling of iodine. To assign these novel bands, absorption spectra of PmmimI / $PmmimTf_2N$ and EpyI / $EpyTf_2N$ mixtures were observe.

Figure 6-3 show normalized absorption spectra of neat I^- salt, neat Tf_2N^- salt, and

their mixture with molar fraction of X_{I^-} as (a) 0.40, (b) 0.50, and (c) 0.75 for $Pmmim^+$-based ILs at 363 K and with molar fraction of X_{I^-} as (d) 0.23, (e) 0.48, and (f) 0.79 for Epy^+-based ILs at 373 K. Simulated spectra with various molar fraction of I^- are also shown in each figure. The absorption spectra of PmmimI / $PmmimTf_2N$ mixture were almost reproduced by sum of the spectra for neat PmmimI and $PmmimTf_2N$ with their corresponding molar fraction as shown in Figure 6-3 (a) ~ (c). Meanwhile, as shown in Figure 6-3 (d) ~ (f), those of EpyI / $EpyTf_2N$ mixture were not reproduced around 230 nm by sum of neat EpyI and $EpyTf_2N$ with their corresponding molar fraction. The spectral difference around 230 nm is considered to be enhanced CTTS transition band of iodide atom ($^2P_{3/2}$) in the binary solvent. Another discrepancy is found in high energy region around 200 nm in both PmmimI / $PmmimTf_2N$ mixture and EpyI / $EpyTf_2N$ mixture. This difference would be attributed to (1) the spectral shifts in the absorption bands in vacuum ultraviolet wavelength region or (2) appearance of CTTS transition in vacuum ultraviolet region as details described later.

Then, molar absorption coefficients of chromophores were estimated from the ratio of absorbance for CT and ππ* bands together with molar fraction. Figure 6-4 shows plots of the absorbance ratio for CT and ππ* bands against molar fraction of I^- in (a) PmmimI / $PmmimTf_2N$ mixture and (b) EpyI / $EpyTf_2N$ mixture, and their fitting lines. Fitting was done by eq.(1) ~ (3) as described below,

$$A_{\pi\pi^*} = \varepsilon_{\pi\pi^*} c_{Tf_2N^-} l \qquad (1)$$

$$A_{CT} = \varepsilon_{CT} c_{I^-} l \qquad (2)$$

$$\frac{A_{\mathrm{CT}}}{A_{\pi\pi^*}} = \frac{\varepsilon_{\mathrm{CT}}}{\varepsilon_{\pi\pi^*}} \frac{c_{\mathrm{I}^-}}{c_{\mathrm{Tf_2N}^-}} = \mathrm{C} \frac{X_{I^-}}{1 - X_{I^-}} \qquad (3)$$

where *A* stands for the normalized absorbance (a) at 211 nm for ππ* and 233 nm for CT transitions and (b) at 257 nm for ππ* and 330 nm for CT transitions, ε for the molar absorption coefficient, *c* for the molar concentration, *l* for the light path length, and *X* for the molar fraction of I^-. The plots are well fitted in both binary liquids. In neat liquids, spectral carriers would be ion pairs as suggested in chap 3 [4], therefore these liquids may be composed of two 1:1 ion pairs, namely, Epy^+I^- and $Epy^+Tf_2N^-$ for EpyI / $EpyTf_2N$ mixture and, $Pmmim^+I^-$ and $Pmmim^+Tf_2N^-$ for PmmimI / $PmmimTf_2N$ mixture, as being similar to the results in BmimI / $BmimTf_2N$ mixture [2]. No free ions such as I^- and Tf_2N^- are expected in these binary liquids. In the case of $Pmmim^+$-based ILs as shown in Figure 6-4 (a), the molar absorption coefficient ratio, C was determined as 2.09 ± 0.03 by the fitting analysis. Value of $\varepsilon_{\pi\pi^*}$ for $Pmmim^+$ was estimated as 5.6 x 10^3 mol^{-1} dm^3 cm^{-1} in acetonitrile solution. Eventually, ε_{CT} is estimated to be 1.2 x 10^4 mol^{-1} dm^3 cm^{-1} at 233 nm. Meanwhile, in the case of Epy^+-based ILs as shown in Figure 6-4 (b), the molar absorption coefficient ratio, C of 1.13 ± 0.05, $\varepsilon_{\pi\pi^*}$ for Epy^+ of 4.7 x 10^3 mol^{-1} dm^3 cm^{-1} in acetonitrile and, ε_{CT} of 5.2 x 10^3 mol^{-1} dm^3 cm^{-1} at 330 nm were estimated by similar analysis.

6-3-2. *Analysis of absorption spectra in neat liquid*

In the above section, spectral feature was roughly attributed to the bands due to $S_1(\pi\pi^*)$ of cation, CT transition with spin orbit states $^2P_{1/2}$ and $^2P_{3/2}$, CTTS transition,

and red-edge region of higher electronic transitions in VUV wavelength. For further understanding of these transitions in neat RTILs, it is important to evaluate absorption coefficients of these bands and their spectral band shapes.

To analyze absorption spectra, the following spectral features were assumed. First, it is presumed there are $S_1(\pi\pi^*)$ of cation even in neat I^- salt and CT transition with spin orbit states $^2P_{1/2}$ and $^2P_{3/2}$. Rough peak energy and band width of $S_1(\pi\pi^*)$ of cation were set refer to that in neat Tf_2N^- salt. Rough band width of two CT bands was presumed from red-edge of absorption band of neat I^- salt which was not overlapped by $S_1(\pi\pi^*)$ of cation. Second, CTTS transition band is assumed to be in VUV region for PmmimI and in 230 nm for EpyI as mentioned in previous section.

Figure 6-5 shows the absorption spectrum of neat PmmimI and its deconvoluted spectrum. The obtained absorption band was almost perfectly deconvoluted by four Gaussian lineshape components. The second lowest electronic absorption band was assigned to $\pi\pi^*$ transition of $Pmmim^+$ moiety because transition energy and band width were almost the same as that of neat $PmmimTf_2N$. The first and third lowest electronic absorption bands were assigned to CT transitions from I^- to $Pmmim^+$ because CT transition band should split within 7600 cm^{-1} by the spin-orbit coupling between $^2P_{1/2}$ and $^2P_{3/2}$ states of iodide atom. In the present case, splitting energy is about 5300 cm^{-1}, which is reasonable for the assignment. This value is discussed in next section. The highest electronic absorption band was assigned to sum of other higher transitions of $Pmmim^+$. In neat PmmimI, there is no longer CTTS band in near ultraviolet light region.

Figure 6-6 shows the absorption spectrum of neat EpyI and its deconvoluted spectra. The same algorithm used above was applied to this deconvolution process. The absorption band was deconvoluted well by five components written in Figure 6-6. The lowest and the second lowest electronic absorption bands were assigned to CT transitions, and their splitting is 5960 cm^{-1}. The third lowest electronic absorption band was assigned to ππ* transition of Epy^+ moiety, and the highest electronic absorption band was assigned to sum of other higher transitions of Epy^+ moiety including higher ππ* transition. Additionally, the second highest electronic absorption band at 43900 cm^{-1} was assigned to CTTS band from Epy^+I^- to surroundings, because CTTS band for EpyI dissolved in N,N,N-trimethyl-n-propylammonium (TMPA)Tf_2N solution appears at the same wavelength region [2].

According to these deconvolution analysis, spectral parameters were determined and the results were listed in Table 1. From these parameters, transition dipole moment, μ_{CT} and oscillator strength, f were calculated for neat PmmimI and neat EpyI. As a reference, μ_{CT} and f of EpyI / CH_2Cl_2 were also listed in Table 1. It is noteworthy that the μ_{CT} and f of neat liquids are larger than those of CH_2Cl_2 solution.

The present result of the existence of CTTS band in near ultraviolet region is remarkably different from that of PmmimI and BmimI where no CTTS bands were seen in UV/VIS region. Since the CTTS band should have non-negligible absorption coefficient as shown in the EpyI result, there would be CTTS bands in PmmimI and BmimI in much higher wavelength region. This point is described in the next section.

As shown in Figure 6-6, ε_{CTTS} at peak wavelength is about 9.4 x 10^3 mol^{-1} dm^3 cm^{-1}, and this value is about two-third as large as that in TMPATf$_2$N whose ε_{CTTS} is 15800 mol^{-1} dm^3 cm^{-1} [2]. This result would be explained as follows. CTTS transition moment is normally large because electron transfers from ion to surroundings with long distance and electric dipole moment of excited state becomes very large. In the present case, electrons might not depart from ion relative to that in TMPATf$_2$N solution.

6-3-3. *Estimation of charge transfer interaction in neat liquid phase*

CT interaction of ion pairs in neat RTILs can be estimated from oscillator strength and/or transition dipole values derived from the deconvoluted CT transition absorption bands. This provides the details of intermolecular interaction of ion pair in neat RTILs which depends significantly on RTILs. In the following, CT interaction by Mulliken theory is briefly explained and then, dependence of CT interaction of ion pair on RTILs is discussed based on experimentally determined oscillator strength values and the CT theory [5].

Wave functions of electronic states are expressed as,

$$\Psi_G = a\Psi_I + b\Psi_N \qquad (1)$$

$$\Psi_E = -b\Psi_I + a\Psi_N \qquad (2)$$

where Ψ_G and Ψ_E stand for electronic states of the ground and excited states, Ψ_I and Ψ_N for zero-order states of ion complex in the ground state and neutral complex in the excited state, and a and b for coefficients of wave functions. Meanwhile, transition

dipole moment, $\boldsymbol{\mu}_{CT}$ is expressed as follows,

$$\boldsymbol{\mu}_{CT} = ab(\boldsymbol{\mu}_N - \boldsymbol{\mu}_I) \sim eRb \qquad (3)$$

where *e* stands for elementary charge, μ_I and μ_N for permanent electric dipole of the ground and excited states, and *R* for the distance between cation and anion as an ion pair in the ground state.

In section 5-3-4, ion pair of EpyI in CH_2Cl_2 solution [1] was discussed. Positive and negative excess charges are separated in cation-anion complex ($Epy^+ I^-$) in the ground state. In the excited state, an excess electron transfers from anion to cation with forming the neutral complex ($Epy^{\cdot} I^{\cdot}$). This feature corresponds to the case where resonance between Ψ_I and Ψ_N are very small and gives rise to a small value of b coefficient. Therefore, small oscillator strength of CT absorption bands is derived from eq.(3). This oscillator strength value roughly gives intermolecular distance between cation and anion of about 3 Å. Small resonance between the ground and excited states provides spin-orbit coupling (ΔE_{SO}) of iodine atom between $^2P_{1/2}$ and $^2P_{3/2}$ states as about 7660 cm^{-1} in the excited state of CT bands. This value is close to the literature value of I atom in the gas phase of nearly 7600 cm^{-1}.

Meanwhile, in the present study for neat EpyI liquid, the values of μ_{CT} and *f* are larger than those of CH_2Cl_2 solution. This result insists that charges of cations and anions in the ground state in neat liquid are more delocalized than those in diluted solution. In EpyI ion pair in neat EpyI, resonance between the ground and excited states must be larger. This trend is also explained from the spin-orbit splitting of I, ΔE_{SO}. ΔE_{SO}

of neat liquid is 5960 cm^{-1} which is smaller than the literature value of 7600 cm^{-1} for I atom. This is interpreted by smaller and larger splitting by spin-orbit coupling in the excited and the ground states of the complex, respectively. This is schematically shown in Figure 6-7 for electronic transitions for weakly and strongly coupled CT complexes. The stronger CT interaction in the complex results in smaller spin-orbit splitting in absorption band, which is in good consistent with the results of EpyI complex diluted in CH_2Cl_2 and in neat EpyI liquid.

In PmmimI complex in neat PmmimI liquid, μ_{CT} and f values are larger than those of EpyI. This suggests that CT interaction is stronger in PmmimI complex than that of EpyI complex. As the theory indicates, stronger CT interaction gives smaller ΔE_{SO} value, which agrees well with the present result where ΔE_{SO} is 5300 cm^{-1} which is smaller than those of EpyI. Unfortunately, no successful deconvolution was done for absorption spectrum of neat BmimI because of non-structural absorption band. However, this non-structural nature implies that ΔE_{SO} is smaller than those of neat PmmimI and neat EpyI. This implication also shows that CT interaction in neat BmimI is larger than that in other two ILs. Therefore, trend of CT interaction strength would be in the order of BmimI > PmmimI > EpyI. It is noteworthy that this order is inverse relation with that of melting points of ILs; melting point is in the order of BmimI (below 300 K) < PmmimI (353 K) < EpyI (370K).

As for $h\nu_{CT}$ of neat EpyI and EpyI / CH_2Cl_2 shown in Table 6-1, neat liquid shows larger value than diluted solution. This result is explained by two reasons as follows; (1)

the electronic state of the ground state complex is more stabilized in neat liquid (ε ~ 15) than dichloromethane solution (ε ~ 9.1) due to polar solvation effect, and (2) transition energy between the zero-order states of the ground and excited states become larger in neat liquid due to larger charge transfer interaction. Difference of $h\nu_{CT}$ should originate from combination of these reasons. Another interesting feature is full width at half maximum (FWHM) of CT bands in neat EpyI and EpyI / CH_2Cl_2 shown in Table 6-1. Neat liquid shows larger FWHM of Gaussion lineshape absorption band than that of diluted solution. This suggests that there are more numbers of configurations of ion pair in neat liquid than in diluted solution.

6-4. Conclusion

Absorption spectra of imidazolium and pyiridinium-based ILs which have halide ions as neat liquid phase were observed by using UV/Vis absorption spectroscopy. In neat liquids, there are only ion pairs which shows CT absorption bands near $\pi\pi^*$ band of cations. In neat EpyI, CTTS band was also observed and its molar absorption coefficient at absorption maximum wavelength was estimated to be 1.0 x 10^4 mol^{-1} dm^3 cm^{-1}. This value is smaller than that of diluted solution because solvated electrons are relatively not far from ion pairs. Oscillator strength of CT bands in neat liquids are much larger than that of isolated ion pair in non-polar solvent, CH_2Cl_2. This result means that charge transfer interaction of ion pairs in neat ILs is large and, excess negative and positive charges on anion and cation, respectively, are rather delocalized

within ion-pair.

References of Chapter 6

[1] ”Charge transfer interaction of pyridinium-based salts as studied by UV/Vis absorption spectroscopy”, T. Ogura, N. Akai, A. Kawai, K. Shibuya, *in preparation.*

[2] R. Katoh, Y. Yoshida, Y. Katsumura, K. Takahashi, *J. Phys. Chem. B* **111**, 4770 (2007).

[3] R. Katoh, *Chem. Lett.* **36**, 1256 (2007).

[4] T. Ogura, N. Akai, A. Kawai, K. Shibuya, *Chem. Phys. Lett.* **535**, 110 (2013).

[5] N. Mataga, *“Molecular Interactions and Electronic Spectra”*, M. Dekker, New York (1970).

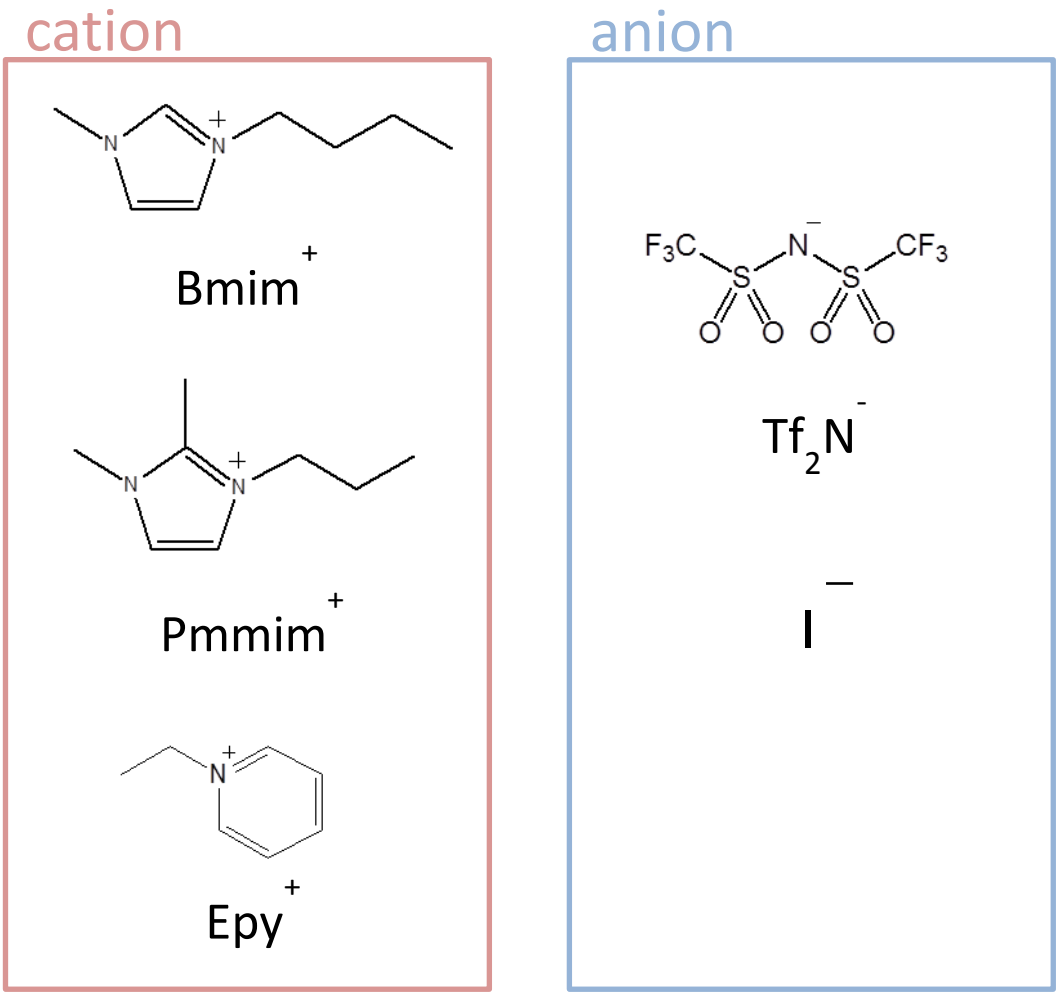

Chart 6-1.

Chemical structures and abbreviations of cations (left) and anions (right) composing RTILs in the present experiment.

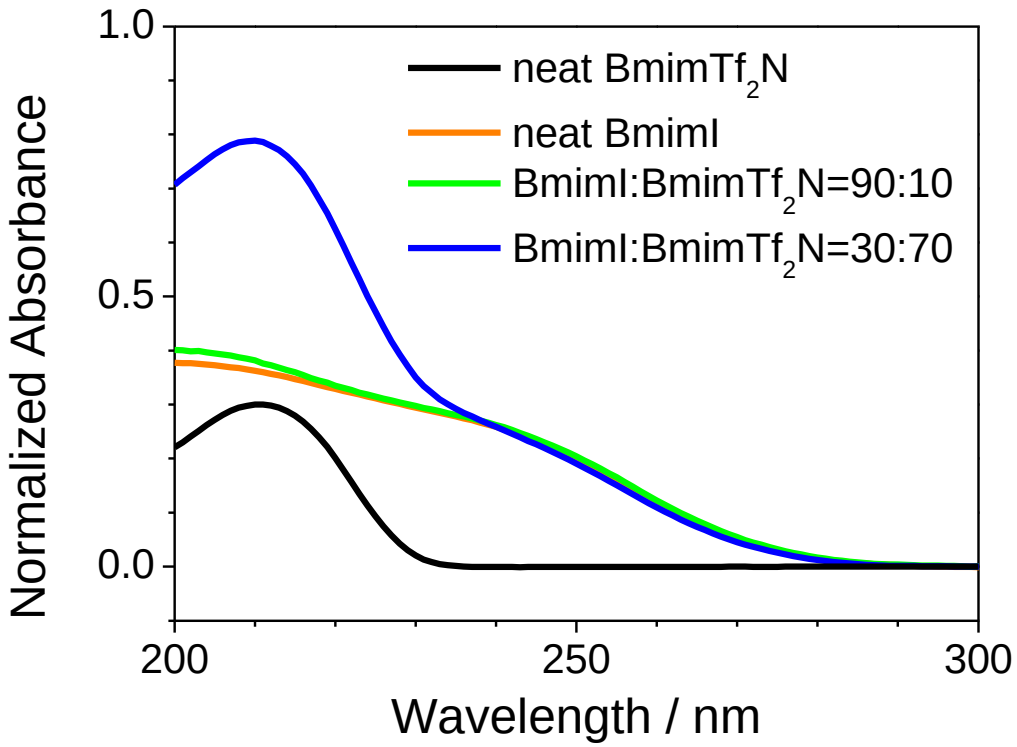

Figure 6-1.

Normalized absorption spectra of $BmimTf_2N$, BmimI and their mixture at 363 K. Molar ratios of the mixture are given.

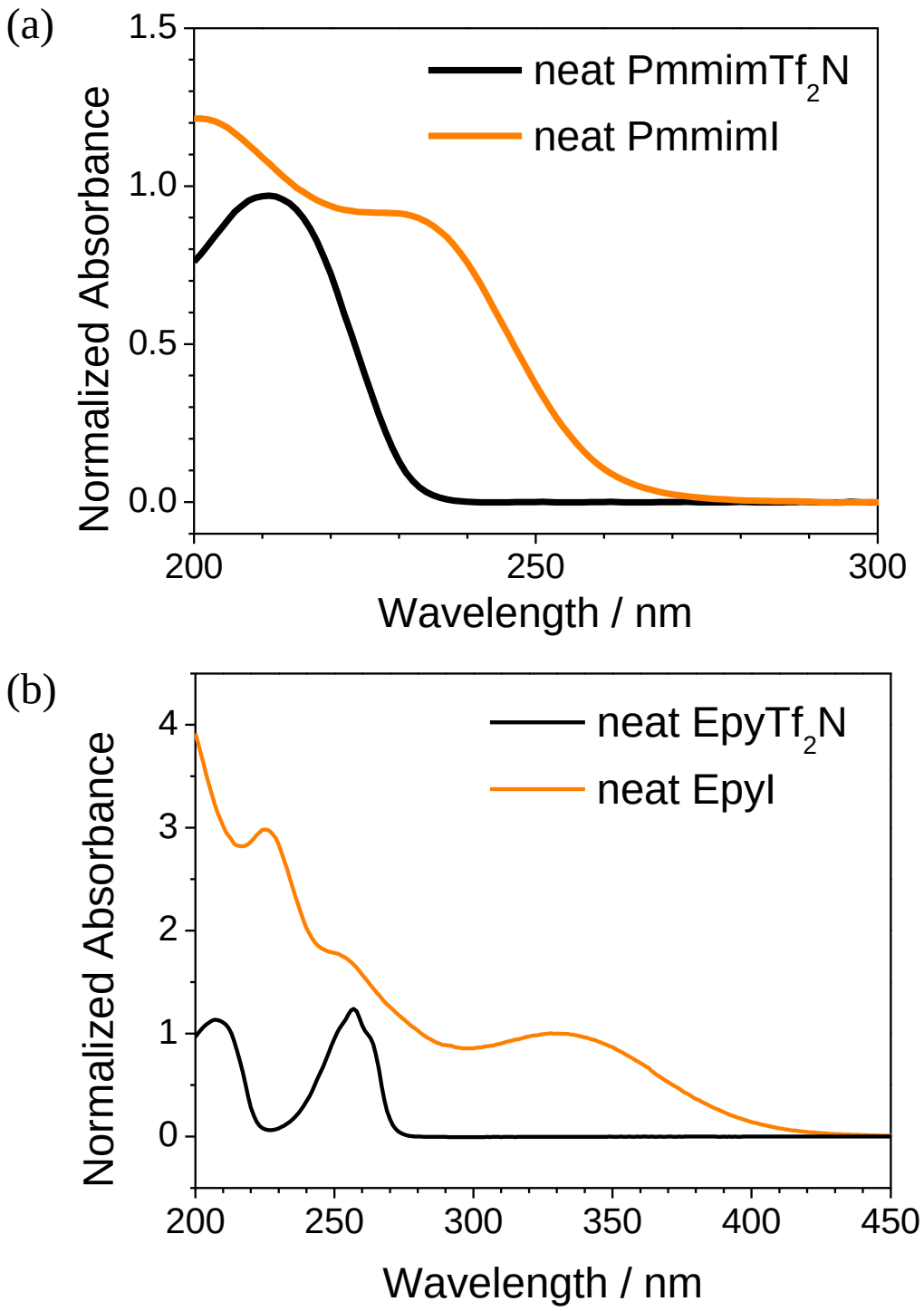

Figure 6-2.

Normalized absorption spectra of (a) neat PmmimI and neat $PmmimTf_2N$ liquids at 363 K and (b) neat EpyI and neat $EpyTf_2N$ liquids at 373 K.

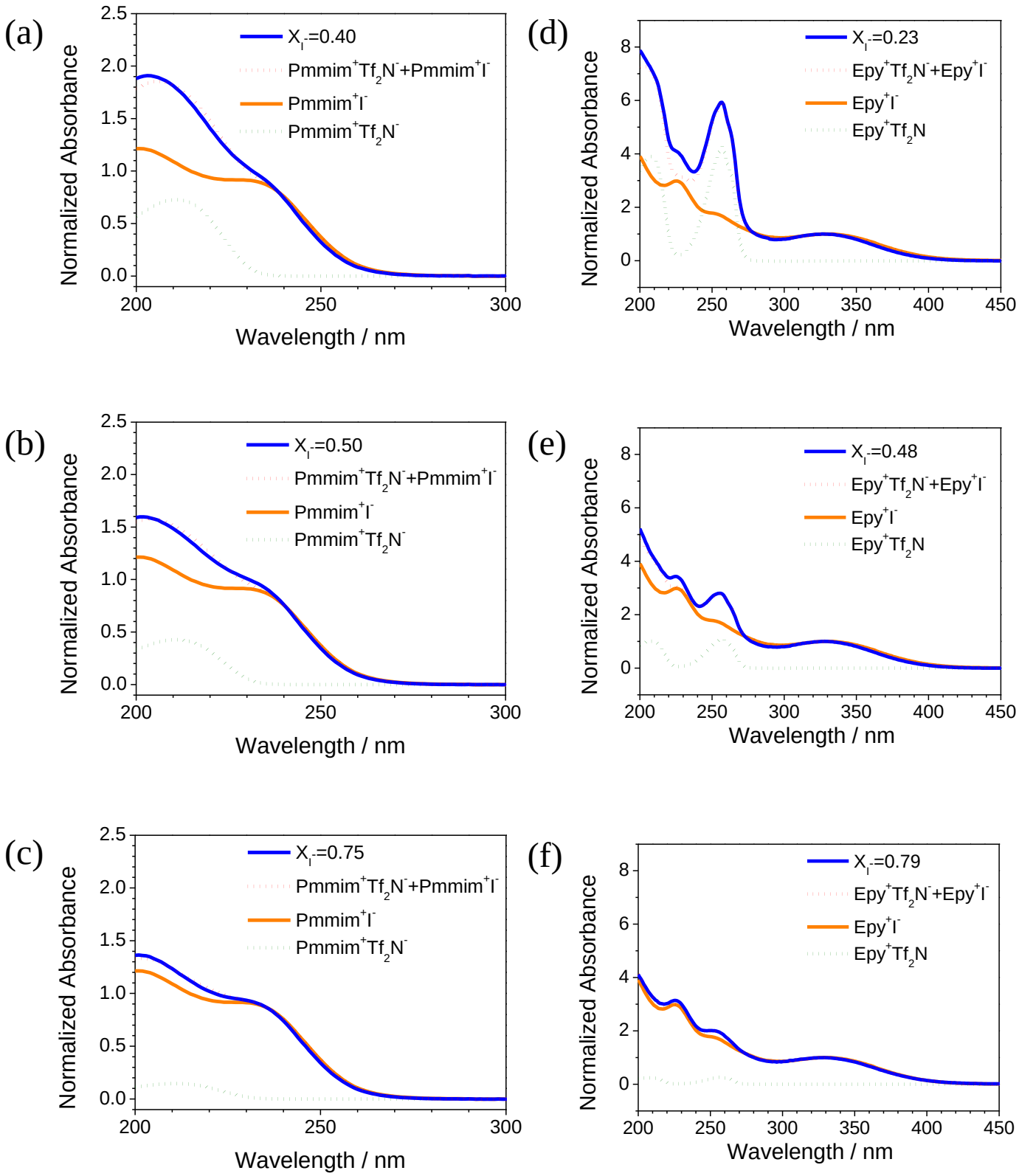

Figure 6-3.

Normalized absorption spectra of neat I^- salt (orange line), Tf_2N^- salt (green dotted line), their mixture (blue line), and simulated spectra (red dotted lines) with molar fraction of X_I- as (a) 0.40, (b) 0.50, and (c) 0.75 for $Pmmim^+$-based ILs at 363 K and (d) 0.23, (e) 0.48, and (f) 0.79 for Epy^+-based ILs at 373 K.

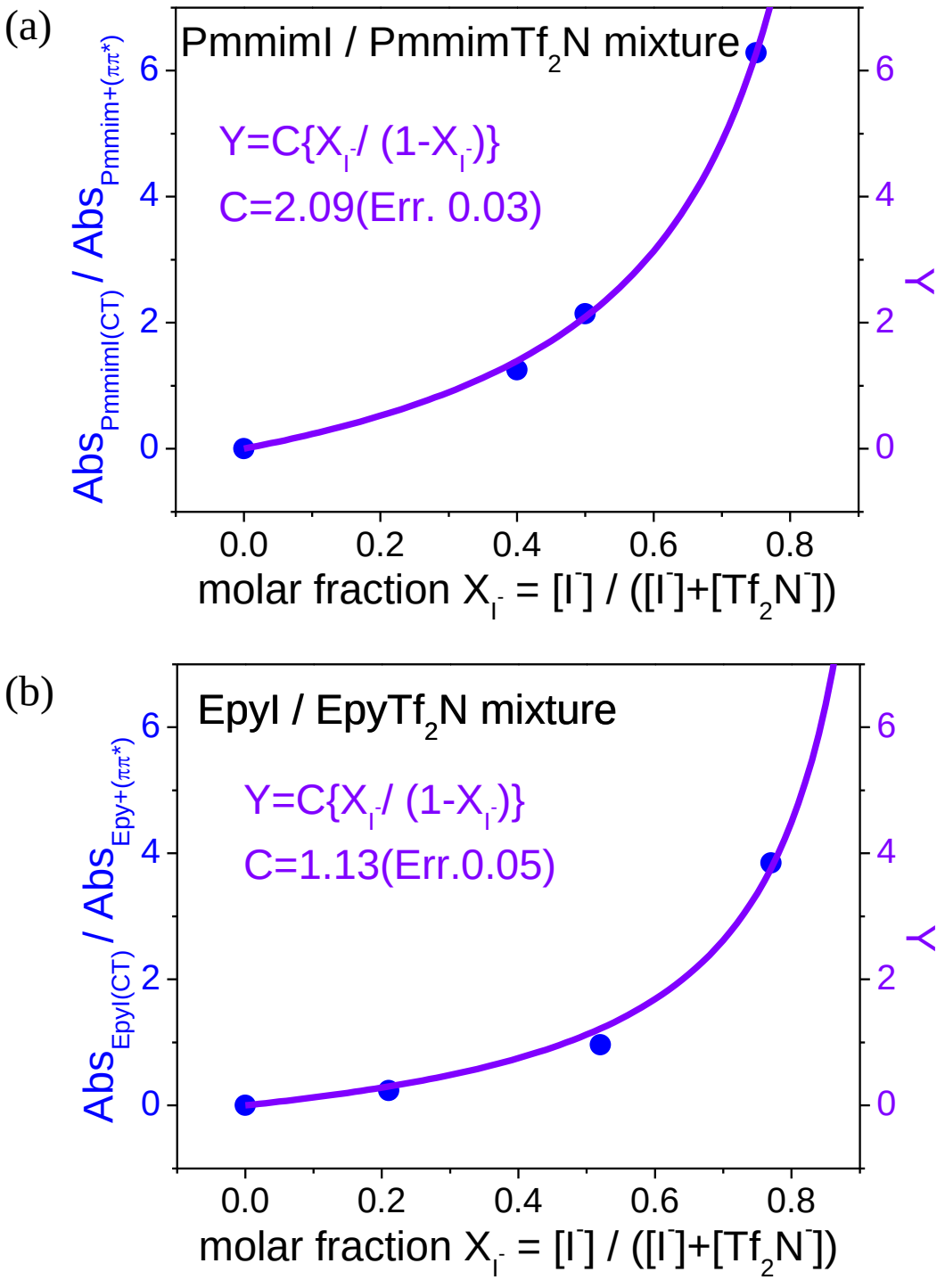

Figure 6-4.

Plots of absorbance ratio vs. molar fraction of X_{I^-} in (a) EpyI / $EpyTf_2N$ mixture, (b) PmmimI / $PmmimTf_2N$ mixture and their fitting curves.

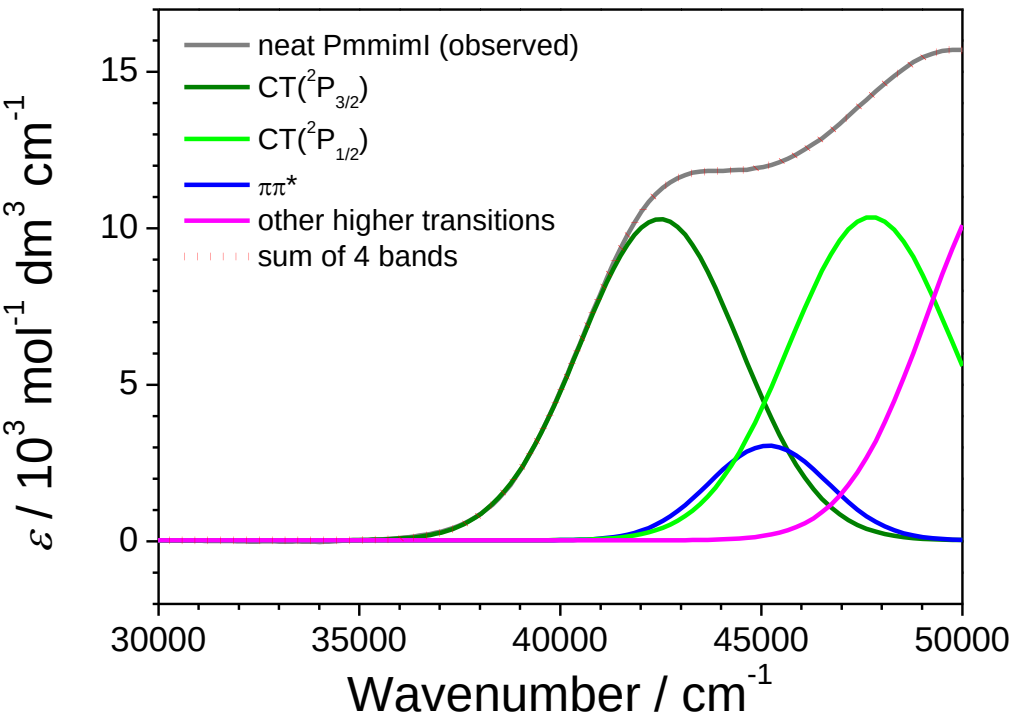

Figure 6-5.

Absorption spectrum of neat PmmimI (grey) and its deconvoluted spectra with 4 bands.

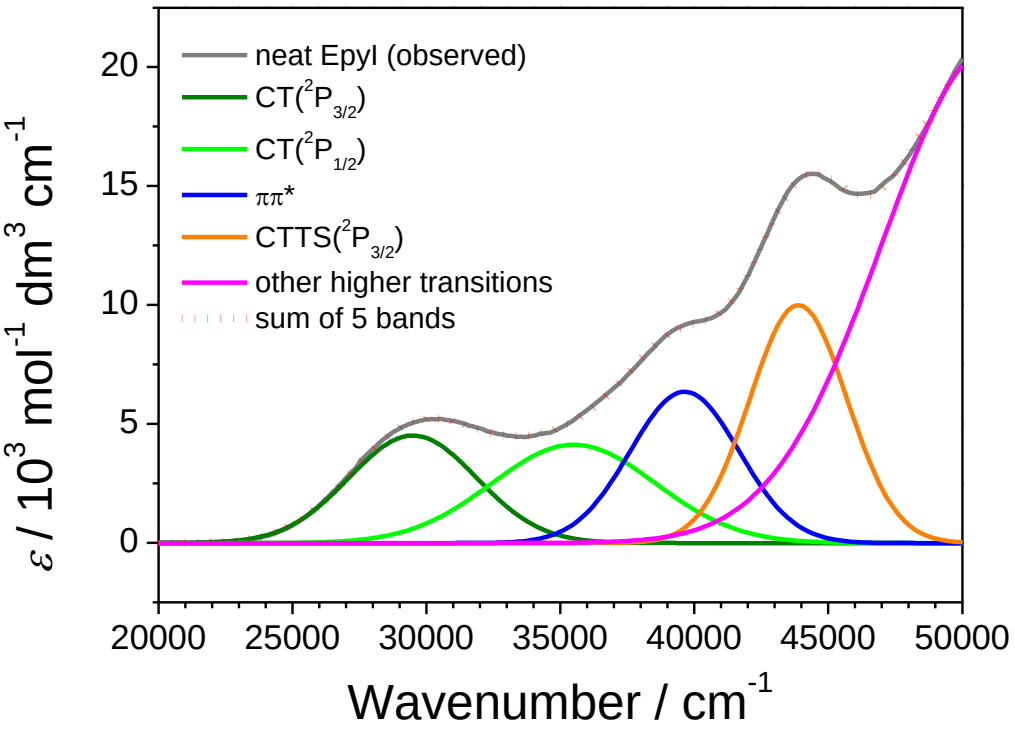

Figure 6-6.

Normalized absorption spectrum of neat EpyI (grey) and its deconvoluted spectra with 5 bands.

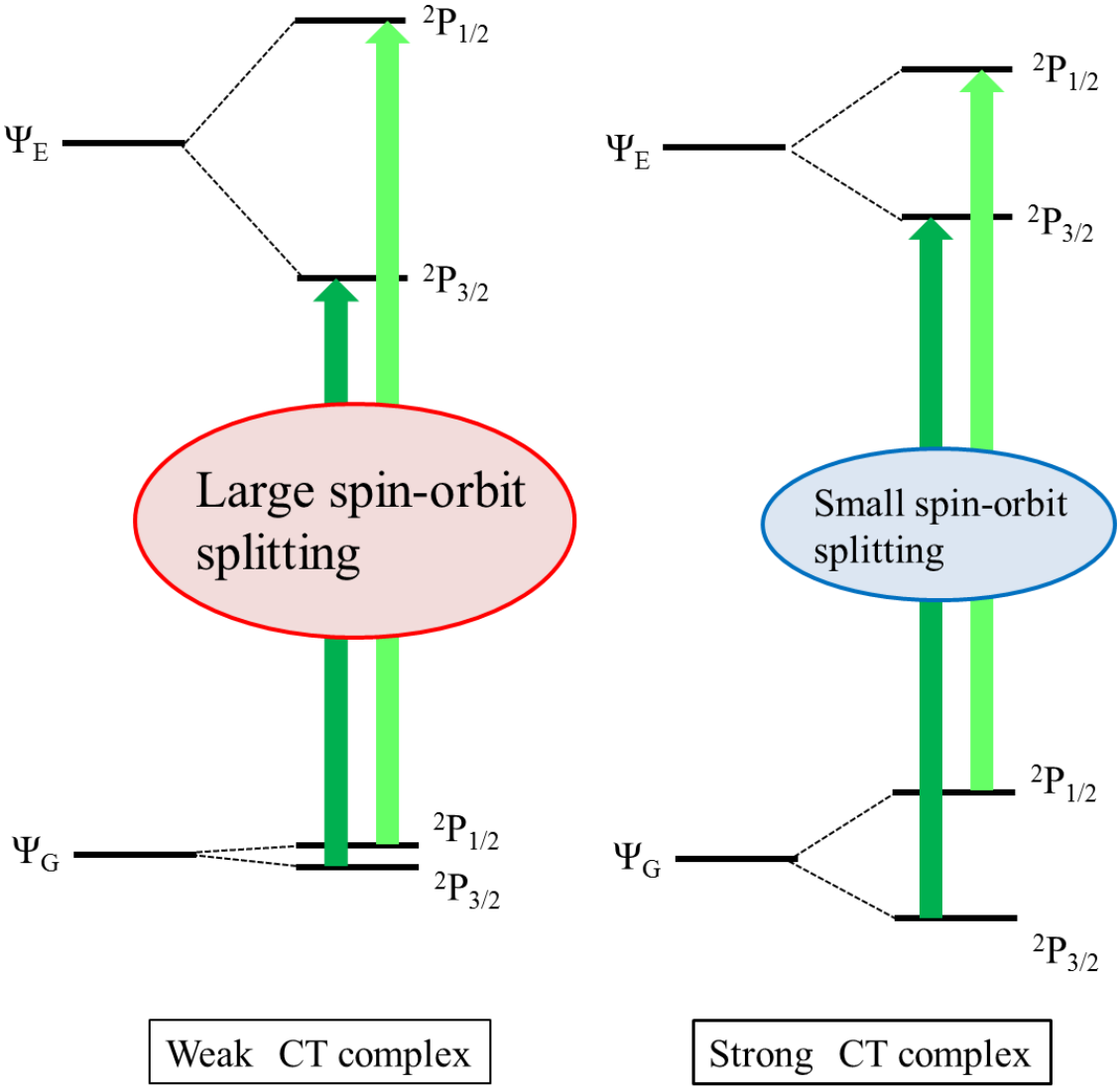

Figure 6-7.

Schematic picture of CT transitions with spin-orbit splitting due to iodine atom. Weak CT complex gives large splitting in absorption bands, while strong CT complex gives small one.

Chapter 7. Charge transfer interaction near ionic liquid-solid interface studied by evanescent wave absorption spectroscopy

7-1. Introduction

7-1-1. *Structure of RTILs near solid-liquid interface*

In the previous chapters from 3 to 6, CT interaction in various phases such as gas, solution, and neat liquid phases are discussed based on UV/VIS absorption spectroscopy. Besides CT interaction, there are various other interactions such as hydrogen-bonding, Coulomb interaction, and van der Waals interaction in neat RTILs, and various unique structures might develop as details were described in Chapter 1-2. Structural heterogeneity develops due to self-aggregation effects between alkyl chains leading to strongly ordered local environments predicted by MD simulation [1,2]. Many spectroscopic studies utilizing various techniques were focusing on RTIL structures [3-9]. Additionally, various different methods such as atomic force microscopy (AFM) [10], X-ray reflectivity studies [11], and sum-frequency generation (SFG) measurement [12-14] have been applied for the investigation of solid-RTIL interfaces, and they suggested that there are unique structures near interfaces. Mezger *et al.* suggested that the ordering structure of RTILs is up to about 1 nm from solid surface [11]. More recently, it is reported that there are longer unique structures with about 100 nm thickness and that translational diffusion of solutes has been influenced [15]. As

described above, there are many outstanding and interesting problems near solid-RTIL interface.

7-1-2. *Experimental results indicating interface's specialty*

There is another example that indicates solid-liquid interface's specialty. Asaka et al. reported synthesis of novel photochromic RTILs as shown in Chart 7-1 and studied [16,17] isomerization dynamics of $[2PA\text{-}Mmim]^+$ diluted in various solvents by transient absorption spectroscopy [18]. They also reported kinetic studies on thermal isomerization of neat $[2PA\text{-}Hmim]Tf_2N$ and neat $[2PA\text{-}MOEmim]Tf_2N$ liquids. Figure 7-1 (a) shows the absorption spectra of $[2PA\text{-}Hmim]Tf_2N$ recorded during thermal isomerization after UV irradiation. For this measurement, thin layer neat liquid was used to reduce absorbance. There are absorption bands of $S_1(n\pi^*)\leftarrow S_0$ transition around 460 nm and $S_2(\pi\pi^*)\leftarrow S_0$ transition around 350 nm due to E- and Z- form mixture. The absorption due to $S_1(n\pi^*)\leftarrow S_0$ transition of Z-form around 465nm decreases immediately after UV irradiation, and $S_2(\pi\pi^*)\leftarrow S_0$ transition of E-form around 300 nm decreases slightly. There are clear isosbestic points at 265 nm, 315 nm, and 429 nm.

Figure 7-1 (b) shows time evolution curve of measured absorbance at 365nm during thermal isomerization and their fitting curves with single and bi-exponential decay functions. It is obvious that bi-exponential fitting is better than single exponential fitting. In addition, decay curve of thermal isomerization becomes single exponential decay when the sample thickness increases. These results indicate that there would be

influence of solid-liquid interface. In absorption measurement by using 1 cm fused silica cell, most samples in light path are in bulk phase and small amount is in near interface region. However in thin layer sample with μm scale thickness, influence of interface would not be negligible. This may result in two components as bulk and interface in thermal isomerization process.

There are possible unique properties at interfaces such as liquid structures, optical properties, CT interaction, and so on. It is not obvious which factors have effect on thermal isomerization process at solid-liquid interface. One approach along the present study is to investigate CT interaction at interface region by absorption spectroscopy. Therefore, CT interaction of ion pairs near solid-liquid interface was focused to elucidate whether CT interaction near interface has effect on thermal isomerization process or not.

7-1-3. *Purpose of the present study*

Figure 7-2 shows normalized absorption spectra of (a) Toluene, (b) Pyridine, and (c) EmpyTf$_2$N as neat liquid and acetonitrile solution. The horizontal axes of Figure 7-2 (a) and (b) are wavenumber shift from 0-0 vibronic transition band. It is obvious that there are almost the same absorption band shapes of the lowest ππ* transitions between neat liquid and solution in three systems. Meanwhile, the absorption intensities of neat liquid around 200 nm are larger than those of solution. These results might suggest that the electronic transition dipole moments of absorption bands in VUV region are very

large, and red-shift of absorption band becomes larger due to solute-solute interaction in molecular solvent or CT interaction in RTILs. To study near interface region by absorption spectroscopy, interface sensitive method should be required. Therefore, attenuated total reflection (ATR) –UV/Visible (ATR-UV/Vis) absorption spectroscopy was introduced in the present study. Details of newly developed apparatus and analysis of the obtained spectra are explained in this chapter. CT interaction near solid-liquid interface is discussed by comparing the absorption spectra near solid-liquid interface with that of bulk phase.

7-2. Experimental

7-2-1. *Samples*

Details of samples were described in Chapter 2. Synthetic product of [2PA-MOEmim]Tf_2N was a kind gift from D.Kawamori [19] and it shows red color due to its absorption in VIS wavelength region. RTILs were used after purification by recrystallization from water to remove impurities of residual synthetic materials such as *n*-alkanes and pyridine. Water in RTILs was removed under vacuum.

7-2-2. *Attenuated Total Reflection (ATR) –UV/Visible spectroscopy*

Some research groups developed their original method of attenuated total reflection (ATR) –UV/Visible spectroscopy (ATR-UV/Vis) [20-23]. Principle of evanescent wave generation and ATR absorption method are explained in Section 7-3-1. In the present

section, an apparatus for ATR-UV/Vis absorption spectroscopy is explained by using scheme in Figure 7-3 (a). Absorption spectra were measured by using a UV/Vis fiber optic spectrophotometer (Stellar Net, EPP2000C) at room temperature. Accumulated time is one second, and wavelength resolution is 0.5 nm.

Excitation light was shaped as parallel light by two lenses as a telescope and was led to a sapphire prism of λ/20 profile irregularity. The sapphire prism could move along vertical axis depending on direction of excitation light which is controlled by the equipped rotary stage, and angle of optical fiber for monitor light was also controlled. Some optical properties are examined for the present spectrometer. Figure 7-3 (b) shows schematic picture of refraction angle (θ'), reflection angle (θ) and angle of incident light (φ). Relation of θ' and θ, as a function of φ are calculated based on Snell's law and the results were listed in Table 7-1.

Sample was dropped on the sapphire prism and was stored as thin layer by putting a cover glass on it. The sapphire prism was fixed by a holder with a sheet heater to make samples warm.

7-3. Results and discussion

7-3-1. *Principle of evanescent wave absorption spectroscopy*

Figure 7-4 (a) shows the principle of evanescent wave generation. Incident light which comes from inside of a crystal (refractive index; $n_D = n_1$) partially reflects and is refracted at the boundary surface with a sample ($n_D = n_2 < n_1$). When reflection angle

(θ) is larger than critical angle (θ_c), whole incident light reflects and is not refracted. In this case of so-called total reflection condition, evanescent wave is generated in sample side. If the sample absorbs evanescent wave, reflected light intensity decreases. This attenuation of the reflected beam is measured as absorbance by a UV/Vis spectrophotometer.

Absorbance (A) is defined as the logarithm of the ratio between intensities of the incident light (I_0) and of the reflected light (I) as eq. (1).

$$A = \log\left(\frac{I_0}{I}\right) \qquad (1)$$

Absorbance is also defined by Lambert-Beer's law described as eq. (2),

$$A(\lambda) = \varepsilon(\lambda)cl = \varepsilon(\lambda)c \cdot zd_{\mathrm{p}}(\lambda) \qquad (2)$$

where λ stands for excitation light wavelength, ε for a molar absorption coefficient, c for concentration of sample, l for the light path length, z for the number of reflections, and d_{p} for the depth of penetration of evanescent wave. Contrary to transmission spectroscopy, l is not constant because d_{p} into the sample is a function of θ, λ, n_1 and n_2 varying with temperature and wavelength.

Müller *et al*. suggested that the estimation of d_{p} changed whether media can absorb incident light or not [20]. The refractive index ($\tilde{n}$) is a complex number and is represented as the sum of the real refractive index (n) and the imaginary absorption index (κ) described by eq. (3).

$$\tilde{n} = n + i\kappa \qquad (3)$$

The latter component depends on the media's absorption feature. For media with

non-negligible κ, d_p is estimated by eq. (4).

$$d_p = \frac{\sqrt{2}\lambda}{2\pi n_1 \sqrt{\sqrt{\mu^2 + \nu^2} + \nu}} \qquad (4)$$

with

$$\mu = 2\kappa^2 \left(\frac{n_2}{n_1}\right)^2 \qquad (5)$$

$$\nu = (\sin\theta)^2 + \left(\frac{n_2}{n_1}\right)^2 (\kappa^2 - 1) \qquad (6)$$

Meanwhile in the case of non-absorbing media, κ is negligibly small, and eq. (4) is simplified to eq. (7).

$$d_p = \frac{\lambda}{2\pi \sqrt{{n_1}^2 (\sin\theta)^2 - {n_2}^2}} \qquad (7).$$

In the present section, eq. (7) was utilized for analysis of the results to obtain rough understanding of near liquid-solid interface region.

Figure 7-4 (b) shows estimated wavelength dispersion of refractive indices from Cauchy dispersion formula and some experimental values. The data of wavelength dispersion of refractive indices of EmpyTf$_2$N does not exist therefore data for N-butylpyridinium Tf$_2$N (BpyTf$_2$N) was used. It is obvious that refractive indices of toluene are larger than those of BpyTf$_2$N in whole UV/Vis wavelength region, and total reflection condition might be achieved by using a sapphire as a substrate. Figure 7-4 (c) shows the estimated d_p depending on light wavelength from eq. (7). The value of d_p changes depending on reflection angle, and estimated values are around 90 nm for θ=67° at the absorption peak wavelength indicated by an arrow. This 90nm is much

smaller than light path length of about 1000 nm in transmission measurement of neat liquid. Therefore, it is worth to measure electronic absorption using ATR near solid-liquid interface.

7-3-2. *ATR-UV/Vis absorption spectra of toluene and RTILs as neat liquids*

Figure 7-5 shows the absorption spectra of three samples, (a) toluene, (b) EmpyTf$_2$N, and (c) [2PA-MOEmim]Tf$_2$N measured by using ATR absorption spectroscopy. As a reference, spectra measured by a conventional transmission method were also shown. In the measurement of toluene as shown in Figure 7-5 (a), the number of reflection was 4, and measured absorbance was about 0.20. Molar absorption coefficient of toluene in aqueous solution at 260 nm was 225 mol^{-1} dm^3 cm^{-1} [24] and molar concentration of neat liquid was 9.5 mol dm^{-3}. From these numbers, d_p of 240 nm was estimated for the given wavelength region. It is obvious that there is cut-off wavelength. Cut-off wavelength is defined as breaking point of total reflection condition, appearing around 240 nm in toluene spectrum. Vibronic band structure is consistent with that of transmission spectrum.

In the measurement of EmpyTf$_2$N as shown in Figure 7-5 (b), the number of reflection was 2, and measured absorbance was about 0.24. Molar absorption coefficient of EmpyTf$_2$N in acetonitrile solution at 265 nm was 4.0 x 10^3 mol^{-1} dm^3 cm^{-1}, and molar concentration of neat liquid was assumed as 3.5 mol dm^{-3} from the density of BmimTf$_2$N. Therefore, estimated value of d_p is 90 nm. Absorption band in ATR

spectroscopy is slightly red-shifted from that of transmission, and there was no cut-off in the present wavelength region.

As for [2PA-MOEmim]Tf_2N shown in Figure 7-5 (c), number of reflection was 1, and measured absorbance was about 0.44. Molar absorption coefficient of [2PA-MOEmim]Tf_2N in toluene solution at 363 nm was 1.86 x 10^4 mol^{-1} dm^3 cm^{-1}, and molar concentration of neat liquid was assumed to be 2.73 mol dm^{-3}, which gave 70 nm as estimated value of d_p. $S_2(\pi\pi^*)$ band was due to allowed transition, and absorbance of the band was too high to measure even in thin film of neat liquid condition. Absorption band in ATR spectroscopy was red-shifted from that in transmission method in toluene solution, and there was no cut-off in this wavelength region.

These three samples of toluene, EmpyTf_2N, and [2PA-MOEmim]Tf_2N have much different values of molar absorption coefficients as described above. This difference is very important to consider relationship between existence of spectral shifts and value of electronic transition dipole moment. However, large electronic transition dipole moment causes anomalous dispersion of refractive indices, which requires detailed analysis of the data considering imaginary part of refractive index in eq.(3) to obtain exact absorption band shapes observed by ATR-UV/Vis spectroscopy.

7-3-3. *Simulation of ATR-UV/Vis absorption spectra*

Simulation of ATR-UV/Vis absorption spectra can be achieved by using measured absorption band by transmission and Kramers-Kronig relation. Extinction coefficient

$\kappa(\omega)$ was derived from eq. (8),

$$\kappa(\omega) = \frac{\varepsilon c \cdot \lambda}{4\pi} \qquad (8)$$

where ω stands for excitation light wavenumber. Then, refractive indices can be derived from eq.(9) as Kramers-Kronig relation.

$$n(\omega) = 1 + \frac{2}{\pi} \mathrm{P} \int_0^{\infty} \frac{\omega' \kappa(\omega')}{\omega'^2 - \omega^2} \mathrm{d}\omega' \qquad (9)$$

However, eq.(9) itself is not applicable for $n(\omega)$ calculation because integral can not be applied for whole wavenumber region. Therefore we applied eq. (10) as approximation,

$$n(\omega) = 1 + \frac{2}{\pi} \left\{ \int_0^{\omega_1} \frac{\omega' \kappa(\omega')}{\omega'^2 - \omega^2} \mathrm{d}\omega' + \int_{\omega_1}^{\omega_2} \frac{\omega' \kappa(\omega')}{\omega'^2 - \omega^2} \mathrm{d}\omega' + \int_{\omega_2}^{\infty} \frac{\omega' \kappa(\omega')}{\omega'^2 - \omega^2} \mathrm{d}\omega' \right\}$$

$$= 1 + \frac{2}{\pi} \left\{ 0 + \int_{\omega_1}^{\omega_2} \frac{\omega' \kappa(\omega')}{\omega'^2 - \omega^2} \mathrm{d}\omega' + n'(\omega) \right\} \qquad (10)$$

where ω_1 and ω_2 stand for the lowest and highest wavenumbers of measured spectral wavenumber region. The first term in parenthesis might be negligible because IR or microwave absorption coefficients are considerably small comparing to electronic absorption. The second term in parenthesis can be calculated from observed absorption spectra. The last term in parenthesis is complicated because large absorption above UV region enhances the refractive indices which is not constant and depends on excitation light wavelengths. Therefore, refractive indices derived from Cauchy dispersion formula assuming absorbing media as non-absorbing media were estimated to replace the last term in parenthesis.

Figure 7-6 shows plots of calculated $n(\omega)$ and $\kappa(\omega)$ values vs. excitation light wavenumber. To show $n(\omega)$ and $\kappa(\omega)$ in the same figure, $n(\omega)$-1.6 and $\kappa(\omega)$ were taken in vertical axis. It is clear that $\kappa(\omega)$ and anomalous dispersion of $n(\omega)$ become larger as ε increases in the order of (a) toluene < (b) $EmpyTf_2N$ < (c) [2PA-MOEmim]Tf_2N. Real part of refractive index, $n(\omega)$, increases drastically in the UV region above 30,000 cm^{-1} as shown in Figure 7-6 (a) and (b).

Figure 7-7 shows plots of d_p against wavelength for various reflection angle for the three liquids. Band shapes of $\kappa(\lambda)$ are also presented. In toluene and $EmpyTf_2N$, d_p is almost the same value in whole wavelength region because absorption of these materials are weak and influence of imaginary $\kappa(\lambda)$ is negligible. Meanwhile, in [2PA-MOEmim]Tf_2N, the values of d_p at the red wavelength side of $S_2(\pi\pi^*)\leftarrow S_0$ transition absorption band drastically change depending on reflection angle. This calculation result implies that the reflection angle must be appropriately controlled to suppress influence of $\kappa(\lambda)$ for absorption band shapes in ATR-UV/Vis absorption spectroscopy. Meanwhile, d_p in wavelength region being shorter than 350nm does not depend on reflection angle. This region corresponds to higher energy region from $S_2(\pi\pi^*)\leftarrow S_0$ transition absorption band. Absorption spectra near solid-liquid interface in this wavelength region can be observed for about 50 nm depth independent on reflection angle as shown in Figure 7-7 (c).

Figure 7-8 shows calculated absorption spectra for various reflection angles. Absorption band shape obtained by the transmission method is also presented. It is

obvious that there is peak shift in the calculated absorption band for [2PA-MOEmim]Tf_2N. This is due to changes of optical properties around intense $S_2(\pi\pi^*)$ band as mentioned above. Meanwhile, in toluene and EmpyTf_2N, simulated absorption bands and observed one by transmission method were good consistent with each other.

Figure 7-9 shows comparison of observed and simulated absorption spectra for the three liquids. It is obvious that experimental and simulated results are not good consistent with each other. It is necessary to clarify whether this result is due to difference of electronic absorption near solid-liquid interface or incomplete data processing in ATR spectroscopy. Major four reasons of difference due to incomplete data processing in ATR spectroscopy are considered to understand why simulated and observed absorption spectra disagrees; (1) the parameter, $\kappa(\lambda)$ in solution is used instead of value in neat liquid, (2) estimated $n(\lambda)$ is not precise value because Cauchy dispersion formula in VIS wavelength region is extended to obtain $n(\lambda)$ in UV region, (3) actual value of d_p has experimental error because excitation light is not perfect parallel beam, and (4) wavelength dispersion of incident light in the sapphire prism results in distributed reflection angle for excitation light. By analyzing details of experimental and simulated results, these four reasons abbreviated as R1 ~ R4, respectively, were discussed in the following.

First, R3 is easily excluded. The error bar of incident light angle was estimated as about 2^o from measurement of light expansion degree, and this value does not have

large error for ATR-UV absorption measurement. Second, R4 is relatively not important. Wavelength dispersion of incident light in sapphire prism is summarized as reflection angle θ in Table 7-1. As seen in example of ϕ=60^{o}, the wavelength dispersion as reflection angle θ from 230 nm to 300 nm is not large, as about 2^{o}. This slight change is not important for d_p of toluene and EmpyTf$_2$N as shown in Figure 7-7 (a) and (b). Meanwhile, in [2PA-MOEmim]Tf$_2$N, d_p changes drastically depending on reflection angle as shown in Figure 7-7 (c). However, this value is almost constant in visible wavelength region. After that, R3 might not be important in the present measurement. Therefore, R1 and R2 are focused in following paragraph.

In toluene shown in Figure 7-9 (a), observed absorption intensity is much larger than simulated one, and there is cut-off wavelength in the experimental result. This result implies that actual d_p is much larger than simulated one. In the present case, R1 is not important due to very small $\kappa(\lambda)$ even in neat liquid. Therefore, the main reason is considered to be R2, and actual refractive indices of toluene in UV region are larger than estimated values from Cauchy dispersion formula due to influence of very large anomalous dispersion in VUV region. Estimated refractive index of toluene from Cauchy dispersion formula at 240 nm is 1.66, and experimental result under breaking of total reflection condition indicates actual refractive index of refractive index is 1.76. It is likely that there is difference by about 0.1 between these values in UV region. Additionally, it is obvious that there are no peak shifts between simulated and experimental spectra.

In EmpyTf$_2$N shown in Figure 7-9 (b), observed absorption intensity is much larger than simulated one. This result means that actual refractive indices of EmpyTf$_2$N are larger and perhaps close to those of sapphire. In the present case, R1 is considered not to be important due to small $\kappa(\lambda)$ in neat liquid. Therefore, the main reason is also R2 in EmpyTf$_2$N. Then, there are peak shift and change of band shape between simulated and experimental spectra.

In [2PA-MOEmim]Tf$_2$N shown in Figure 7-9 (c), absorption intensity in observed spectrum is much smaller than that of simulated one. This experimental and simulated results show two possibilities as follows; (1) $\kappa(\lambda)$ in toluene solution is slightly lower than that in neat liquid concerning R1, and (2) $n(\lambda)$ of azobenzene used as the parameter of [2PA-MOEmim]Tf$_2$N is larger than that of [2PA-MOEmim]Tf$_2$N for R2. We consider that R2 is the most important reason. Azobenzene and [2PA-MOEmim]$^+$ have almost the same absorption intensities at almost the same wavelength region. However, there is significant difference between the two materials: all molecules are chromophore in neat azobenzene, meanwhile, neat [2PA-MOEmim]Tf$_2$N includes only 50 % of choromophore, 2PA-MOEmim$^+$. This fact implies that $n(\lambda)$ of [2PA-MOEmim]Tf$_2$N might be smaller than those of azobenzene. Then, there are peak shift and change of band shape between simulated and experimental spectra.

It is worthwhile to compare the absorption peaks obtained by ATR-UV/Vis absorption spectroscopy with that obtained by absorption spectroscopy of transmission method. According to the results, $\pi\pi^*$ absorption peaks near solid-liquid interface are

more red-shifted than those in bulk phase in EmpyTf_2N and [2PA-MOEmim]Tf_2N neat liquids. This experimental finding implies that polarity of RTILs near solid-liquid interface is larger than that in bulk phase due to unique interface structure. However, in the case of large $\kappa(\lambda)$, simulation of absorption bands near solid-liquid interface are complicated, which results in large analytical and experimental errors. Therefore, whether observed red-shift has physical meanings or not cannot be elucidated. It is very important to overcome this problem by measuring concentration dependence on absorption band shapes.

7-3-4. *ATR-UV/Vis absorption spectra of RTILs depending on chromophore concentration*

Figure 7-10 shows ATR absorption spectra for various concentration of solutes. In the case of EmpyTf_2N diluted by TMPATf_2N as shown in Figure 7-10 (a), absorption band shape does not change. This result indicates that absorption peak shifts are not derived from $\kappa(\lambda)$ of EmpyTf_2N. If peak shifts were derived from simple dependence on $d_p(\lambda)$, this shift quantity would be too large to reproduce observed spectrum as described in next section. Therefore, it is concluded that the difference between band shapes in the spectra by ATR-UV/Vis and by transmission methods originates from physical meanings. Meanwhile, in the case of [2PA-MOEmim]Tf_2N diluted by BmimTf_2N as shown in Figure 7-10 (b), absorption band shape changes drastically. This result means that absorption peak shifts are derived from $\kappa(\lambda)$ of [2PA-MOEmim]Tf_2N. From simulated result as shown in Figure 7-7 (c), there found almost the constant value of d_p

below 370 nm. Therefore, spectrum in limitary region from 370 nm to 300 nm are discussed for [2PA-MOEmim]Tf_2N. It is obvious that there are no peak shift of $S_2(\pi\pi^*)\leftarrow S_0$ transition absorption band as 363 nm pointed out by an arrow in Figure 7-10 (b) . However, this value of 363 nm is not consistent with that obtained by transmission method of 361 nm. From these results, two novel facts were found: (1) $S_2(\pi\pi^*)\leftarrow S_0$ transition energies of [2PA-MOEmim]Tf_2N in diluted solution and neat liquid are almost the same, and (2) there are slight transition energy changes between solid-liquid interface and bulky phase.

7-3-5. *ATR-UV/Vis absorption spectra of dyes diluted in RTILs*

Figure 7-11 (a) shows calculated d_p as a function of light wavelength from eq. (7). Obtained wavelength dispersion of RTILs was only for $BpyTf_2N$ [25], and thus, $BpyTf_2N$ was chosen as the representative to estimate $d_p(\lambda)$. The d_p value changes linearly depending on reflection angle, therefore, d_p vs. λ can be approximately obtained by the following equation; $d_p(\lambda) = 0.19\lambda + 9$ [nm] from 300 nm to 600 nm. Absorption band peaks do not change largely under calibration by this equation as shown in Figure 7-11 (b) and (c). In the present case, red-shifted absorption bands were observed by ATR-UV/Vis absorption spectroscopy. However, there still remains unknown why transition energies of dyes in RTILs decreases near solid-liquid interface.

7-3-6. *Charge transfer interaction near solid-liquid interface*

Absorption spectrum of neat EpyI near solid liquid interface were observed by ATR method to understand CT interaction through analysis of CT transition absorption band. Figure 7-12 shows absorption spectra of neat EpyI obtained by transmission and reflection methods. There is obvious spectral shift of the lowest CT transition absorption band from 330 nm to 397 nm. Unfortunately, there are not enough optical data of EpyI to simulate the absorption spectra obtained by reflection method. Therefore, discussion was focused on spectral shift of absorption bands obtained by the transmission and the reflection methods qualitatively.

In neat [2PA-MOEmim]Tf_2N as shown in Figure 7-5 (c), spectral shift is estimated as almost 2700 cm^{-1}. Meanwhile, in neat EpyI shown in Figure 7-12, spectral shift is estimated as almost 5100 cm^{-1}. This is the curious result showing remarkably large spectral shift near interface region. The $\kappa(\lambda)$ of [2PA-MOEmim]Tf_2N is about 4 times as large as that of EpyI, therefore anomalous dispersion and spectral shift of [2PA-MOEmim]Tf_2N should be larger than those of EpyI. However, spectral shift of [2PA-MOEmim]Tf_2N is smaller than that of EpyI. This result implies that there is red-shifted absorption band between EpyI near solid-liquid interface region and in bulk phase.

From the results in the previous sections, it was concluded that polarity of RTILs near solid-liquid interface would be larger than bulk phase. High polarity leads low CT interaction between cation and anion because charge would be more localized on individual ions. Therefore, there is reduction of CT transition energy near solid –liquid

interface. This means that charge distribution of ion pairs near solid-liquid interface is close to that of isolated ion pair diluted in non-polar solvent. Further experiments and revise theoretical simulation are in necessity to answer these implicative questions.

7-4. Conclusion

Experimental apparatus for ATR/UV-Vis absorption spectroscopy was set up to measure absorption spectra near liquid-solid interfaces. Electronic transition absorption bands of chromophores near solid-liquid interface were measured for about 60 nm in depth from the interface. Based on simulated results, it was elucidated that there would be decrease of transition energies of chromophores near solid-liquid interface in RTIL solution and neat RTILs. This finding implies that CT interaction is lowered near interface region.

References of Chapter 7

[1] J.N.A. Canongia Lopes and A.A.H. Pádua, *J. Phys. Chem. B* **110**, 3330 (2006).

[2] A.A.H. Pádua, M.F. Costa Gomes, and J.N.A. Canongia Lopes, *Acc. Chem. Res.* **40**, 1087 (2007).

[3] H. Hamaguchi, S. Saha, R. Ozawa, S. Hayashi, ACS. Symp. Ser. **901**, 68 (2005).

[4] N. Akai, A. Kawai, K. Shibuya, *Chem. Lett.* **37**, 256 (2008).

[5] H. Shirota, J.F. Wishart, E.W. Castner Jr., *J. Phys. Chem. B* **111**, 4819 (2007).

[6] M.-M. Huang, Y. Jiang, P. Sasisanker, G.W. Driver, H. Weingärtner,

J. Chem. Eng. Data **56**, 1494 (2011).

[7] H. Tokuda, K. Hayamizu, K. Ishii, Md.A.B.H. Susan, M. Watanabe, *J. Phys. Chem. B* **108**, 16593 (2004).

[8] D.C. Khara, A. Samanta, *Phys. Chem. Chem. Phys.* **12**, 7671 (2010).

[9] A. Triolo, O. Russina, H.J. Bleif, and E. Di Cola, *J. Phys. Chem. B* **111**, 4641 (2007).

[10] R. Hayes, G.G. Warr, R. Atkin, *Phys. Chem. Chem. Phys.* **12**, 1709 (2010).

[11] M. Mezger, S. Schramm, H. Schroder, H. Reichert, M. Deutsch, E.J. De Souza, J.S. Okasinski, B.M. Ocko, V. Honkimaki, H. Dosch, *J. Chem. Phys.* **131**, 094701 (2009).

[12] S. Baldelli, *Acc. Chem. Res.* **41**, 421 (2008).

[13] B.D. Fitchett, J.C. Conboy, *J. Phys. Chem. B* **108**, 20255 (2004).

[14] T. Iimori, T. Iwahashi, H. Ishii, K. Seki, Y. Ouchi, R. Ozawa, H. Hamaguchi, D. Kim, *Chem. Phys. Lett.* **389**, 321 (2004).

[15] S. Iwata et al., Annual Meeting of Japan Society for Molecular Science (2011).

[16] T. Asaka, N. Akai, A. Kawai, K. Shibuya, *J. Photochem. Photobio. A* **209**, 12 (2010).

[17] A. Kawai, D. Kawamori, T. Monji, T. Asaka, N. Akai, K. Shibuya, *Chem. Lett.* **39**, 230 (2010).

[18] A. Ida, B. Cohen, T. Asaka, A. Kawai, J.A. Organero, K. Shibuya, A. Douhal, *Phys. Chem. Chem. Phys.* **13**, 20318 (2011).

[19] D. Kawamori, Master thesis (2011).

[20] G. Müller, K. Abraham, A. Schaldach, *Appl. Opt.* **20**, 1182 (1981).

[21] H. Schlemmer, J. Katzer, *Anal. Chem.* **329**, 435 (1987).

[22] Y. Morisawa, A. Ikehata, N. Higashi, Y. Ozaki, *Chem. Phys. Lett.* **476**, 205 (2009).

[23] P. Billot, M. Couty, P. Hosek, *Org. Process Res. Dev. 14*, 511 (2010).

[24] J.R. Dyer, Applications of Absorption Spectroscopy of Organic Compounds, Prentice-Hall, Englewood Cliffs, N.J., 1965.

[25] U. Brackmann, Lambdachrome Laser Dyes (2nd revised Edition), Lambda Physik, Göttingen, Germany, 1994.

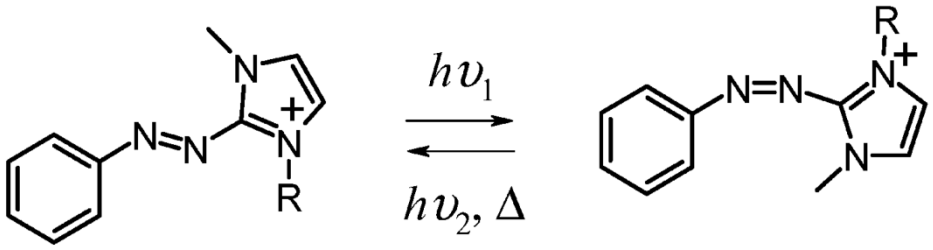

E-form Z-form

$[2PA\text{-}Rmim]^+$

$[2PA\text{-}Hmim]^+$ for R=Hexyl

$[2PA\text{-}Mmim]^+$ for R=Methyl

$[2PA\text{-}MOEmim]^+$ for R=Metoxyethyl

Chart 7-1. Photochemical and thermal E–Z isomerization reaction of $[2PA\text{-}Rmim]^+$ cation. [2PA-MOEmim] Tf_2N : 2-phenylazo-1-metoxyethyl-3-methylimidazolium bis(trifluoromethanesulfonyl)amide.

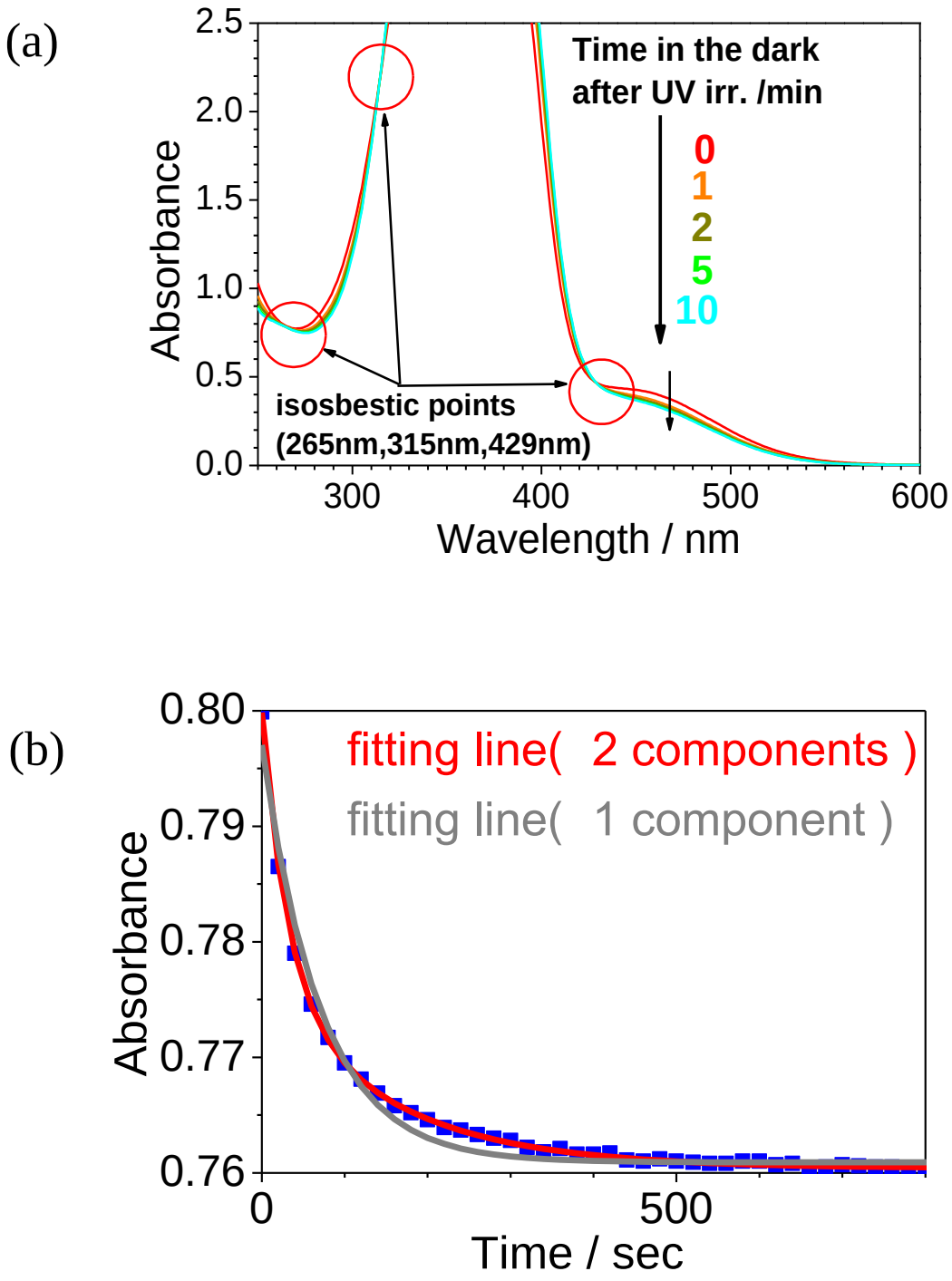

Figure 7-1. (a) Absorption spectra of neat [2PA-Hmim]Tf_2N during thermal isomerization after UV irradiation stopped. (b) The measured change in absorbance during thermal isomerization, and their fitting curves by single exponential and biexponential decay functions.

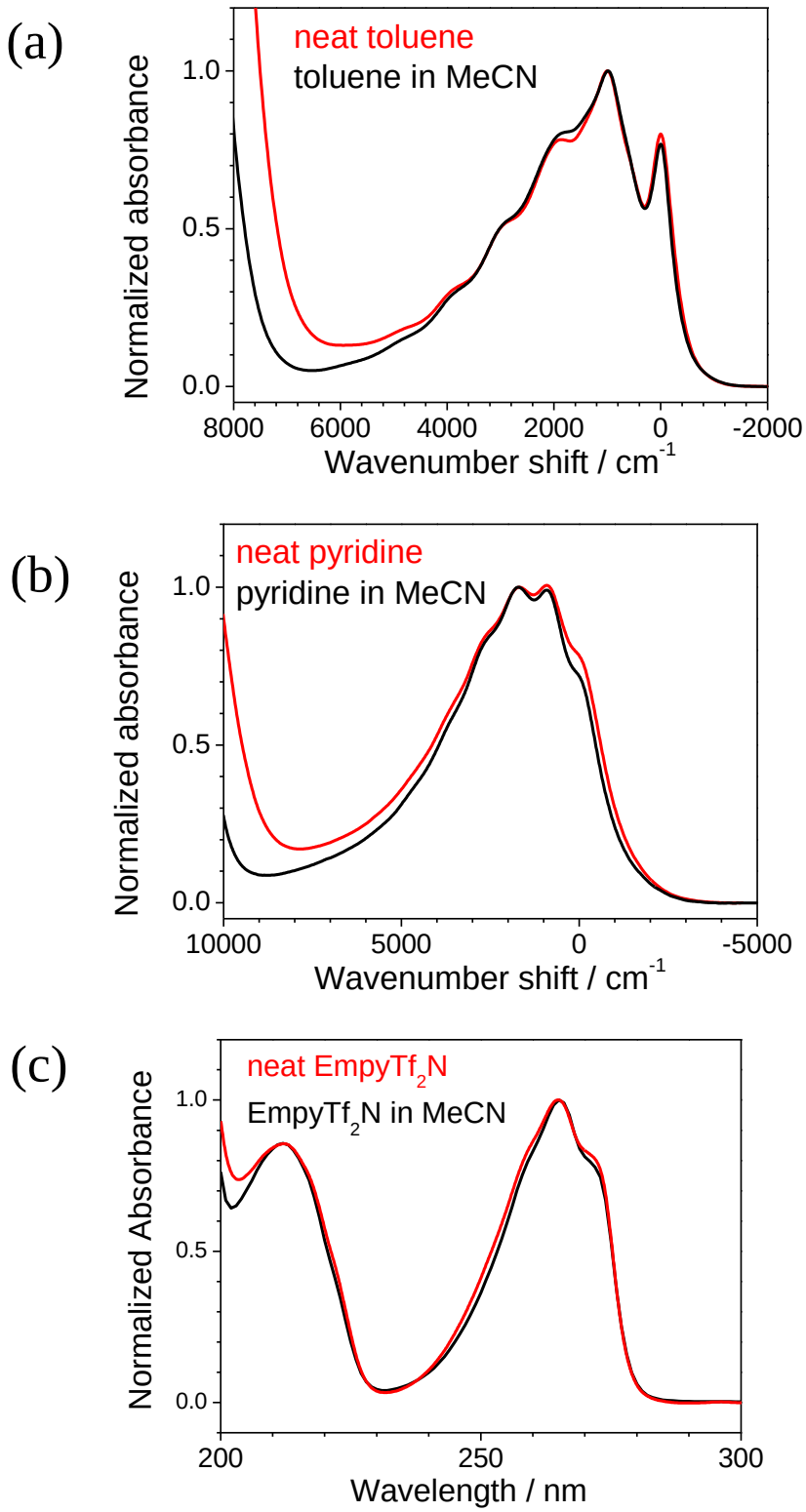

Figure 7-2. Normalized absorption spectra of (a) Toluene, (b) Pyridine, and (c) $EmpyTf_2N$ as neat liquids and acetonitrile solutions.

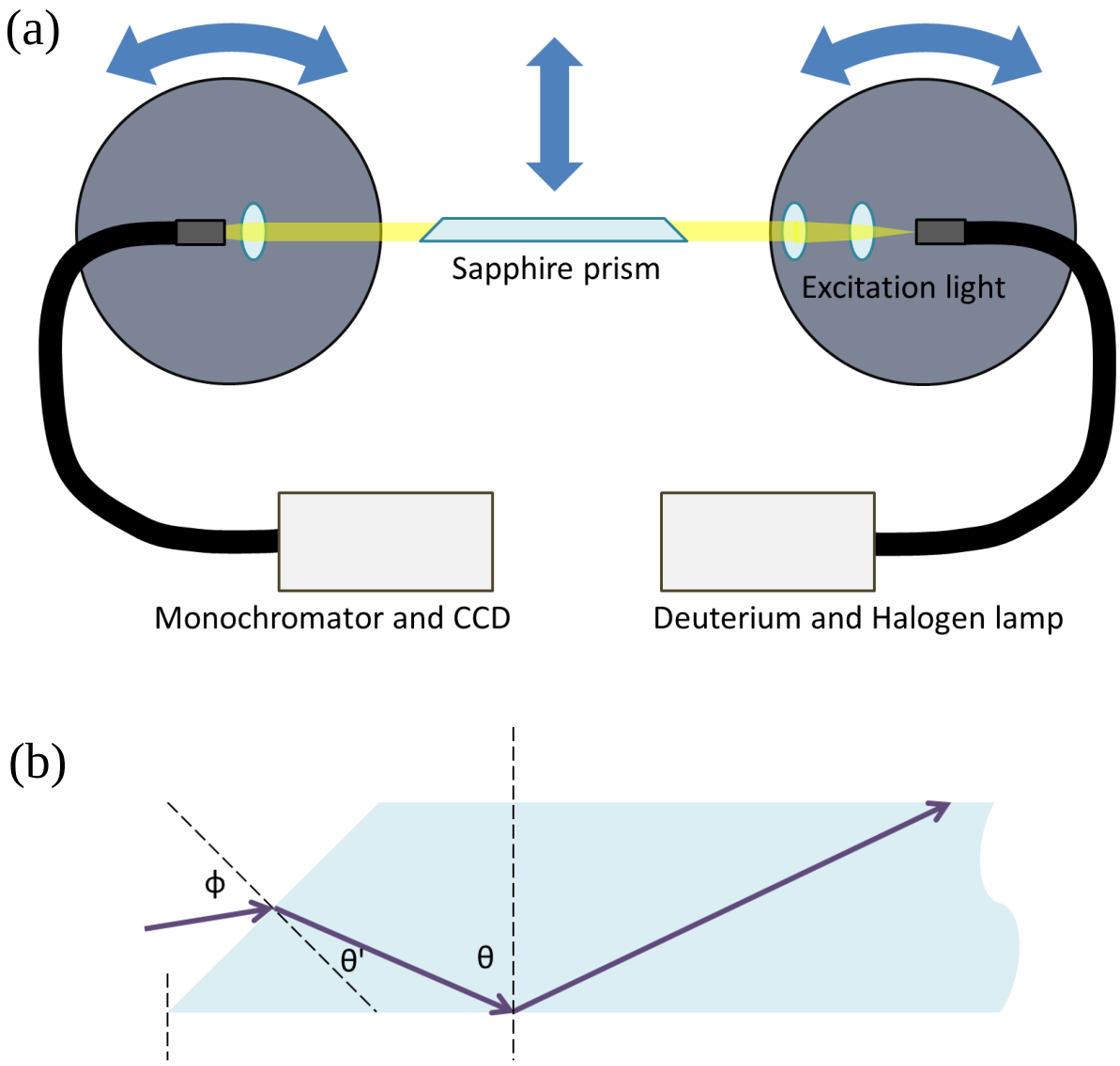

Figure 7-3. (a) Experimental apparatus for ATR-UV/Vis absorption spectroscopy, and (b) View of incident light and sapphire prism.

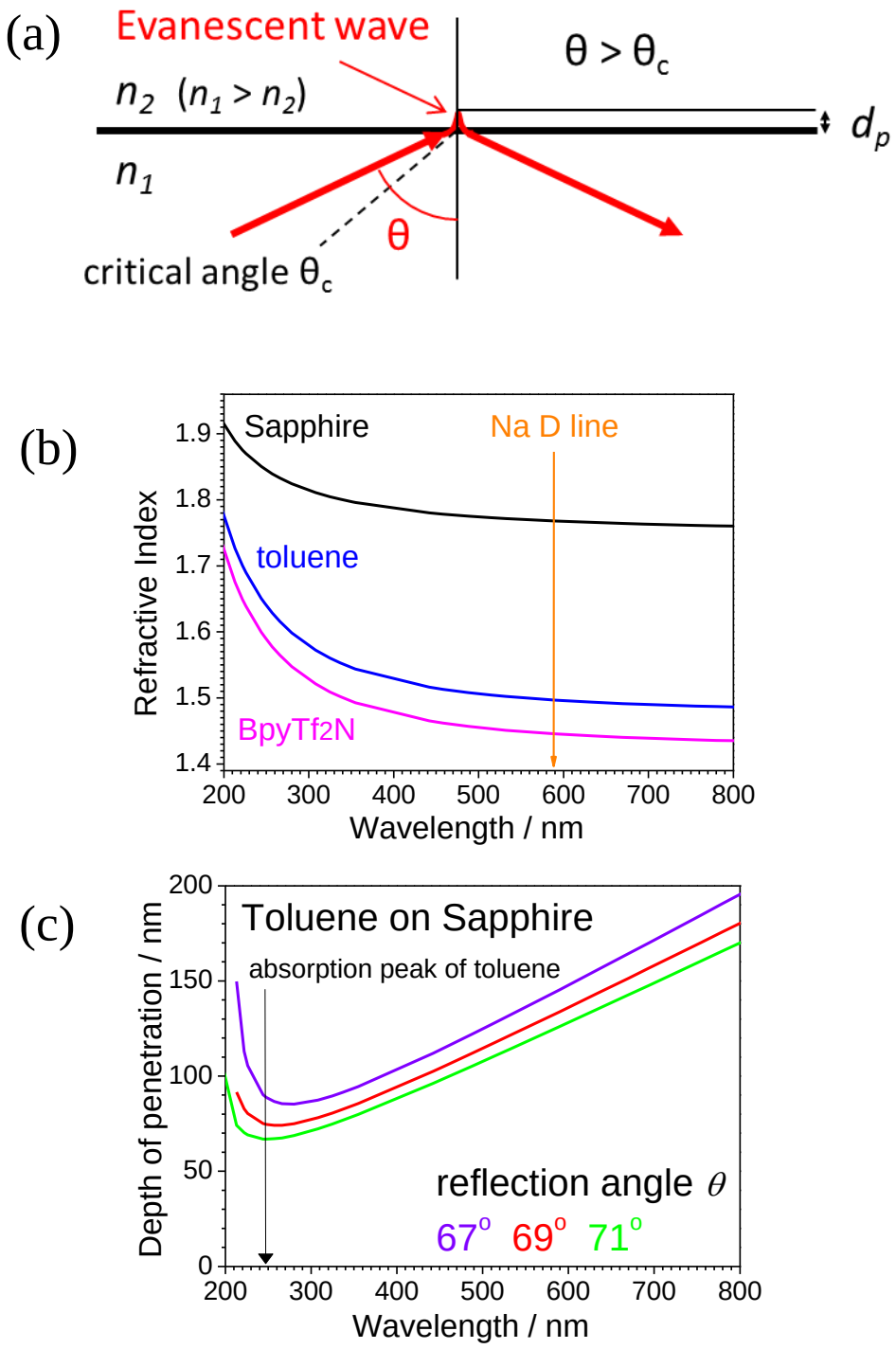

Figure 7-4. (a) Principle of evanescent wave generation, (b) estimated wavelength dispersion of refractive indices, and (c) estimated depth of penetration (d_p) depending on light wavelength in the case of toluene on sapphire.

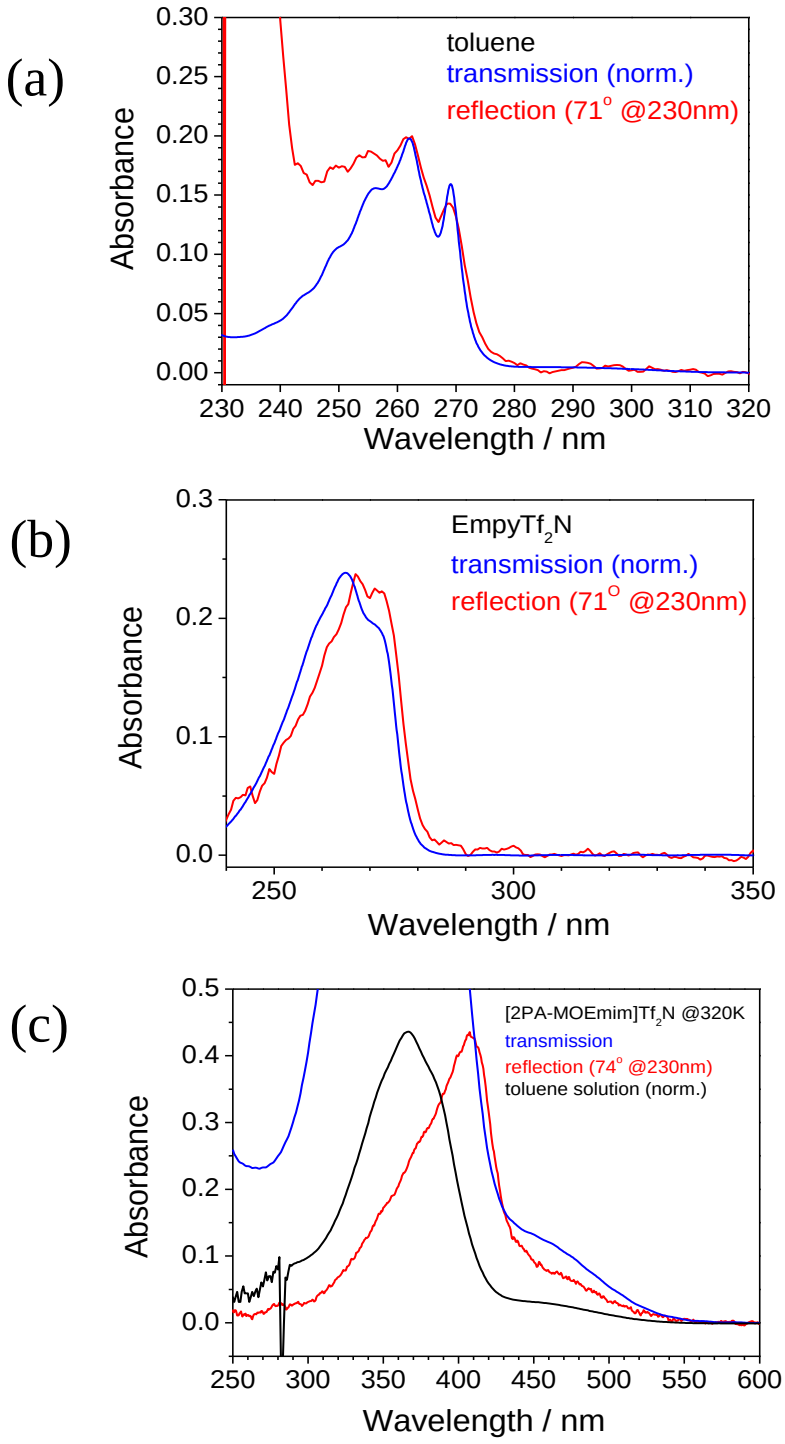

Figure 7-5. Absorption spectra of neat liquids by using reflection method (red), transmission method (blue), and that of toluene solution by using transmission method (black) as (a) toluene, (b) $EmpyTf_2N$, and (c) $[2PA\text{-}MOEmim]Tf_2N$.

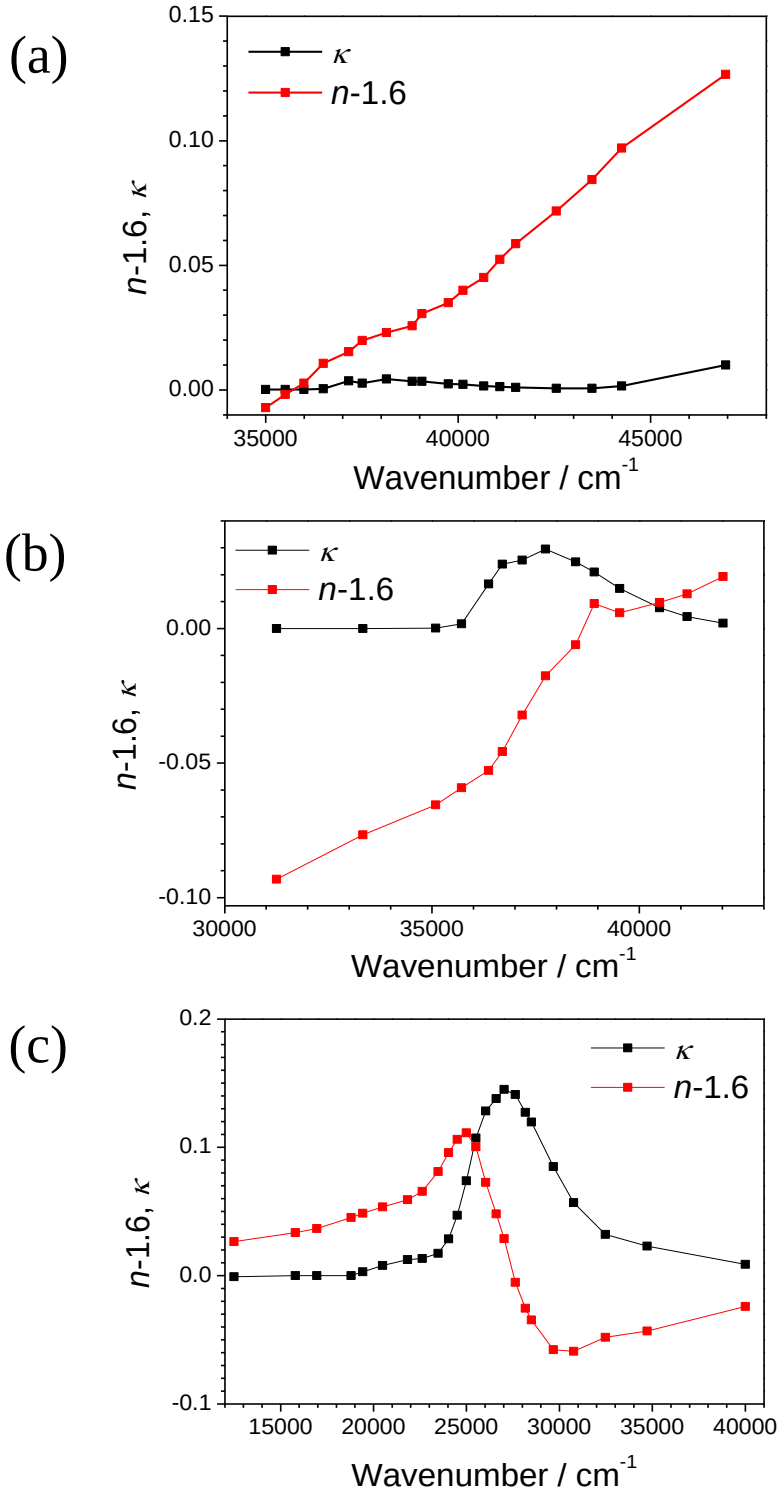

Figure 7-6. Plots of calculated values for refractive index (n) and extinction coefficient (κ) vs. excitation light wavenumber of (a) toluene, (b) EmpyTf$_2$N, and (c) [2PA-MOEmim]Tf$_2$N..

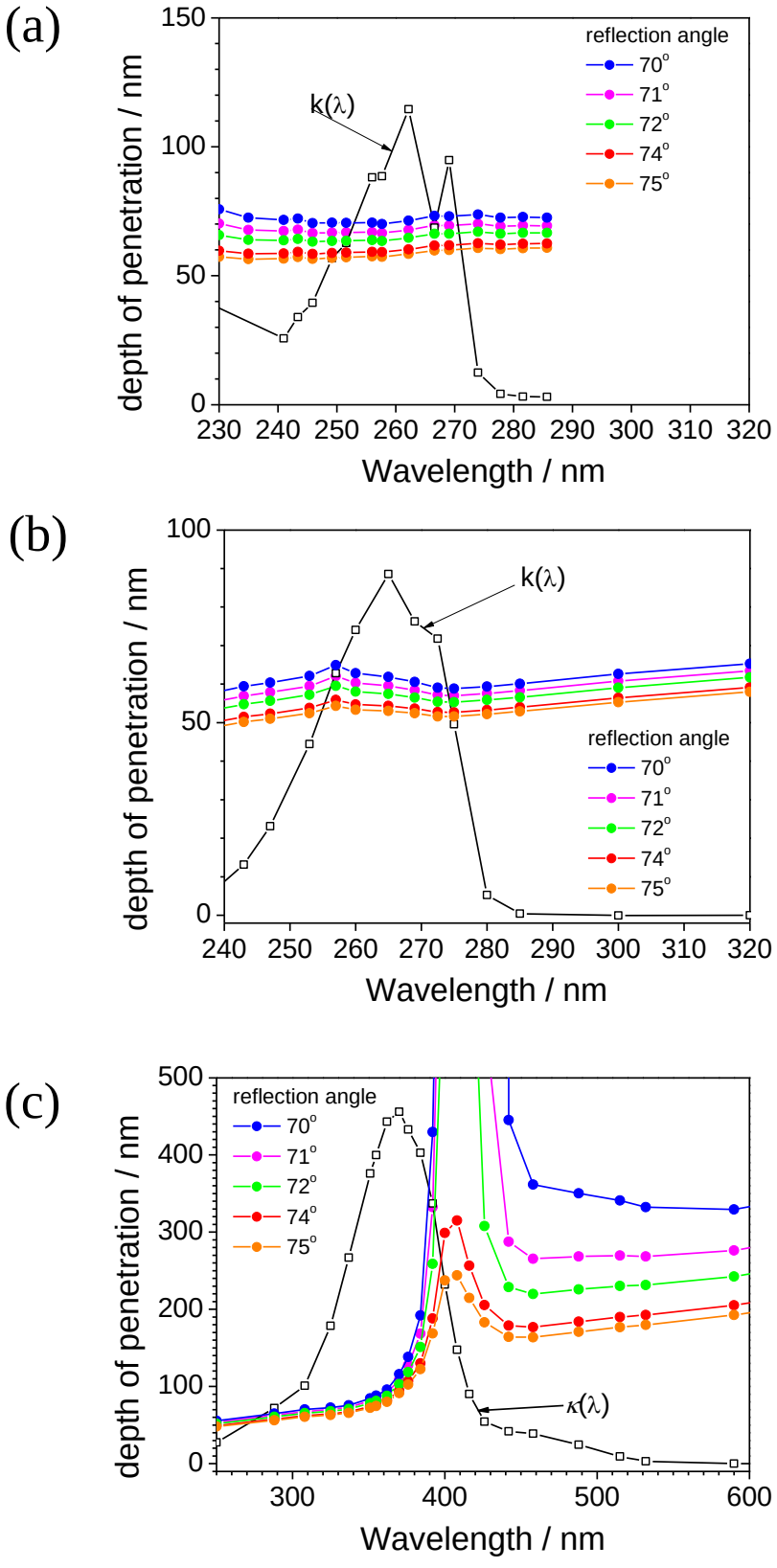

Figure 7-7. Theoretically estimated depth of penetration (d_p) depending on reflection angle comparing with band shape of κ for (a) toluene, (b) EmpyTf$_2$N, and (c) [2PA-MOEmim]Tf$_2$N.

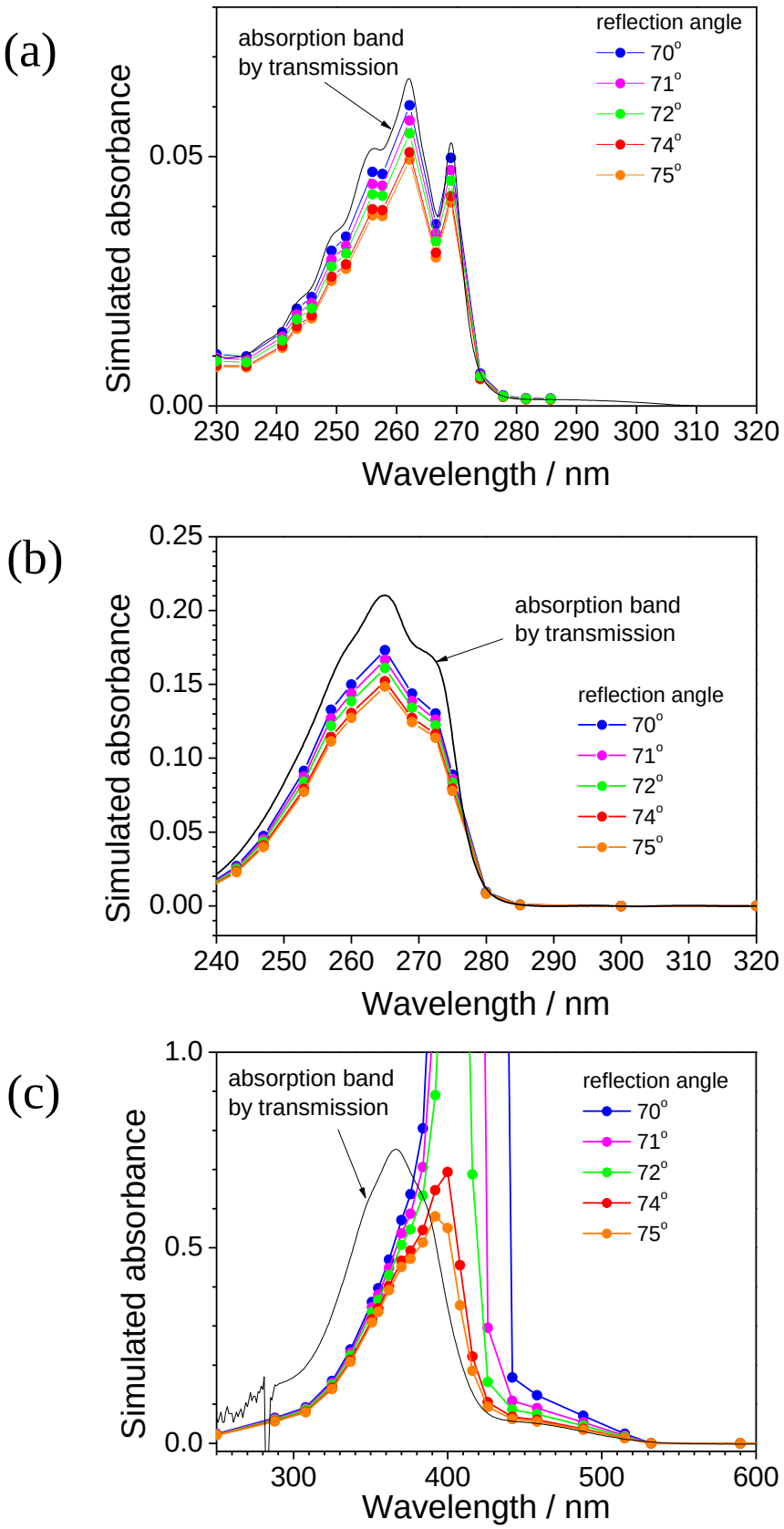

Figure 7-8. Calculated absorption band for various reflection angle and observed one by transmission method. (a) toluene (z=4), (b) EmpyTf$_2$N (z=2), and (c) [2PA-MOEmim]Tf$_2$N (z=1).

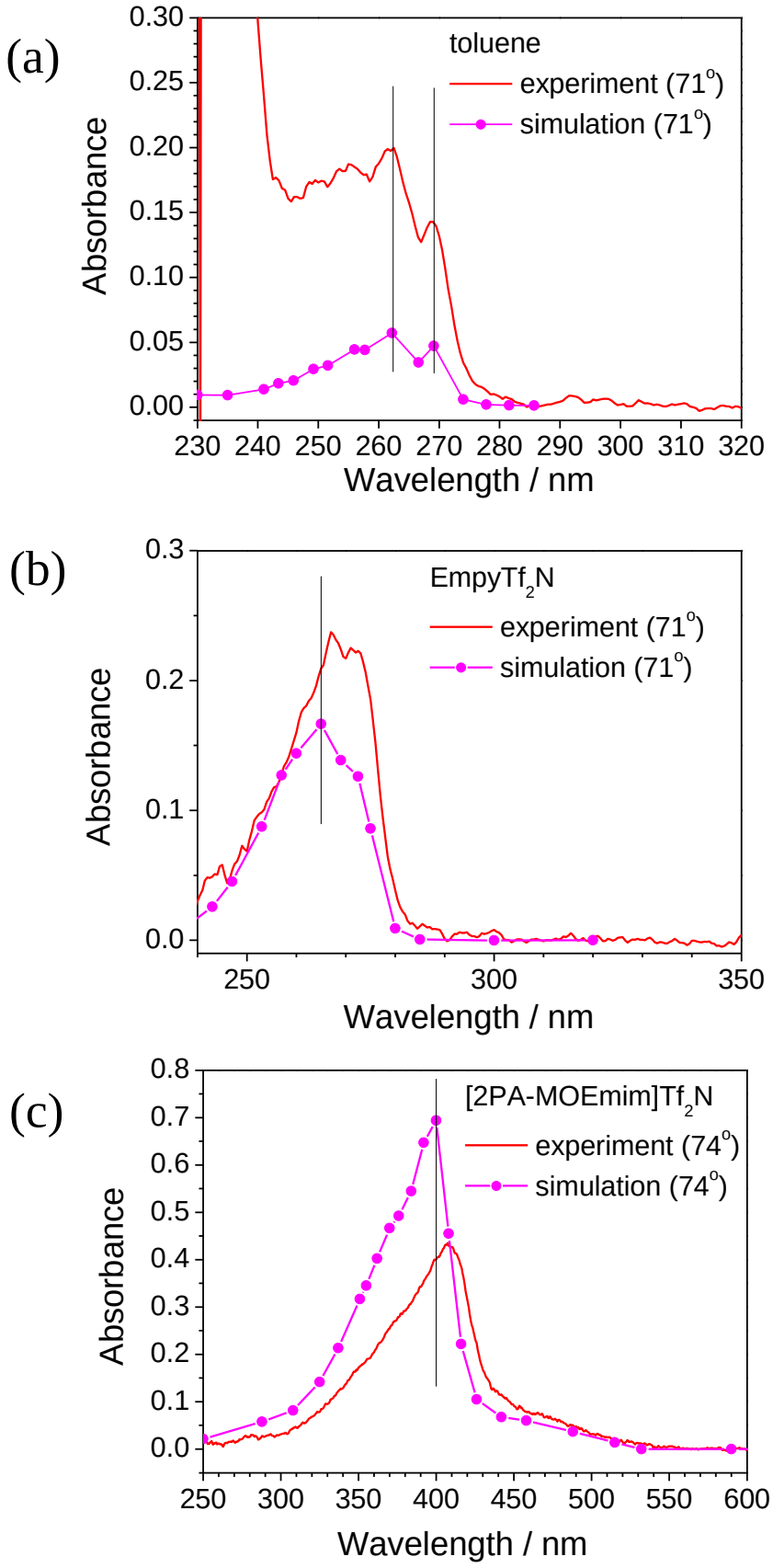

Figure 7-9. Observed ATR and simulated absorption spectra of (a) toluene, (b) $EmpyTf_2N$, and (c) $[2PA\text{-}MOEmim]Tf_2N$. The numbers in parenthesis mean the reflection angle.

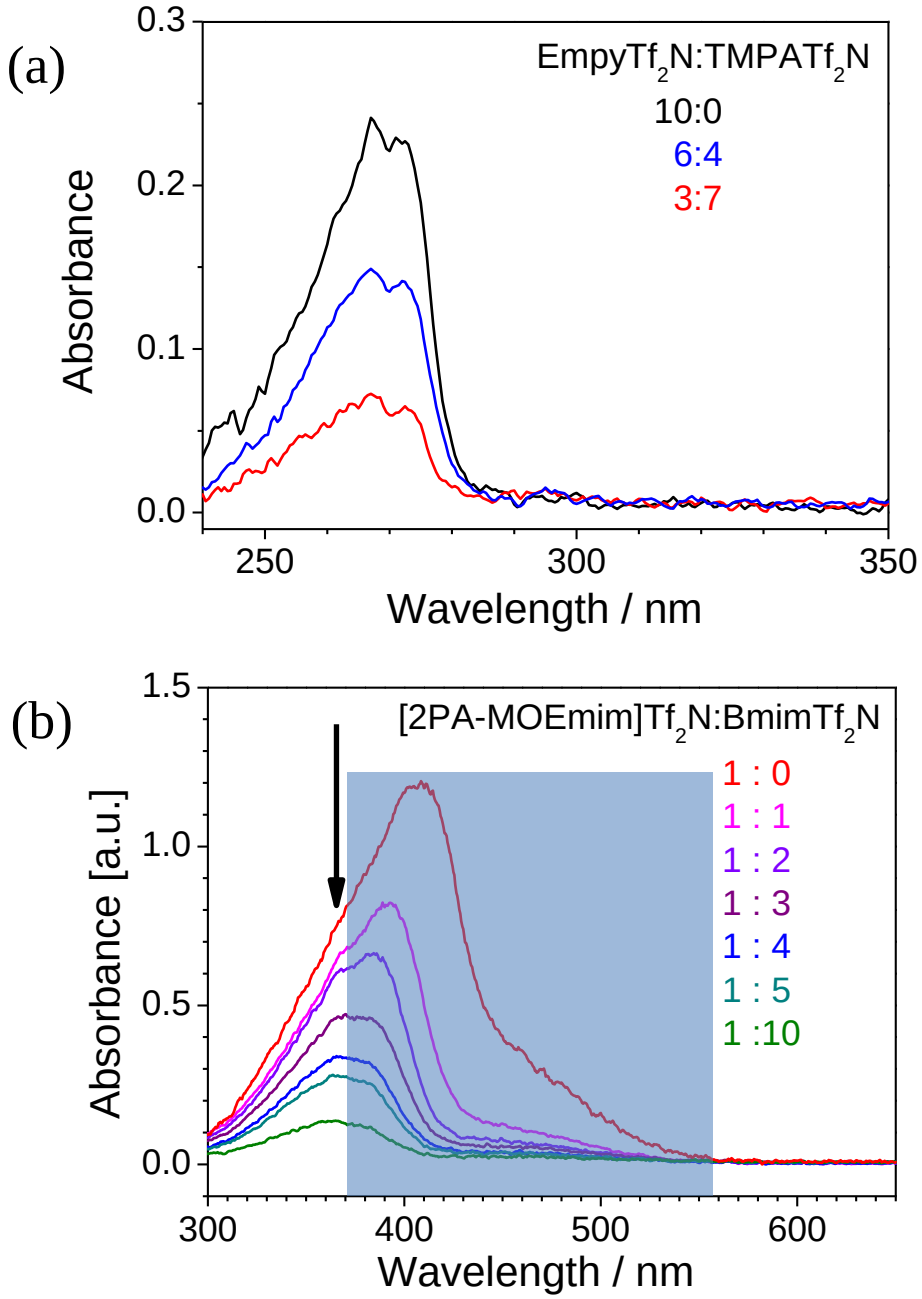

Figure 7-10. Absorption spectra by ATR method for various concentration of (a) $EmpyTf_2N$ in $EmpyTf_2N/TMPATf_2N$ mixture, and (b) $[2PA\text{-}MOEmim]Tf_2N$ in $[2PA\text{-}MOEmim]Tf_2N/BmimTf_2N$ mixture . The numbers in vertical axis of (b) are arbitrary units due to various number of reflections for each samples.

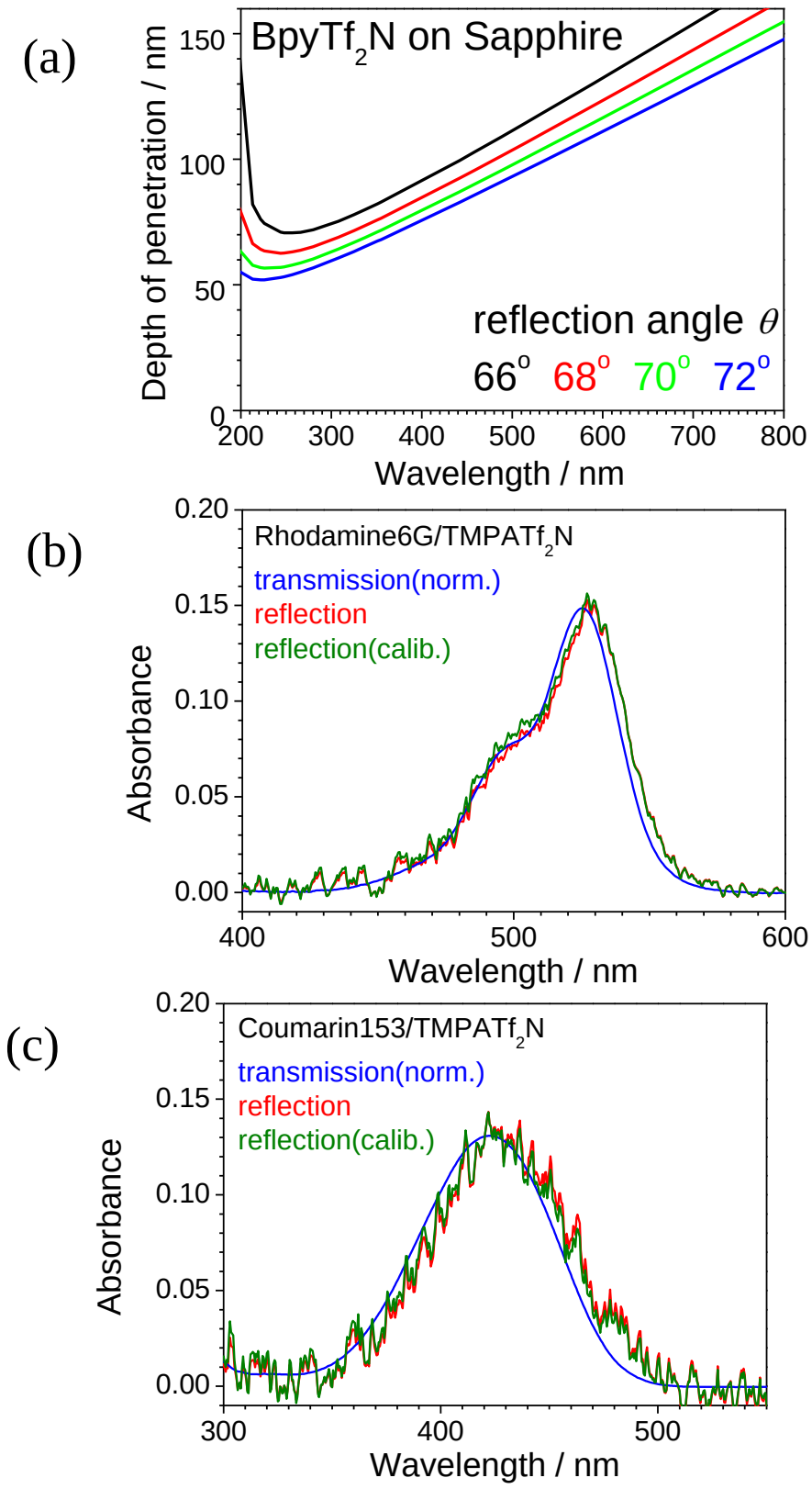

Figure 7-11. (a) Calculated depth of penetration (d_p) against light wavelength for $BpyTf_2N$ which is the representative of RTILs on sapphire. Absorption spectra of neat liquids by using transmission method (blue), reflection method (red), and that after calibration of *d*p (green) for (b) rhodamine 6G/$TMPATf_2N$ and (c) coumarin 153/$TMPATf_2N$.

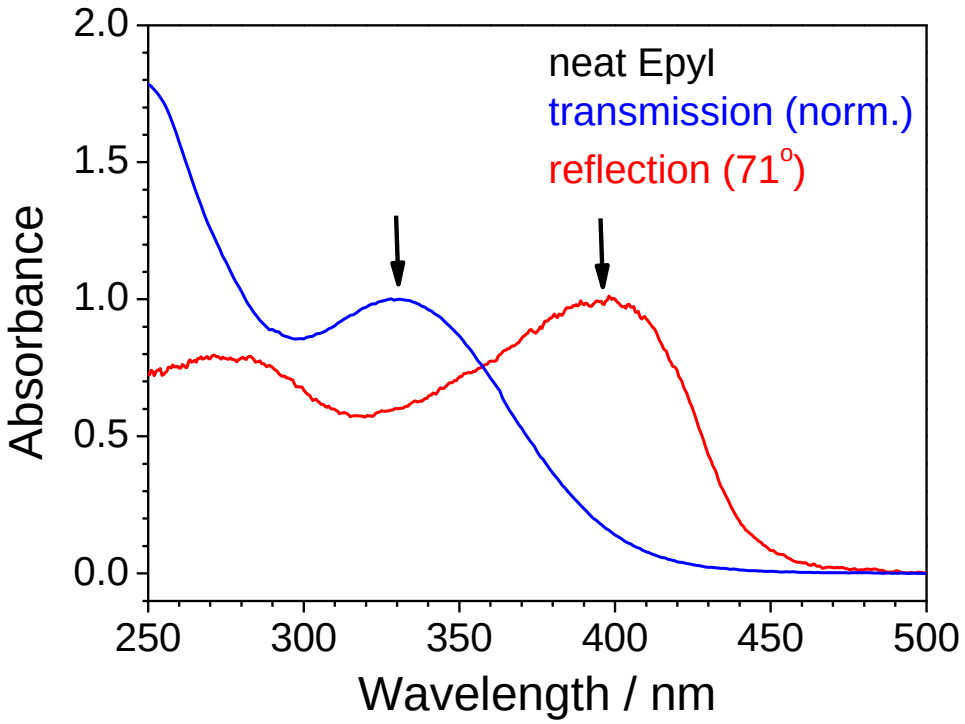

Figure 7-12. Absorption spectra of neat liquid by using reflection method (red), and transmission method (blue) at about 473 K. Arrows indicate absorption

Table 7-1. Estimated reflection angle of incident light depending on light wavelengths and refractive indices of sapphire prism depicted in Figure 6-3 (b).

Sapphire										
incident light	RI	reflection angle θ								
λ / nm	n_D	φ =45	50	55	60	65	70	75	80	85
200	1.94	66.38	68.26	69.98	71.51	72.85	73.97	74.86	75.51	75.90
230	1.87	67.22	69.18	70.98	72.59	73.99	75.17	76.10	76.78	77.19
300	1.80	68.13	70.19	72.07	73.76	75.23	76.47	77.45	78.17	78.60
vis	1.77	68.55	70.64	72.57	74.29	75.80	77.07	78.07	78.81	79.25

Chapter 8. Summary and concluding remarks

RTILs have attracted much interest since they show many unique physicochemical properties whose clear origin has not been found yet. Many scientists believe that RTILs are composed of polar and non-polar domain structures in bulk phase but this picture does not directly give answers for various questions about unique properties of RTILs. In particular, structure and dynamics near RTIL-solid interface region remains unknown. It is important to understand more details of microscopic interactions in neat RTILs because unique physicochemical properties and structures in RTILs introduced in previous sections would be due to the balance of these interactions. This is a basic motivation of the present thesis, and CT interaction between cation and anion was widely studied in gas phase, in diluted solution, in bulk neat liquid and near liquid-solid interface region by using various electronic absorption spectroscopic methods.

In Chapter 3, solvent effect for electronic states of $EmpyTf_2N$ and $BmimTf_2N$ were examined by using Cavity Ring-Down Spectroscopy for gas and liquid phases. Contrary to conventional molecular liquids, no remarkable differences were observed between the absorption spectra of RTILs in the gas and neat liquid phases. Small spectral shifts of the absorption bands of these RTILs from gas to neat liquid phases are discussed on the basis of ion pair absorption both for gas phase and for neat liquid. A large Onsager volume of ion pair reduces the spectral shifts due to the reaction field of liquids, which account for the reason why gas-phase spectra is similar to that of neat liquid. This result

indicates that there are mainly ion pairs in neat RTILs. It was proposed that a relatively small spectral shift in electronic absorption spectra between the gas and neat liquid phases is common for RTILs.

In Chapter 4, electronic state of cations affected by CT interaction from nearby anion was examined. The electronic absorption spectra of RTILs were measured for RTILs such as $BmimTf_2N$, $BmimPF_6$, $BmimBF_4$, and BmimTfO as neat liquid phases. $S_1(\pi\pi^*)\leftarrow S_0$ transition energy of $Bmim^+$ becomes large in the order of $TfO^- < Tf_2N^- < BF_4^- < PF_6^-$ as corresponding to the inversed order of RTILs' DN. Meanwhile, there is no correlation between transition energies and solvent polarities such as dielectric constant and empirical parameter (E_N^T), and this result also suggests that transition energy changes due to CT interaction between cation and counter anion within the ion pair.

In Chapter 5, CT complex of pyridinium-based cation and halide anion pair in diluted solution was studied. This gave important and fundamental information to understand those of neat RTILs which would have CT interaction within ion pairs forming CT complex. Oscillator strength of CT bands of RTILs in dichloromethane solution were estimated to be 0.02 by absorbance of the spectra and by measured concentration of ion pairs derived from electric conductivity measurements. Remarkable experimental finding is that CT interaction between the cation, Epy^+ and halide anions is very small as compared to usual CT complexes studied previously. This complex is composed of ion and anion with their charge being negligibly transfered from anion to

cation. From NMR spectroscopy and DFT calculation on EpyCl and EpyTf_2N ion pairs, we determined configuration of EpyCl ion pair which is isolated in dichloromethane solution. The complex is well characterized by the weak bonding of Cl^- anion attached to the hydrogen atoms at carbon atoms of 1' and 2 positions of Epy^+ cation.

In Chapter 6, CT complexes of cation and anion pair in neat RTILs, EpyI, PmmimI and BmimI, were studied by absorption spectroscopy. Oscillator strength of CT bands in neat liquids is much larger than that of isolated ion pair in non-polar solvent, CH_2Cl_2. This result means that CT interaction of ion pairs in neat ILs is large and, excess negative and positive charges on anion and cation, respectively, are rather delocalized within ion-pair. In neat liquids, there are only ion pairs which shows CT absorption bands near ππ* band of cations. In neat EpyI, CTTS band was also observed and its molar absorption coefficient at absorption maximum wavelength was estimated to be 1.0 x 10^4 mol^{-1} dm^3 cm^{-1}. This value is smaller than that of diluted solution, which indicates solvated electrons locates in surrounding near region from ion pairs.

In Chapter 7, CT interaction of ion pair in RTILs near solid-liquid interface was examined. Experimental apparatus for ATR/UV-Vis absorption spectroscopy was set up to measure absorption spectra near liquid-solid interfaces. Electronic transition absorption bands of chromophores near solid-liquid interface were measured for about 60 nm in depth from the interface. Based on simulated results, it was elucidated that there would be decrease of transition energies of chromophores near solid-liquid interface in RTIL solution and neat RTILs. This finding implies that CT interaction is

lowered near interface region.

In summary, this thesis has concluded the following three points to understand microscopic interactions within RTILs by various absorption spectroscopic studies.

(1) Neat RTILs is dominated by ion pairs as a unit of liquid phase. CT interaction within ion pairs in neat RTILs is stronger than that between cation and anion as isolated ion pair in non-polar solvent, which was given by discussion of oscillator strength based on Mulliken's theory.

(2) Solvent effect for ion pairs is small due to large Onsager volume of ion pairs in neat RTILs, and CT interaction strongly depends on anions' donor number.

(3) CT interaction near solid-liquid interface region is lower than that in bulk phase, which is presumably due to unique structure formed liquid-solid interaction.

These spectroscopic findings, in particular CT interaction within ion pair, may be useful in understanding of unique macroscopic properties of RTILs, in near future.

Acknowledgements

I wish to express my gratitude to Professor Akio Kawai for his valuable advice and support. I am most grateful to Professor Kazuhiko Shibuya for his helpful suggestion, valuable advice and encouragement. I am also obliged to Professor Nobuyuki Akai (Tokyo University of Agriculture and Technology) for his helpful advice and encouragement. I also thank to Professor Tetsuo Okada for his unfailing supports on electric conductivity measurements and the data analysis.

I thank Mr. Tooru Asaka and Mr. Daiki Kawamori to measure NMR spectrum. I also thank Dr. Yusuke Miyake and Dr. Takehiro Hidemori for their helpful support and suggestion. Then, I thank Mr. Yanagibashi as the same project member of ionic liquid-solid interface. Thanks are given to all the laboratory members for their various help.